UNIVERSIDAD NACIONAL AUTÓNOMA DE MÉXICO

PROGRAMA DE MAESTRÍA Y DOCTORADO EN INGENIERÍA

INGENIERIA CIVIL – ESTRUCTURAS

INELASTIC SEISMIC DEMANDS OF ONE-STORY PLAN-ASYMMETRIC BUILDINGS SUBJECTED TO BIDIRECTIONAL GROUND MOTIONS CHARACTERISTIC OF SOFT SOIL SITES IN THE VALLEY OF MEXICO

TESIS QUE PARA OPTAR POR EL GRADO DE:

MAESTRO EN INGENIERÍA

PRESENTA:

LUIS DANIEL PANCARDO GARCÍA

TUTOR PRINCIPAL:

DR. SAUL ESTEBAN LÓPEZ RÍOS PROGRAMA DE MAESTRÍA Y DOCTORADO EN INGENIERÍA

CIUDAD DE MÉXICO. JUNIO 2020

Universidad Nacional Autónoma de México
UNAM
Biblioteca Central
Dirección General de Bibliotecas de la UNAM

UNAM – Dirección General de Bibliotecas
Tesis Digitales
Restricciones de uso

DERECHOS RESERVADOS ©
PROHIBIDA SU REPRODUCCIÓN TOTAL O PARCIAL

Todo el material contenido en esta tesis esta protegido por la Ley Federal del Derecho de Autor (LFDA) de los Estados Unidos Mexicanos (México).

El uso de imágenes, fragmentos de videos, y demás material que sea objeto de protección de los derechos de autor, será exclusivamente para fines educativos e informativos y deberá citar la fuente donde la obtuvo mencionando el autor o autores. Cualquier uso distinto como el lucro, reproducción, edición o modificación, será perseguido y sancionado por el respectivo titular de los Derechos de Autor.

JURADO ASIGNADO:

Presidente:	Dr. Amado Gustavo Ayala Millán
Secretario:	M.I. Leonardo Emmanuel Flores Corona
Vocal:	Dr. Saúl Esteban López Ríos
1 er. Suplente:	Dr. Darío Rivera Vargas
2 do. Suplente:	Dr. Mauro Pompeyo Niño Lázaro

Lugar o lugares donde se realizó la tesis:

Facultad de Estudios Superiores Acatlán, UNAM

TUTOR DE TESIS:

Dr. Saul Esteban López Ríos

FIRMA

ACKNOWLEDGEMENTS

This thesis is dedicated to my family who have been by my side at every step of my life. To my mother, Maria Luisa Garcia, who taught me how to live a righteous life, your wisdom and advice will always be invaluable to me. To my father, Danilo Pancardo, who taught me the importance of working to achieve my goals, your unconditional support throughout both my bachelor and master studies made possible the fulfillment of this work. Finally, to my brother, Alex Pancardo, who taught me to never give up, your achievements will always inspire me.

Mainly, I dedicate this thesis to my wife, Guille Herrera, my partner and support, who has been with me all these years, thanks for being there when I needed and for your patience during the development of these research, thank you for believing in me. And to my son, Fernando, I hope that the hard work of your mother and mine will serve as inspiration to fulfill your dreams.

I would like to express my gratitude to Dr. Saul López, for your support throughout my master studies. Thank you for the opportunity to collaborate with you, and the professional development I experienced under your guidance.

I thank Dr. Gustavo Ayala, M.I. Leonardo Flores, Dr. Darío Rivera and Dr. Mauro Niño for the review of this thesis and their comments, which made possible the realization and development of this work.

I also acknowledge the National Council of Science and Technology (CONACyT) for my master studies scholarship and the PAPIIT project IA104519 "Formulation and validation of a displacement-based seismic design procedure for buildings considering the effects of in-plan torsion" for granting me additional support; both made possible the completion of the present thesis.

Finally, I thank God, for giving me the strength and knowledge to finish this work, for all the blessings in my life and the support.

INDEX

ABSTRACT

Seismic events like the earthquakes of Mexico in 1985 and recently in 2017, as well as several analytical studies, have proven the ill seismic performance of buildings with an asymmetric distribution of mass and/or lateral load resisting elements. The building codes' criterion for ultimate limit state design of irregular buildings consists on limiting the ductility demand through penalization of the seismic reduction factor, in accordance with the level of structural irregularity. However, this simple criterion, although practical, does not allow a rational control of the structural response under severe seismic demands, which might be significantly different between structures with different types and levels of irregularity.

Given the limitations of current design criteria for structures with in-plan asymmetry, this dissertation presents the results of a parametric analysis of the non-linear dynamic response of plan-asymmetric one-story buildings, with different levels of irregularity, subjected to bidirectional seismic loads, obtained from real seismic events' records from the Valley of Mexico, for both subduction and intraplate seismic sources. Specifically, the following demands were obtained:

- The displacement amplification of the flexible side of the structure, with respect to the displacement of the center of mass.
- The ductility demand at the center of mass
- The combination factor of the orthogonal base shear and displacement demands.

A non-linear regression analysis was carried out, from which equations were obtained that allow to approximate such seismic demands as a function of the parameters that define the level of irregularity of a building.

The results attained from this investigation allow to define rational seismic design demands, for its use in the design of in-plan irregular buildings with different levels of inelastic behavior, particularly, for its use with displacement-based design methods, which provide better control of seismic performance than the traditional force-based design methods of most building codes.

RESUMEN

Eventos símicos como los de México en 1985 y recientemente en 2017, así como diversos estudios analíticos, han demostrado el comportamiento sísmico inadecuado de edificios con una distribución asimétrica de masas y/o elementos resistentes a fuerzas laterales. El criterio reglamentario para el diseño de edificios irregulares para el estado límite último, consiste en limitar la demanda de ductilidad a través de la penalización del factor de reducción sísmica, de acuerdo con el nivel de irregularidad. Sin embargo, este criterio, si bien simple y práctico, no permite un control racional de la respuesta sísmica ante demandas intensas, el cual puede resultar muy distinto para estructuras con diferentes tipos y niveles de irregularidad.

Dadas las limitaciones de los criterios de diseño para estructuras con asimetría en planta, el presente trabajo presenta un análisis paramétrico de la respuesta no lineal de edificios de un nivel con asimetría en planta, con diferentes niveles de irregularidad, sujetos a cargas sísmicas bidireccionales, obtenidas de registros de eventos sísmicos reales del Valle de México, tanto para fuentes sísmicas de subducción como de intraplaca. De los resultados del análisis paramétrico, se obtuvieron las siguientes demandas:

- La amplificación del desplazamiento del lado flexible de la estructura, con respecto al desplazamiento del centro de masas.
- La ductilidad desarrollada en el centro de masas.
- El factor de combinación de las demandas ortogonales.

A partir de tales parámetros de demanda obtenidos del análisis, se realizó un ajuste de regresión no lineal, del cual se obtuvieron ecuaciones que permiten aproximar las demandas sísmicas como una función de los parámetros que definen el grado de irregularidad de una estructura. Con estas ecuaciones es posible calcular las demandas sísmicas inelásticas de cualquier edificio con asimetría en planta, utilizando propiedades básicas que son fácilmente obtenibles en el proceso de diseño.

Los resultados obtenidos en esta investigación permitirán definir demandas sísmicas de diseño razonables, para su uso en el diseño de edificios con irregularidad en planta con diferentes niveles de comportamiento inelástico, particularmente, para su uso en métodos de diseño basados en desplazamientos, los cuales permiten un mejor control del desempeño estructural que los métodos tradicionales basados en fuerzas de la mayoría de los reglamentos.

Chapter 1. INTRODUCTION

1.1. Background

Seismic events such as Kanto, Japan in 1923; the 1971 San Fernando, California earthquake; the 1985 Algarrobo, Chile earthquake; and particularly the earthquakes in Mexico in 1985 and more recently in 2017, have proven the ill performance of buildings with a plan-asymmetric distribution of mass and/or lateral load resisting elements. This type of structures exhibits significant in-plane torsional response when subjected to seismic ground motions, due to the offset between the resultants of the inertial and stiffness forces. This offset is known as stiffness eccentricity and its magnitude is an indicator of the level of irregularity of the building

Several analytical studies also show the vulnerability of buildings with in-plan asymmetry, which is a consequence of inelastic demand concentrations in its flexible side, which may lead to local collapse (Anagnostopoulos *et al.*, 2010; De Stefano and Rutenberg, 1999; Lucchini *et al.*, 2011; Ruiz *et al.*, 1989; Rutenberg and De Stefano, 1997). Likewise, experimental studies have shown such trend, both in-plan and in elevation (De Stefano *et al.*, 2013; Jeong and Elnashai, 2004; Moehle, 1984).

The seismic performance of buildings with in-plane torsion depends on several parameters relative to its geometry and its distribution of mass and/or resisting elements, particularly, stiffness eccentricity and rotational stiffness, and it has been the subject of several analytical studies with different levels of detail in the numerical modeling, from simplified one-story monosymmetric buildings (Bensalah *et al.*, 2012; De Stefano and Rutenberg, 1999; Ghersi and Rossi, 2000; Myslimaj and Tso, 2002), one-story buildings with two-way eccentricity (Lucchini *et al.*, 2011; Stathopoulos and Anagnostopoulos, 2007), or multi-story buildings modeled with plastic hinges (Anagnostopoulos *et al.*, 2010). Even though it has been well-recognized that in-plan asymmetric buildings will likely exhibit inadequate seismic performance and, thus, it has been recommended to avoid such structural configurations (Bazán and Meli, 1985), they are still a common feature in modern architectonic projects.

Although, the response of in-plan irregular multistory buildings is much more complex than that of one-story buildings, the response of the former can be studied via simplified one-story models with similar dynamic properties (Anagnostopoulos *et al.*, 2008). For this reason, there have been several analytical studies that use such approach. However, the number of different models and assumptions used on the analysis of irregular buildings have derived in conclusions that, although correct for the model used, have been generalized and contradict the conclusions obtained from different models and hypothesis (Anagnostopoulos *et al.*, 2015).

Particularly, the problem of inelastic behavior of buildings with in-plan torsion is quite complex, as the dynamic properties of the system vary through the different damage states attained during seismic response. Moreover, as in any dynamic problem, seismic response of a system depends

significantly on the characteristics of the ground motion, e.g. frequency content, phase angle and intensity, which makes the design and evaluation of the seismic behavior of in-plan irregular buildings an even more challenging task.

The criterion for the design of irregular buildings given in most design building codes, e.g., Complementary Technical Norms for Earthquake Resistant Design of the Mexico City Building Code 2017, NTC-DS (2017b), for the ultimate limit state, ULS, consists on limiting the ductility demand through the penalization of the seismic reduction factor, *Q'*, in accordance with the level of structural irregularity. However, this simple criterion, although practical, does not allow a rational control of the seismic response under severe seismic demands, in accordance with the current performance-based earthquake engineering approach. This is due to the fact that the ductility demand of the structure is unclear, as it may be significantly different between structures with different types and levels of irregularity. Moreover, the distribution of force and deformation demands may be significantly different in the inelastic range of behavior, aspect that cannot be adequately accounted for in an explicit manner by means of modal spectral analysis of elastic models.

As an alternative to the traditional design methods, displacement-based methods have been developed, which allow to use clearer criterion for the consideration of the effect of torsion, e.g. the extended N2 method (Fajfar *et al.*, 2005), which considers the effect of torsion through the superposition of the displacement of the center of mass obtained from an static non-linear analysis and the plan-displacement obtained from an elastic modal analysis.

Although the response of torsionally irregular buildings has been investigated since the emergence of earthquake engineering, as pointed out by Anagnostopoulos *et al*. (2015), seismic design of this type of buildings is still an open area of research

1.2. Objectives of this investigation

Given the limitations of the current design criteria given in building codes for structures with in-plan asymmetry, the objective of this investigation is to provide more rational design demands for irregular structures as a function of the parameters that define the level of irregularity, e.g. the stiffness eccentricity, the rotational stiffness and the fundamental period of the structure, in order to develop criteria for the consideration of the effects of seismic torsion, which can be incorporated in seismic design methods, particularly displacement-based design methods.

In this study, a parametric analysis of the seismic response of one-story in-plan irregular buildings with 3 degrees of freedom, 3DOF, two translational displacements and a floor rotation, subjected to bidirectional seismic accelerations characteristic of soft soils of the Valley of Mexico was carried out. The parametric analysis was performed using as seismic intensity measure the spectral pseudo-acceleration corresponding to the fundamental period, T_n, of the larger horizontal component.

From the results of the parametric analysis, the following demands were obtained:

- The displacement amplification of the flexible side of the structure, with respect to the displacement of the center of mass.
- The ductility demand developed at the center of mass.
- The combination factor of the orthogonal demands.

Furthermore, non-linear regression analysis was used to define equations that allow the calculation of inelastic seismic demands of in-plan asymmetric building considering the essential structural parameters that may be defined in practical design applications.

1.3. Outline

The background and objectives of this investigation were given in the current chapter. In the second chapter, the effect of seismic torsion on asymmetric buildings is reviewed, with emphasis on the seismic behavior of plan-irregular buildings. Subsequently, a summary of the current design methods of irregular buildings, for both force-based and displacement-based methods, is presented.

The third chapter present the parametric analysis of the seismic response o monosymmetric buildings. First, the study cases are presented along with the model specifications. Subsequently, the seismic ground motions used for the analysis are listed, along with its characteristics and the intensity measure considered in the parametric analysis. Finally, the modelling and analysis of the case studies is described.

The fourth and fifth chapters present the seismic demands obtained from the parametric analysis, for structures of moderate to high rotational stiffness (M-System) and structures with extremely high rotational stiffness (X-System). For both analysis of results the trends of the obtained seismic demands are identified, along with the discussion of the influence of the parameters considered in the analysis.

Chapter 6 presents equations, obtained from a non-linear regression analysis, which allow to calculate seismic demands as a function of the parameters that define the level of irregularity of a building. The main conclusions of this investigation are presented in Chapter 7Chapter 6, where a discussion of the results attained is given.

Finally, the expressions used to obtain the dimensions of the resisting elements, as a function of the parameters used in this work, are presented in Appendix A.

Chapter 2. SEISMIC TORSION ON ASYMMETRIC BUILDINGS

2.1. Basic concepts of torsional response

When a building is subjected to seismic loads, inertial and stiffness force generate on the floor and lateral load resisting elements, respectively. Generally, the in-plane stiffness of the floor systems is large, hence, they can be modelled as a rigid diaphragm. The point of the floor where the resultant of the inertial forces is located is known as center of mass, C_m, and the location of the resultant of the stiffness forces is known as center of stiffness, C_s. If the distribution of lateral load resisting elements is asymmetric an offset exists between the center of mass and stiffness, which generates a torsional moment that produce floor rotation, thus, the displacements in one edge of the plan are greater than the displacement of the center of mass and smaller on the opposite edge. The edges where the maximum displacements are generated is known as *flexible side* and where the minimum displacements are generated is known as *rigid side* (Fig. 2.1).

Under the hypothesis of rigid diaphragm, the displacements in every point in the floor-plan can be calculated as the sum of the displacements due to translation and torsion, hence, the relation between the translational and rotational stiffness and, consequently, the corresponding periods, are of great importance in the analysis of seismic torsion. Several studies show that the most important parameter that defines floor rotation of a building is the uncoupled translational to rotational frequency ratio, known as rotational stiffness factor, Ω (Anastassiadis *et al.*, 1998). $\Omega < 1.0$ denotes a torsionally flexible structure and $\Omega \geq 1.0$ denotes a torsionally stiff structure. Since Ω depends on the rotational stiffness of the structure, its value is a function of several parameters like the plan aspect ratio (B/L), the uncoupled translational periods ratio (R_T) and the resisting elements distribution.

The offset between the center of mass and the center of stiffness of a structure is known as stiffness eccentricity, e_s, and its magnitude is an indicator of the level of irregularity of the structure, which will present a higher level of seismic torsion as the stiffness eccentricity is larger. However, in the non-linear range of behavior, the torsional response depends more on the strength eccentricity, e_r, which is the distance between the center of mass and the point where the resultant of the yield resisting forces of the elements is located, *i.e.*, the center of strength, C_r, (Paulay, 2001). Hence, the yield force distribution is also an important factor in the torsional response, which depends on the distribution of the resisting elements and the shear design forces, obtained from a modal-spectral analysis using a design spectrum affected by a seismic reduction factor, Q'.

Table 2.1. Parameters associated to the seismic torsion effect, symbology and formulas. (De Stefano and Pintucchi, 2010)

Parameter	Symbology
Mass polar moment of inertia	$I_m = \frac{B^2 + L^2}{12}$.
Mass radius of gyration	$\rho = \sqrt{\frac{I_m}{m}}$
Total lateral stiffness along y- and x-direction	$K_y = \sum_{i=1}^{N} k_{yi}; \quad K_x = \sum_{i=1}^{N} k_{xi}$
Rotational stiffness, computed with respect to C_s	$K_\theta = \sum_{i=1}^{N} \left[k_{yi} \left(x_i, C_s \right)^2 + k_{xi} \left(y_i, C_s \right)^2 \right]$
Uncoupled translational and rotational periods	$T_y = 2\pi \sqrt{\frac{m}{K_y}}; \; T_x = 2\pi \sqrt{\frac{m}{K_x}}; \; T_\theta = 2\pi \sqrt{\frac{I_m}{K_\theta}}$
Uncoupled translational periods ratio	$R_T = \frac{T_y}{T_x}$
Stiffness eccentricity along x- and y-direction, non-dimensionalized with respect to parallel plan dimension	$e_{sx} = \frac{1}{L} \frac{\sum_{i=1}^{N} k_{yi} x_i}{K_y}; \quad e_{sy} = \frac{1}{B} \frac{\sum_{i=1}^{N} k_{xi} y_i}{K_x}$
Total system lateral strength	$V_y = \sum_{i=1}^{N} V_{yi}; \quad V_x = \sum_{i=1}^{N} V_{xi}$
Strength eccentricity along x- and y-direction, non-dimensionalized with respect to parallel plan dimension	$e_{rx} = \frac{1}{L} \frac{\sum_{i=1}^{N} V_{yi} x_i}{V_y}; \quad e_{ry} = \frac{1}{B} \frac{\sum_{i=1}^{N} V_{xi} y_i}{V_x}$
Torsional flexibility ratio	$\Omega_y = \frac{T_y}{T_\theta}; \qquad \Omega_x = \frac{T_x}{T_\theta}$

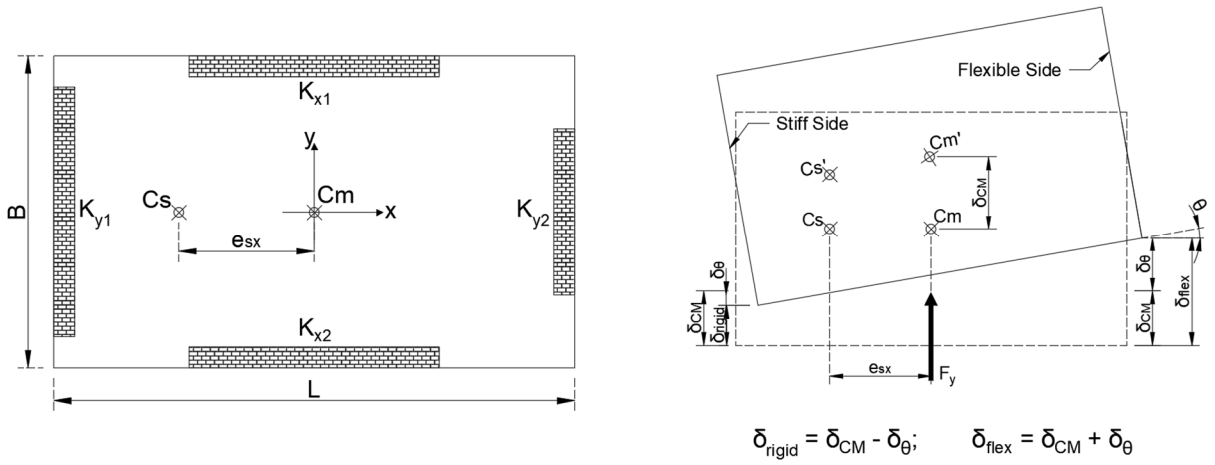

Fig. 2.1. One-story in-plan asymmetric building model
a) terminology associated with seismic torsion and b) deformed shape of an in-plan asymmetric building. (Anagnostopoulos et al., 2015)

2.2. Modern building codes torsional provisions

The most common approach followed in force-based design procedures, contained in building codes, relies on an elastic modal-spectral analysis, where the lateral seismic forces are obtained from a pseudo-acceleration design spectrum, reduced by a seismic reduction factor, *Q'*. The analysis of the structure, from which the shears and moments used for design are obtained, is performed considering two horizontal orthogonal components, 100% in on direction and β% in the other. This combination factor, β, was derived from analysis of elastic systems of 2 DOF, e.g. Rosenblueth and Contreras (1977), implicitly accepting that the combination between the maximum responses in the linear range of behavior and the ones in the non-linear range are similar. However, the use of this combination factor may lead to underestimated design forces for certain elements, particularly on buildings with torsional behavior (Wilson *et al.*, 1995)

The analysis method used for the obtention of the design values depends on the level of irregularity of the building. For structures with none to low irregularity an equivalent static analysis is allowed, where lateral loads are a function of the weight and height of the building. On the other hand, for structures with moderate irregularity, the lateral loads are obtained from a modal-spectral analysis, and for structures with high irregularity, a non-linear dynamic analysis is required. The torsional provisions of different building codes from Mexico (*NTC-DS*, 2017b), Europe (*EN 1998-1*, 2004), USA (*ASCE 7-16*, 2016) and Chile (*NCh 433-12*, 2012), are presented in table 2.2.

The building codes' provisions for the design of irregular buildings, for the ultimate limit state (ULS), consists on limiting the ductility demand through the penalization of the seismic reduction factor, *Q'*, in accordance to the level of structural irregularity. Additionally, different codes prescribe a value of accidental eccentricity, e_{acc}, to consider the uncertainty of the locations of the

center of mass and stiffness. However, this simple criterion, although practical, does not allow a rational control of the seismic response under severe seismic intensities, in accordance to the current seismic engineering performance-based approach, since the ductility demand that the structure develops is unclear, which might result very different between structures with different types and levels of irregularity. Furthermore, the in-plan distribution of forces and deformations is different for elastic and inelastic systems for distinct levels of ductility.

Table 2.2 Torsional provisions of modern codes

Torsion Related Causes	Code			
	Mexico NTC-DS 2017	Europe EN-8 2004	USA ASCE7 2016	Chile NCh 433 2012
Regularity Criteria	Geometric and Structural	Geometric and Structural	Geometric and Structural	Geometric and Structural
Accidental Eccentricity	$\pm\left[0.05+0.05\frac{i-1}{n-1}\right]b_i$	$\pm 0.05 b_i$	$\pm 0.05 b_i A_x$ $A_x=(\delta_{max}/1.2\delta_{avg})^2$	1) $\pm 0.05 b_i$ Or 2) $\pm 0.10 b_i\, h_i/H$
Torsional effects	Apply static moment $M_{0i} = \pm (M_{ai} - M_{a(i+1)})$ $Mai = e_{acci} V_i$	Move masses by $\pm$ eacc or combine with static moment $M_i = e_{acc} F_i$ or move static forces by $\pm e_{acc}$	Apply static moment $M_{ta} = \pm e_{acc} F_i$	1) Move center of mass $\pm e_{acc}$ Or 2) Apply static moment $Mi = \pm e_{acc} F_i$

2.3. Displacement-based design methods for asymmetric buildings

As an alternative to the traditional force-based design method prescribed in building codes, displacement-based methods have been developed, which allow to use a more rational criterion for the consideration of the effects of seismic torsion (Moehle, 1992; Priestley *et al.*, 2007). In such types of methods, the design demands are defined considering in an improved manner the displacement profile of the structures under inelastic response, from which a better estimation of design demands is attained than that achieved with the force-based design procedure. Two of the most widely known displacement-based design methods are the direct displacement-based design method (DDBD) proposed by Priestly *et al* (Priestley, 2003) and the extended N2 method proposed by Fajfar *et al* (2005). Such methods shall be described in the following.

2.3.1. Direct Displacement-Based Design Method

The direct displacement-based design method, DDBD (Priestley, 2003), is based on the assumption that structures must be designed to achieve a certain performance objective, defined by displacement or drift limits. The DDBD method considers an SDOF representation of the building (Fig. 2.2a), characterized by a secant stiffness K_e at maximum displacement Δ_d, and an

equivalent viscous damping ξ, representative of the combined elastic damping and the hysteretic energy absorbed during the inelastic response, which is a function of the level of ductility demand and the structural system type.

The design displacement of the structure depends on the displacement or drift limit state of the most critical element of the story. If the displacement shape is assumed to be equal to the shape of the fundamental mode of vibration, which is a reasonable simplification for low and medium rise buildings, the design displacement is given by the following expression:

$$\Delta_d = \frac{\sum_{i=1}^{n}\left(m_i\Delta_i^2\right)}{\sum_{i=1}^{n}\left(m_i\Delta_i\right)} \qquad 2.1$$

where m_i and Δ_i are the masses and displacements of the n stories of the building.

From the assumption that the substitute SDOF structure is representative of the fundamental mode of vibration, the effective mass and height of the structure are obtained from the following equations:

$$m_e = \sum_{i=1}^{n}\left(m_i\Delta_i\right)\Big/\Delta_d \qquad 2.2$$

$$H_e = \sum_{i=1}^{n}\left(m_i\Delta_i H_i\right)\Big/\sum_{i=1}^{n}\left(m_i\Delta_i\right) \qquad 2.3$$

The ductility demand can be defined assuming that the yield drift depends only on the geometry of the structural elements. Priestley (2003) proposes the following expression to obtain the yield rotation for concrete or steel frame buildings.

$$\theta_y = C_2\varepsilon_y\frac{L_b}{h_b} \qquad 2.4$$

where:

C_2 is a factor equal to factor equal to 0.50 and 0.65 for concrete and steel frames, respectively.

ε_y is the yield strain of steel reinforcement.

L_b y h_b are the beam's length and depth, respectively.

The yield displacement and the expected ductility demand of the system are obtained from the following expressions:

$$\Delta_y = \theta_y H_e \qquad \mu = \frac{\Delta_d}{\Delta_y} \tag{2.5}$$

From the design displacement and the equivalent viscous damping associated with the expected ductility demand (Fig. 2.2c), the effective period T_e at the maximum displacement response, associated with the effective height H_e, can be obtained from a set of displacement spectra with different damping ratios (Fig. 2.2d).

The secant stiffness K_e of the substitute structure at maximum displacement can be estimated in a straightforward manner via the following equation:

$$K_e = 4\pi^2 \frac{m_e}{T_e^2} \tag{2.6}$$

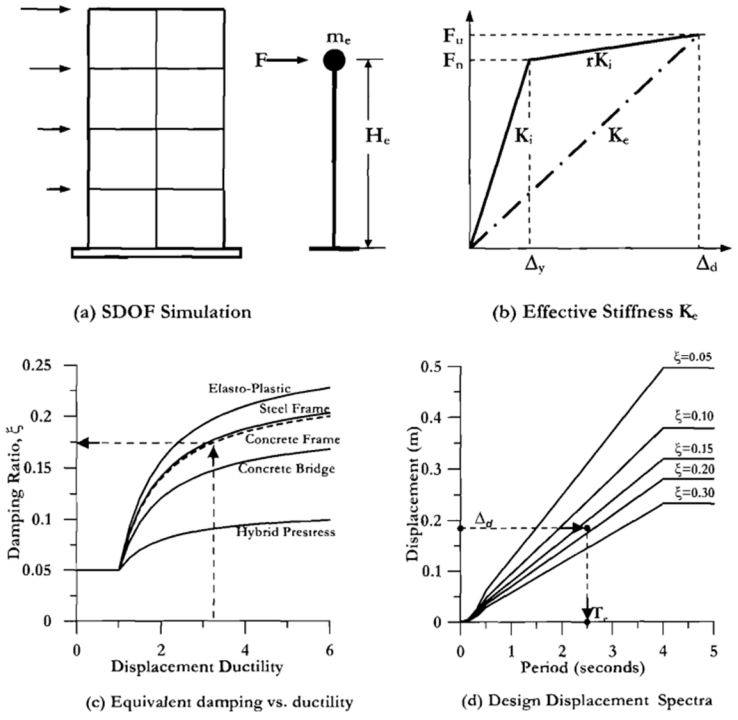

Fig. 2.2 Fundamentals of Direct Displacement-Based Design (Priestley et al., 2007)

2.3.1.1. Direct displacement of the method to account for torsion

In plan-asymmetric buildings, the flexible side of the plan shall exhibit the largest inelastic seismic displacements due to the combined effect of translational and rotational motion. Hence, the drift

of the flexible side of the building governs the design (Fig. 2.3). The displacements of the flexible side can be obtained with the following expressions:

$$\Delta_j = \Delta_{CM} + \Delta_{\theta j}$$
$$\Delta_{\theta j} = \theta(x_j - e_{rx}) \qquad 2.7$$

where Δ_{CM} and $\Delta_{\theta j}$ are the displacements due to translation and torsion, respectively, θ is the floor rotation and x_j is the distance of the element to the center of stiffness. Considering this, the design displacement at the building center of mass used in the SDOF substitute structure, obtained with eq. 2.1, needs to be reduced in proportion to the torsional displacements:

$$\Delta_{d,CM} = \Delta_d - \theta\left(x_j - e_{rx}\right) \qquad 2.8$$

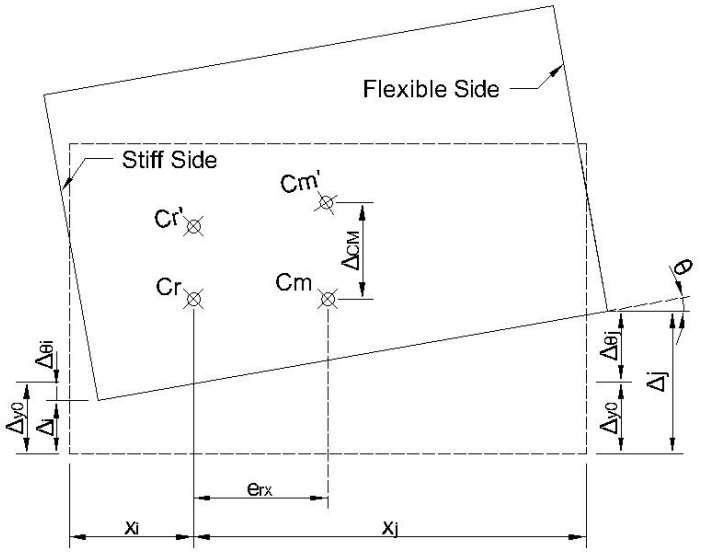

Fig. 2.3 Plan displacement shape of an asymmetric building

It is also possible, particularly for low-rise wall buildings, that the displacement of the rigid side may govern the design. In this case the design displacement at the center of mass will be larger than the displacement of the critical element. For those cases a slight modification of eq. 2.8 should be used:

$$\Delta_{d,CM} = \Delta_d + \theta\left(x_i + e_{rx}\right) \qquad 2.9$$

In general, it will be necessary to adopt an iterative approach to determine the design displacement when torsional effects are significant, since θ depends on K_θ, e_s and e_r which in turn depend on the relative strengths and stiffnesses of the lateral force-resisting elements in both orthogonal directions, and the ductility of the system.

2.3.2. Extended N2 method

The Extended N2 method (Fajfar *et al.*, 2005) is based on the definition of an equivalent SDOF system to determine the seismic demand of an MDOF system. The properties of the former are attained from pushover analysis from which the capacity curve is defined. Such curve is then simplified as an elastic perfectly plastic idealization of the force-displacement relationship, based on the equal energy principle, where the yield displacement is given by:

$$S_{dy} = 2\left(S_{dm} - \frac{E_m}{S_{ay}}\right) \qquad 2.10$$

Where S_{dm} is the displacement when a plastic mechanism occurs and E_m is the actual energy deformation up to the formation of the plastic mechanism.

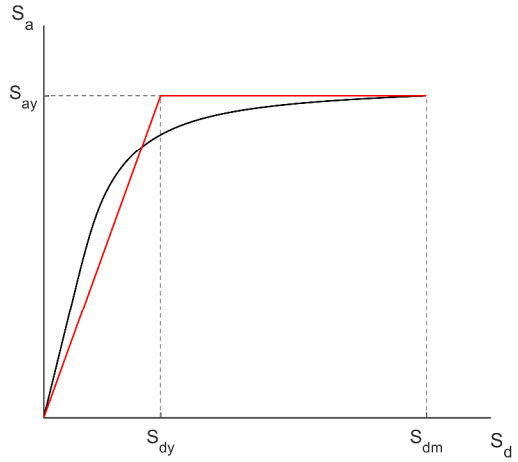

Fig. 2.4. Capacity Curve of the MDOF system (EN 1998-1, 2004)

The displacement and force of the equivalent SDOF system S_d* and F* are defined as:

$$S_d^* = \frac{S_{dt}}{\Gamma}; \qquad S_a^* = \frac{S_a}{\Gamma} \qquad 2.11$$

Where S_{dt} is the top displacement of the MDOF system, S_a is the pseudo-acceleration of the MDOF system in the direction of ground motion and Γ is the modal participation factor. The elastic period of the idealized bilinear system T* can be determined using the yield force and displacement:

$$T^* = 2\pi\sqrt{\frac{S_{dy}^*}{S_{ay}^*}} \qquad 2.12$$

The inelastic ductility and displacement of the SDOF system are determined from the following expressions (*EN 1998-1*, 2004):

$$\mu = \begin{cases} \left(R_\mu - 1\right)\dfrac{T_C}{T^*} + 1; & T^* < T_C \\ R_\mu; & T^* \geq T_C \end{cases} \qquad 2.13$$

$$S^*_{dm} = \begin{cases} \dfrac{S^*_{de}}{R_\mu}\left(1 + \left(R_\mu - 1\right)\dfrac{T_C}{T^*}\right); & T^* < T_C \\ S^*_{de}; & T^* \geq T_C \end{cases} \qquad 2.14$$

where R_μ is the reduction factor due to ductility, which is equivalent to the seismic reduction factor *Q'* used in the Mexican Building Code (*NTC-DS*, 2017a); and T_C is the characteristic period of the ground motion, typically defined as the transition period where the constant acceleration segment of the design spectrum ends. As it can be seen in eqs. 2.13 and 2.14, for periods greater than T_C, the equal displacement rule applies, *i.e.,* the displacement of the inelastic system is equal to the displacement of the corresponding elastic system with the same period.

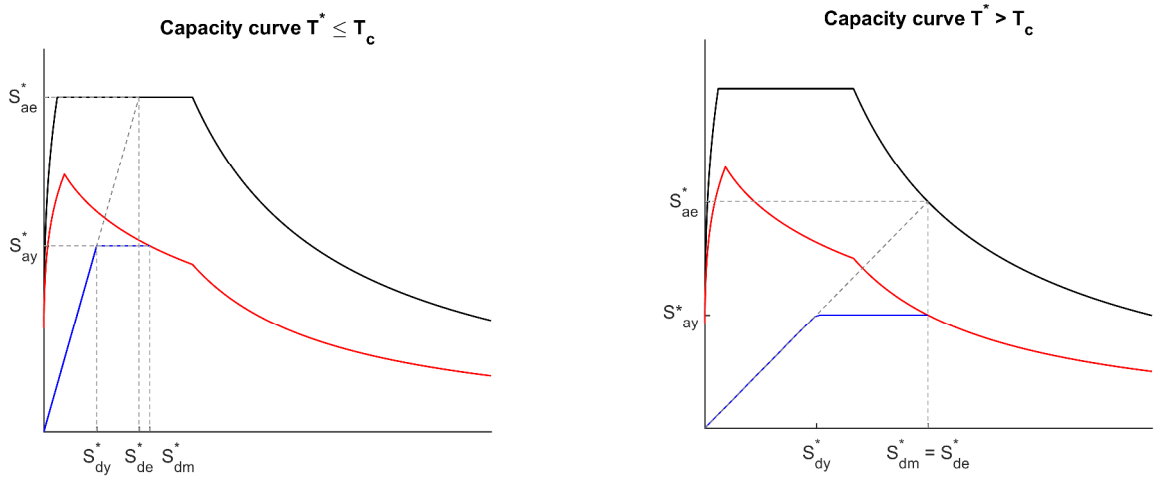

Fig. 2.5. Elastic and inelastic demand spectra vs. capacity curve (Fajfar et al., 2005)

Using the displacement of the SDOF system, the displacement demand at the center of mass of the MDOF system, S_{dm}, is obtained from the eq. 2.11. The displacements of the flexible and rigid sides of the building are obtained from a pushover analysis, taking S_{dm} as the ultimate displacement. It is assumed that the distribution of deformations throughout the height of the building in the pushover analysis approximates the one that would be obtained from non-linear dynamic analysis, However, the transformation of the MDOF structure to an equivalent SDOF system assumes a time-invariant displacement shape, this assumption is appropriate for planar structural models only where the influence of higher modes is negligible.

For the case of asymmetric buildings, where higher modes contribute substantially to the response, the results obtained by pushover analysis of a 3D structural model must be combined with the results of a linear modal-spectral analysis, where the former results control the target displacements and the distribution of deformations along the height of the building, whereas the latter results define the torsional amplifications (Fajfar *et al.*, 2005). Specifically, correction factors, *CF*, are defined as the ratio between the normalized roof displacements obtained from elastic modal analysis and those attained via pushover analysis. The normalized roof displacement is the roof displacement at an arbitrary location divided by the roof displacement at the center of mass. If the normalized roof displacement obtained by the elastic modal analysis is smaller than 1.0, the value 1.0 is used.

$$CF = \begin{cases} \dfrac{S_{di}}{S_{d,CM}}; & S_{d,CM} < S_{di} \\ 1.0; & S_{d,CM} \geq S_{di} \end{cases} \qquad 2.15$$

The aforementioned approach is based on the results of parametric studies that show that in the majority of cases an upper limit for torsional effects can be estimated by a linear dynamic analysis (Marusic and Fajfar, 2005). However, De Stefano and Pintucchi (2010) suggest that the use of the elastic deformed shape to predict the inelastic torsional amplifications is not always conservative, particularly for structures with high torsional stiffness.

Chapter 3. METHODOLOGY USED FOR THE PARAMETRIC ANALYSIS OF SEISMIC RESPONSE OF ASYMMETRIC BUILDINGS

As it was shown in the preceding chapter, for any of the aforementioned seismic assessment and design methods it is necessary to consider robust estimations of torsional demands of in-plan asymmetric structures that allow an appropriate estimation of its maximum seismic response for assessment and design purposes. For this reason, in this study, a full-scale parametric analysis of one-story buildings with one- and two-way in plan-asymmetry subjected to ground motions corresponding to soft soil sites at the Valley of Mexico, with fundamental soil periods between 0.5 s and 2.5 s, was carried out. This type of ground motion was chosen in this study as they exhibit unique characteristics with respect to other ground motions due to large site effects, hence, being the reason behind the severe damage occurred at soft soil sites of Mexico City caused by the 1985 Michoacán Earthquake and the 2017 Puebla Earthquake.

3.1. Description of the case studies

The case studies considered were one-story buildings with rigid diaphragm and plan dimensions B x L. The strength eccentricity was considered the same as the stiffness eccentricity, *i.e.*, the center of strength coincides with the center of stiffness, which is representative of existing buildings (De Stefano and Pintucchi, 2010). The parametric analysis was carried out considering the parameters described in table 2.1, varying their values as follows:

- Plan aspect ratio B/L was varied between 0.25 and 1.00, in increments of 0.25.
- Uncoupled translational period T_y was varied between 0.50 and 3.00 s, in increments of 0.50 s.
- Uncoupled translational periods ratio $R_T = T_y / T_x$ with values of 1.0, 1.5 and 2.0.
- Stiffness/strength eccentricity along the x-direction e_{sx} with values of 0.1, 0.2 and 0.3.
- Stiffness/strength eccentricity along the y-direction e_{sy} with a value of 0, *i.e.* the analyzed structures are monosymmetric.
- Lateral strength associated with seismic reduction factors, *Q'*, between 1.0 and 7.0, a range that is consistent with ductility values from 2.0 to 4.0 in soft soil types of the Valley of Mexico (Ruiz-Garcia and Miranda, 2004).

Two main types of case studies were considered as a function of its rotational stiffness: buildings composed by moment resisting frames, denoted as M – System, which possess a moderate to large rotational stiffness; and buildings with perimetral shear walls, denoted as X – System, which in many cases possess an extremely large rotational stiffness and, thus, exhibit different behavior trends than those less torsionally rigid systems.

3.1.1. Moderate to large torsionally stiff system

The M – System, Fig. 3.1a, presents six vertical resisting elements, which are rectangular column-type elements, with *h/b* ratio equal to R_T, distributed along the perimeter of the building, with each pair of vertical elements aligned in the y-direction having the same dimensions, and stiffness. The vertical resisting elements present a stiffness ratio equal to $k_{xi} / k_{yi} = (R_T)^2$.

The sizing and distribution of elements was performed in such a way that the parameters e_s, **Ω**, T_y and R_T, matched the values considered (see Appendix A). **Ω** is independent of e_s and its value is limited by the combination of different parameters (table 3.1). It is also worth noting that the range of **Ω** for a combination of parameters narrows as e_s, R_T and B/L are larger.

3.1.2. Highly torsionally stiff system

The X – System, Fig. 3.1b, presents four vertical resisting elements, which are wall-type elements, with t/L_m ratio equal to 0.1*,* where *t* is the wall thickness and L_m is the wall length, distributed along the perimeter of the building. The out-of-plane stiffness of the elements is equal to 0.001 of its in-plane stiffness.

This specific number and distribution of elements represent a special case in which **Ω** is dependent of e_s, B/L and R_T, i.e. a single value of **Ω** correspond to a combination set of parameters (see Appendix A). In table 3.2 the values of **Ω** for different combinations of parameters is presented. It can be observed that this value of **Ω** is slightly higher than the maximum limit of its corresponding for the M – System, which confirms that the X – System is significantly more torsionally rigid.

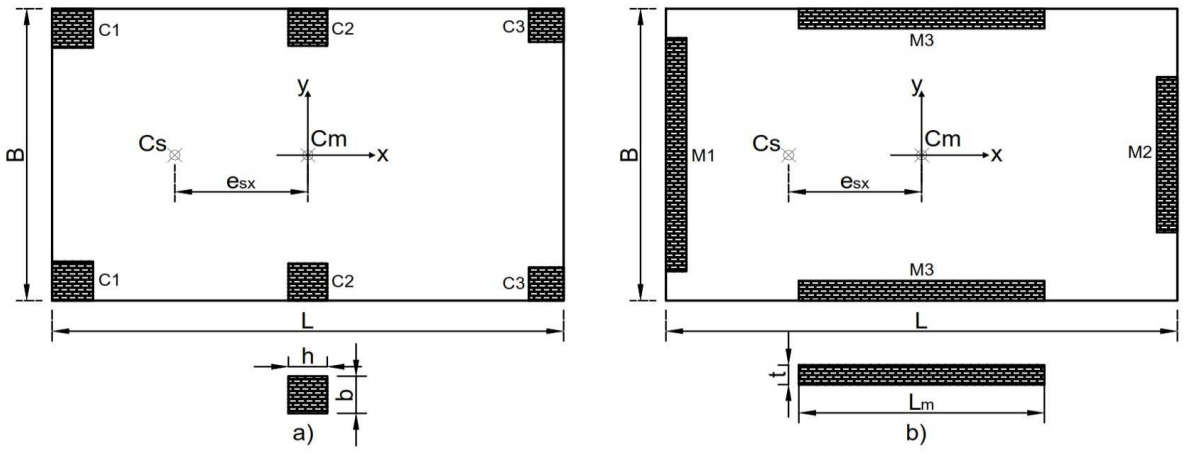

Fig. 3.1. Model representation of one-story 3 DOF one-way asymmetric building with a) Moderate to large rotational stiffness and b) Extremely large rotational stiffness.

Table 3.1. M – System: Ω_y range of values for different combinations of e_s, B/L and R_T.

	B/L								
	0.50			0.75			1.00		
e_{sx} \ R_T	1.0	1.5	2.0	1.0	1.5	2.0	1.0	1.5	2.0
-0.1	1.0 1.7	1.4 1.9	1.7 2.1	1.2 1.7	1.7 2.0	2.2 2.4	1.4 1.7	2.0 2.1	2.5 2.7
-0.2	1.1 1.6	1.4 1.8	1.8 2.1	1.3 1.6	1.8 2.0	2.2 2.4	1.4 1.6	2.0 2.1	2.6
-0.3	1.1 1.4	1.4 1.6	1.8 1.9	1.3 1.5	1.8 1.9	2.2 2.3	1.4 1.5	2.0	2.6

Table 3.2. X – System: Ω_y values for different combinations of e_s, B/L and R_T.

	B/L								
	0.50			0.75			1.00		
e_{sx} \ R_T	1.0	1.5	2.0	1.0	1.5	2.0	1.0	1.5	2.0
-0.1	1.70	1.90	2.15	1.70	2.05	2.46	1.70	2.18	2.71
-0.2	1.61	1.82	2.08	1.63	2.00	2.42	1.65	2.14	2.68
-0.3	1.45	1.68	1.96	1.51	1.90	2.34	1.56	2.07	2.62

3.2. Seismic ground motions

A set of earthquake ground motions corresponding to soft soil sites was selected from the earthquake record database of the UNAM Institute of Engineering (RAII-UNAM, 2018). The selection was carried out considering records of subduction and intraplate earthquake events with predominant periods, T_s, in their velocity spectrum between 1.5 s and 2.5 s, as such periods are similar to the fundamental period of soft soil sites at the Valley of Mexico. Detailed information of the selected records is given in table 3.3.

Table 3.3. Input ground motions, main characteristics and properties

Record	Station	Magnitude	PGA NS [g]	PGA EW [g]	Source
SCT190985dat	SCT B-1	8.1	0.096	0.165	subduction
AL250489dat	ALAMEDA	6.9	0.047	0.038	subduction
AL140995dat	ALAMEDA	7.2	0.042	0.036	subduction
TL250489dat	TLATELOLCO	6.9	0.046	0.032	subduction
CJ140995dat	C.U. JUAREZ	7.2	0.025	0.027	subduction
CUPJ140995dat	CUPJ	7.3	0.025	0.028	subduction
CO140995dat	CORDOBA	7.3	0.045	0.046	subduction
TL140995_2dat	TLATELOLCO	7.2	0.031	0.020	subduction
GA140995dat	GARIBALDI	7.3	0.031	0.027	subduction
TL140995dat	TLATELOLCO	7.3	0.027	0.029	subduction
SCT241093dat	SCT B-1	6.6	0.011	0.011	subduction
SCT101294dat	SCT B-1	6.3	0.011	0.014	subduction
TL101294dat	TLATELOLCO	6.3	0.015	0.015	subduction
SCT21709191	SCT B-2.	7.1	0.092	0.093	intraplate
CI0520170919181440	CIBELES	7.1	0.116	0.116	intraplate
GA6220170919181440	ESC. SEC. TÉC. NO. 2	7.1	0.099	0.086	intraplate
CJ0320170919181440	CENTRO URBANO JUÁREZ	7.1	0.114	0.100	intraplate
PE1020170919181440	ESC. PRIM. "PLUTARCO ELÍAS CALLES"	7.1	0.103	0.127	intraplate
AL0120170919181440	ALAMEDA	7.1	0.119	0.111	intraplate
VG0920170919181440	VALLE GÓMEZ	7.1	0.122	0.104	intraplate
BL4520170919181440	BALDERAS	7.1	0.104	0.117	intraplate
TL0820170919181440	DEPORTIVO "ANTONIO CASO T-II"	7.1	0.084	0.083	intraplate
HJ7220170919181440	HOSPITAL JUÁREZ	7.1	0.092	0.098	intraplate
TL5520170919181440	TLATELOLCO	7.1	0.084	0.071	intraplate

The reference seismic intensities considered in this study were defined from the design pseudo-acceleration spectrum (5% viscous damping ratio) of the seismological station of the Secretaria de Comunicaciones y Transportes, SCT, whose site period is T_s = 1.73 s. The intensity measure (IM) considered in the parametric analyses was the larger value of pseudo-acceleration of the two horizontal components, S_{am}, at the fundamental period of the structure, T_n. Therefore, the ground motions used in the analyses were scaled so that the larger pseudo-acceleration of the horizontal components at T_n, matched the corresponding of the reference design spectrum, S_{ad}.

The pseudo-acceleration response spectra of the scaled ground motions are shown in Fig. 3.2a, for values of T_n = 0.50, 1.5 and 3.0 s. As can be observed in such figure, the spectral ordinates are equal to the target S_{ad} for $T = T_n$. Fig. 3.2b depicts the comparison between the average intensity measure, $\overline{IM}$, and the target spectrum.

3.3. Modeling and analysis of the case studies

The parametric analysis was performed using the OpenSees software (McKenna *et al.*, 2016). The case studies were modeled as generic one-story buildings with rigid diaphragm and 3DOF, two translational displacements and a floor rotation. The center of mass was located at the geometric center and the center of stiffness at a known distance from the center of mass. The buildings were modeled as shear buildings, columns with infinitely rigid beams, hence, the lateral stiffness of the frame is provided entirely by the columns.

Modal analysis of elastic models of the case studies was carried out to obtain their coupled periods and modal participation factors. Subsequently, modal-spectral analysis of the elastic models was performed using the reference design spectrum reduced by seismic reduction factors Q' between 1.0 and 7.0, to define the strength of the structural elements for the purpose of assessing the seismic response of the structures for different levels of inelastic action. Since it was considered that the center of strength of the case studies was located at the same point as their center of stiffness, i.e. $e_s = e_r$, the strength of the structural elements was distributed in proportion to its stiffness.

Non-linear static analysis were performed to define the yield displacement of the buildings and their ductility under monotonic loading in order to serve as a reference to the dynamic response of the case studies. Non-linear dynamic analysis were carried out using both horizontal components of the earthquake records selected to assess the seismic response of the case studies.

For such analyses, the vertical resisting elements were modeled as elastic elements with plastic hinges at both ends considering an elastoplastic behavior model. The flexural-compression interaction in the non-linear range of behavior was modelled using an ellipsoidal moment interaction surface (De Stefano and Pintucchi, 2002), whose limits are the yield moments along the x- and y-axes. For the column-type elements of the M – System, the yield moments were determined through the Bresler equation for biaxial flexion (Bresler, 1960). On the other hand, the wall-type elements were modeled as in-plane uniaxial flexural elements since their out-of-plane strength is not significant.

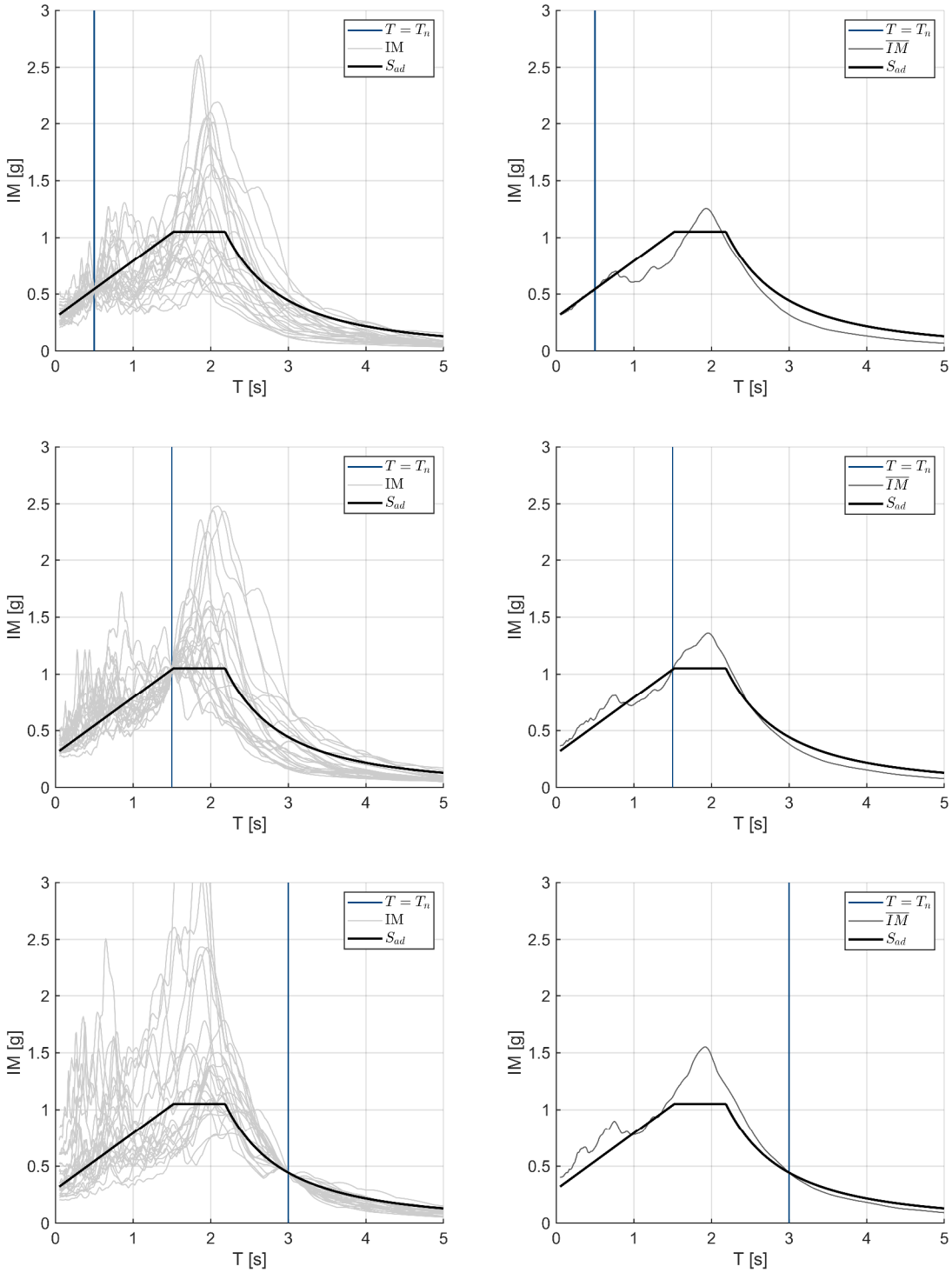

Fig. 3.2. Scaling of ground motions with respect to the design elastic spectrum
a) Intensity Measure spectra; b) Average Intensity Measure spectrum

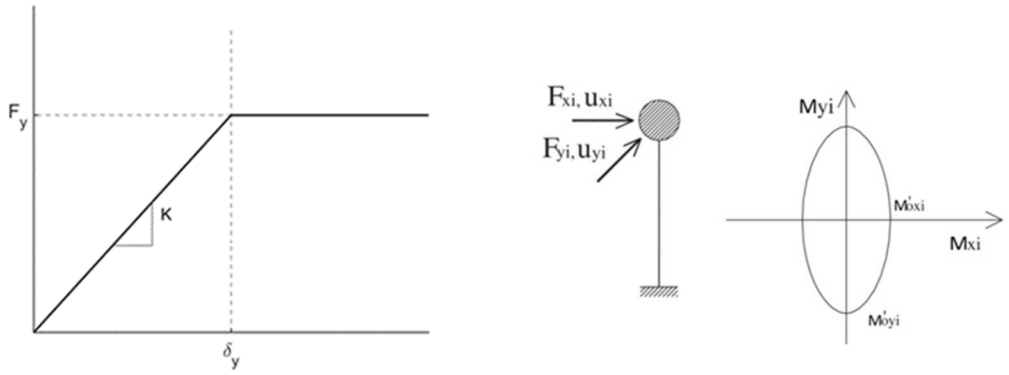

Fig. 3.3 Elastoplastic behavior model and yield interaction surface (De Stefano and Pintucchi, 2002).

The solution of the dynamic equilibrium equation was attained via Newmark's average constant acceleration method (Newmark, 1959), in conjunction with the Newton-Raphson method. The damping of the system was considered by means of a Rayleigh's damping model, with a damping of 5% for the first two modes of vibration.

3.4. Analysis of results

Since multiple non-linear dynamic analyses were performed for each structure, a large data set was obtained for each combination of parameters. In order to have a single value associated with each structure, the median of its corresponding data set was considered as the reference seismic demand, as the median is less affected by skewed data, *i.e.* extremely large or small values, and is a better measure of central tendency when the distribution is not symmetrical. The dispersion of the seismic response of the case studies was measured in terms of the median absolute deviation (MAD), normalized by the median. From the analyses carried out, the following seismic demands parameters were obtained:

3.4.1. Displacement amplification due to torsional effects, δ_F/δ_{CM}.

As mentioned earlier, the extended N2 method uses a correction factor of the displacement at the flexible and rigid sides, which is equal to the ratio of the displacement of the respective side and the displacement of the center of mass, obtained from an elastic modal analysis. However, the use of the elastic deformed shape to estimate the inelastic torsional amplifications is not always conservative, particularly for structures with high torsional stiffness (De Stefano and Pintucchi, 2010).

Therefore, the displacement amplification of the flexible side with respect to the center of mass was obtained, δ_F/δ_{CM}, using the maximum displacements of non-linear dynamic analysis (Fig. 3.4) in order to identify the influence of the torsional stiffness, the fundamental period and the eccentricity on the torsional response. Additionally, the results were compared with the

displacement amplification obtained from a linear dynamic analysis to evaluate the use of the elastic deformed shape to estimate the inelastic torsional amplifications.

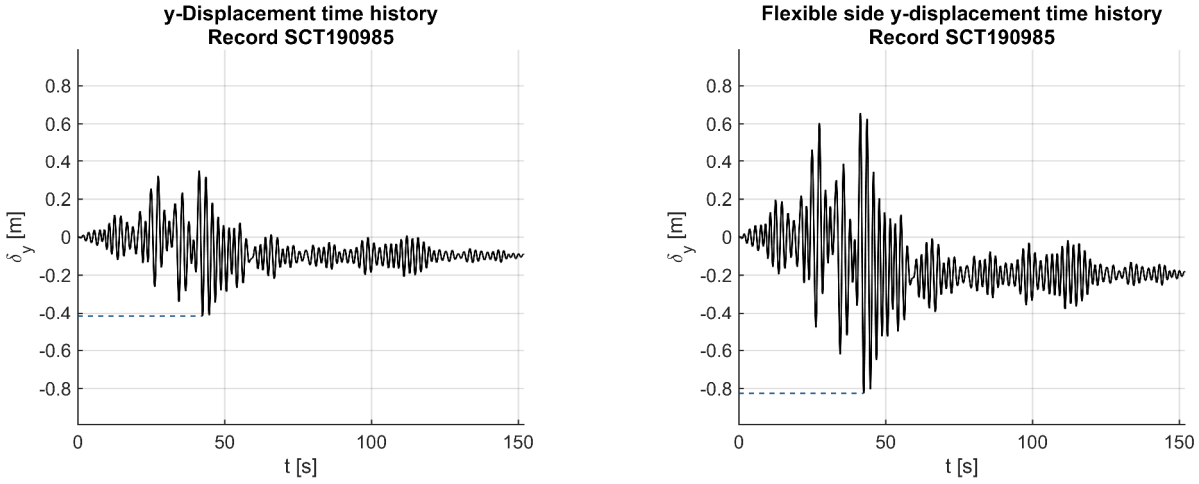

Fig. 3.4 Time history displacement in the y-direction of the center of mass (left) and the flexible side (right)

3.4.2. Ductility demand, μ.

As the ductility demand of an irregular structure is unclear, due to the uncertainties of the seismic response of structures with different types and levels of irregularity, the ductility demand developed at the center of mass of the 3DOF structure was calculated, considering the yield displacement obtained from the bilinear idealization of the capacity curve (Fig. 3.5). For the bilinearization of the capacity curve it is considered that the plastic mechanism is formed at the maximum displacement of the non-linear dynamic analysis, δ_u, therefore, the energy deformation is the area below the capacity curve from 0.0 to δ_u.

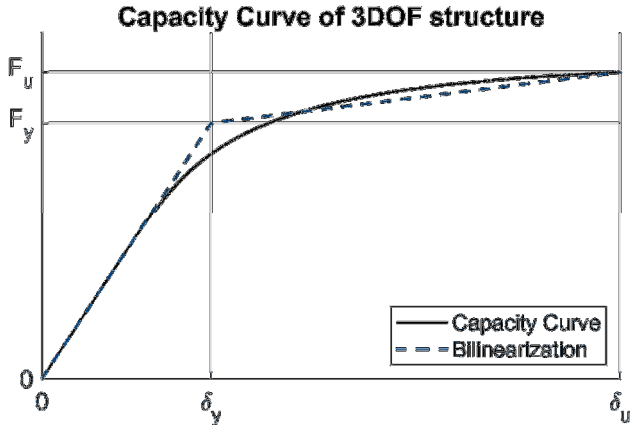

Fig. 3.5 Capacity curve of the 3DOF structure and bilinear idealization.

As the bilinear idealization of the capacity curve is considered to have a residual stiffness, a slight modification of the eq. 2.10 is used to obtain the yield displacement:

$$\delta_y = \frac{2E_m - \delta_u F_u}{K_e \delta_u - F_u} \tag{3.1}$$

3.4.3. Combination factor of orthogonal demands, *β*.

A combination factor, β, of orthogonal demands in the X- and Y-directions was derived as a fraction of the root mean pseudo-acceleration spectrum of both components (eq. 3.2). It was defined in such a way that the use of such spectrum at its natural scale as demand in the critical direction and the same spectrum scaled by β% in the horizontal orthogonal direction in conventional modal-spectral analysis provides approximately the same base shear demands as those obtained from non-linear dynamic analysis (eq. 3.3).

$$a(T) = \sqrt{a_x(T)^2 + a_y(T)^2} \tag{3.2}$$

$$\beta = \frac{V_{\max} - V_{cr}}{V_{ncr}} \tag{3.3}$$

where, V_{max} is the maximum base shear demand obtained from the non-linear dynamic analysis, V_{cr} and V_{ncr} are the base shear obtained from a modal spectral analysis, using the spectrum obtained from eq. 3.2, in the critical and the non-critical directions, respectively.

Additionally, the combination factor obtained from the non-linear dynamic analysis was compared with β = 0.3, which is the combination factor stablished on the Mexico's Building Code (*NTC-DS*, 2017a).

The results attained from the non-linear analyses and behavioral trends of the M-system and the X- systems regarding the aforementioned response parameters are shown and discussed in detail in the subsequent chapters.

Chapter 4. SEISMIC RESPONSE OF M-SYSTEM

4.1. Displacement amplification due to torsional effects, δ_F/δ_{CM}

4.1.1. Median response

Figs. 4.1 and 4.2 show the relation between Ω and the displacement amplification for structures, with B/L = 0.50 and 1.0, respectively, for various values of uncoupled period, T_y. It can be observed that, in general, the amplification is larger for structures with a smaller rotational stiffness, and it decreases as the rotational stiffness is larger, for all R_T and B/L values shown. This agrees with the rigid diaphragm hypothesis, since having a higher rotational stiffness the floor rotation decreases and, hence, the edges of the plan tend to have equal displacements. For rectangular-plan buildings, B/L=0.75, the decrease of δ_F/δ_{CM} with respect to Ω tends to be linear except for $T_y \geq 2.5$ s, where in fact there is an increase of amplification for systems with $Q' \geq 3$, which may be attributed to dynamic effects. For square-plan buildings B/L=1.0, the decrease of δ_F/δ_{CM} as a function of the period is smoother than for buildings with B/L=0.50 and is virtually independent of Ω, particularly for inelastic systems.

Furthermore, as expected in a dynamic system, there is dependency between the response parameter δ_F/δ_{CM} and the period T_y. In particular, the displacement amplification trends, regarding the level of inelasticity, vary significantly for different values of Q', especially for B/L=0.50. As can be observed in Fig. 4.1, for B/L=0.50, $T_y \leq 1.0$ s and $\Omega \leq 1.3$, δ_F/δ_{CM} is similar for elastic and moderately inelastic structures, *i.e.* $1.0 \leq Q' \leq 3.0$, and their values are higher than those corresponding to larger values of Q'. Conversely, for B/L=0.5 and T_y=1.0 s and $\Omega > 1.3$, δ_F/δ_{CM} for moderately inelastic systems tends to be larger than those of elastic systems and more ductile structures. For B/L=0.5 and the period range 1.5 s $\leq T_y \leq$ 2.0 s, δ_F/δ_{CM}, is about the same or slightly larger for systems with $1.0 \leq Q' \leq 4.0$, than for higher values of Q' for $\Omega \leq 1.3$, whereas δ_F/δ_{CM} tends to be smaller for elastic systems than that of inelastic systems for $\Omega > 1.3$. As T_y increases, the amplification of elastic systems tends to be larger than that of inelastic systems with respect to Ω. For B/L=0.5 and T_y=2.5 s, δ_F/δ_{CM} for elastic systems is larger than that of inelastic systems for $\Omega \leq 1.3$, however, for $\Omega > 1.3$ the amplification of inelastic systems tends to be slightly larger than that of elastic structures as Ω increases. However, for T_y=3.0 s, δ_F/δ_{CM} is larger for elastic systems than inelastic ones for all Ω values.

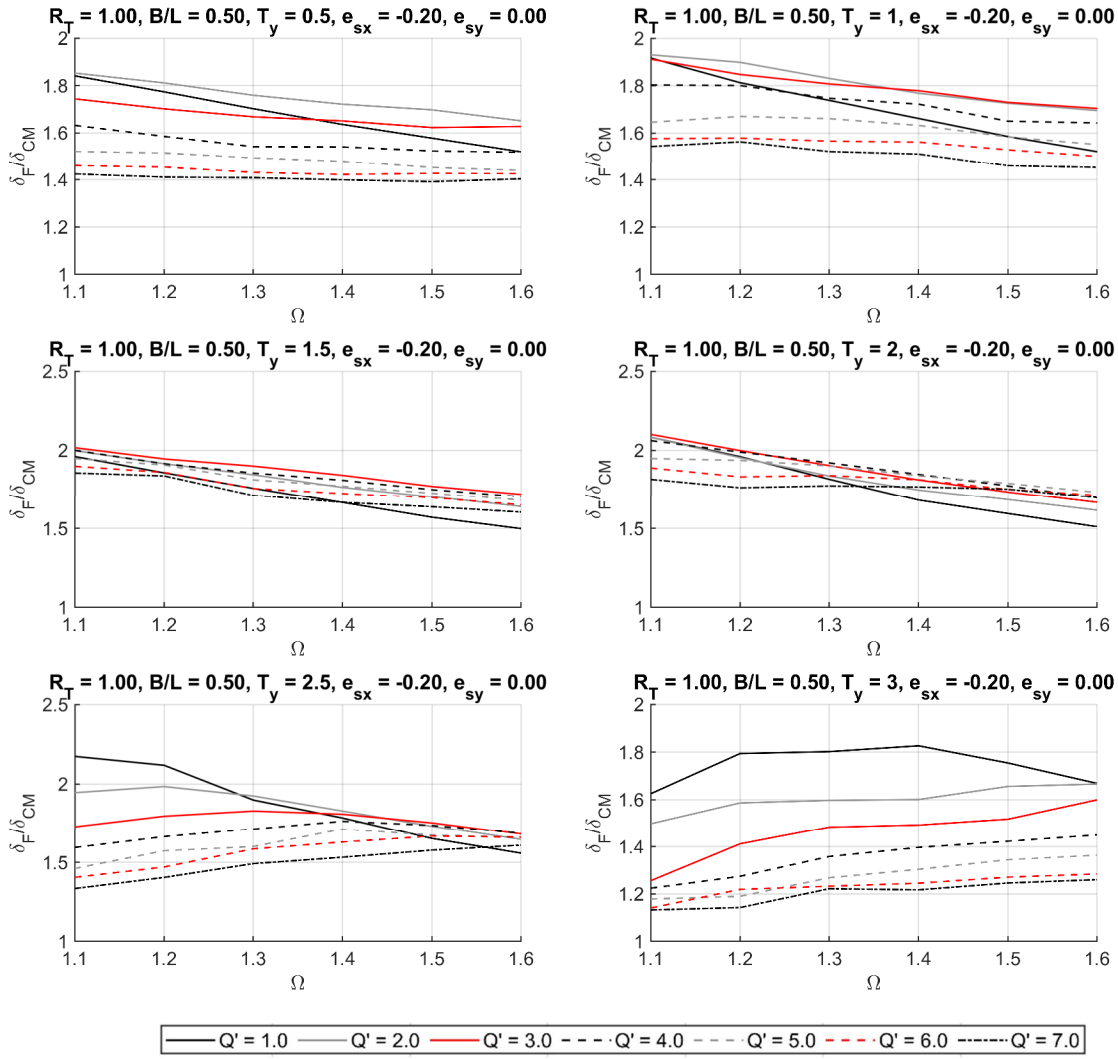

Fig. 4.1. Flexible side displacement amplification, δ_F/δ_{CM}, as a function of Ω*, for B/L = 0.50*

The displacement amplification trends for systems with *B/L*=0.5 (Fig. 4.2) with respect to period are similar than those for *B/L*=0.5, although with some notable differences. For $T_y \leq 1.0$ s and $\Omega \leq 1.5$, δ_F/δ_{CM} is similar for elastic and moderately inelastic structures, *i.e.* $1.0 \leq Q' \leq 3.0$, and their values are higher than those corresponding to larger values of *Q'*. For the period range $1.5 \text{ s} \leq T_y \leq 2.0$ s, δ_F/δ_{CM} of elastic systems is smaller than that of inelastic systems for all values of Ω. For T_y=2.5 s, δ_F/δ_{CM} is larger for elastic and moderately inelastic systems than for more ductile structures for $\Omega \leq 1.5$, while for $\Omega \geq 1.5$, δ_F/δ_{CM} tends to be smaller for elastic systems as Ω increases.

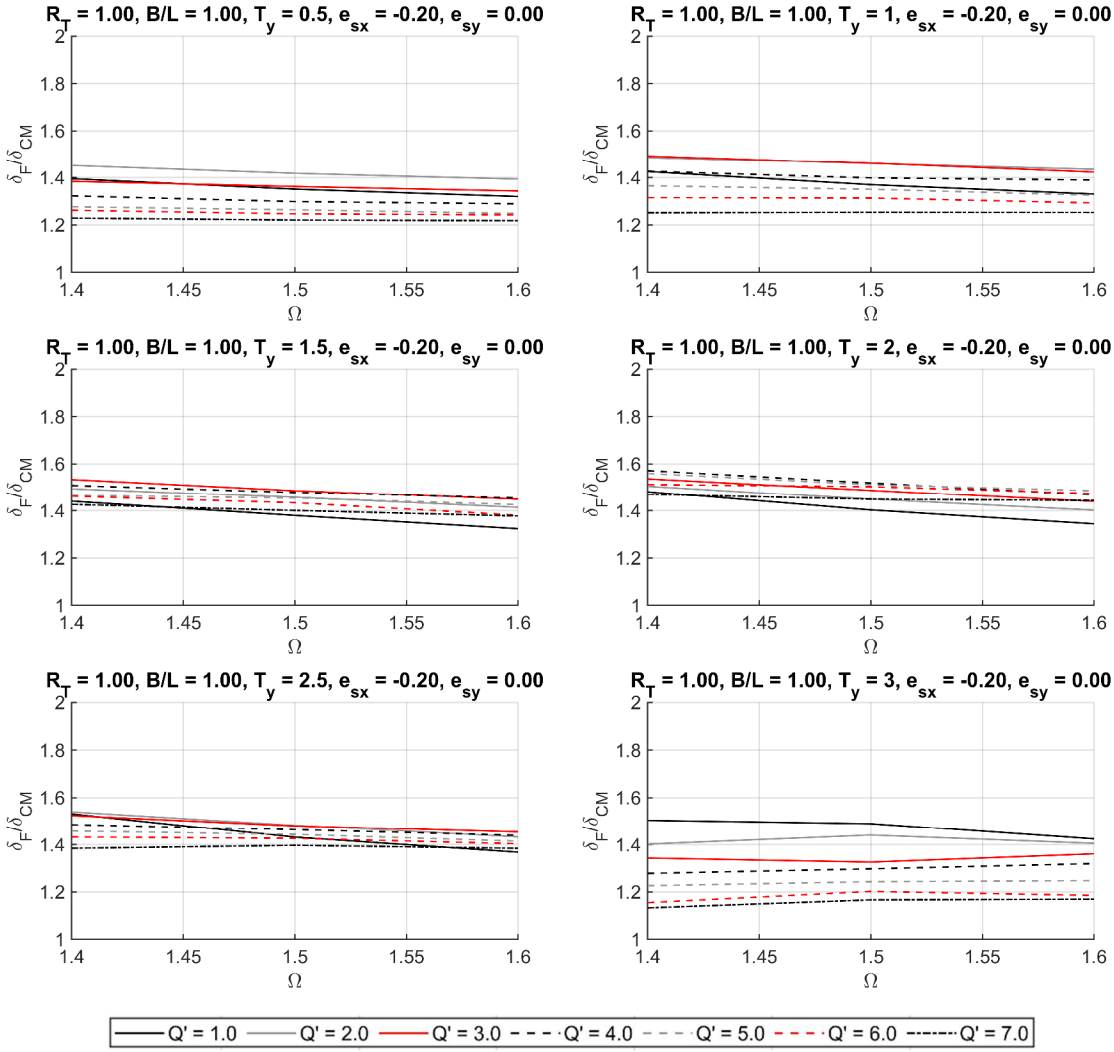

Fig. 4.2. Flexible side displacement amplification, δ_F/δ_{CM}, as a function of Ω, for B/L = 1.00

For the purpose of further identifying the displacement amplification trends with respect to period, Figs. 4.3 and 4.4 depict the relationships between δ_F/δ_{CM} and uncoupled translational period, T_y, for Ω=1.1, 1.3, 1.5 and 1.6. The first two values of Ω correspond to structures with moderate rotational stiffness and the others to systems with high rotational stiffness. It can be observed in such figures that elastic systems follow a different trend than inelastic systems. The former exhibit larger displacement amplification as the period increases and $\Omega \leq 1.3$, whereas such amplification tends to be constant with respect to the period for larger values of Ω. In contrast, δ_F/δ_{CM} of inelastic systems exhibit an increasing relation with the period for $T_y \leq 1.5$ s, reach a maximum value that remains approximately constant in the range 1.5 s $\leq T_y \leq$ 2.0 s, and decreases at larger periods. It should be noted that this plateau of the T_y *vs* δ_F/δ_{CM} plot coincides with the characteristic periods of the design spectrum.

For B/L=0.50 (Fig. 4.3), δ_F/δ_{CM} of elastic systems is larger as the period increases up to T_y=2.5 s and decreases after such period, for both Ω =1.1 and 1.3. However, for the former value, δ_F/δ_{CM} of elastic systems is larger than those of inelastic systems in the entire period range while for Ω =1.3, δ_F/δ_{CM} of elastic structures is smaller than for most inelastic systems in the period range 1.0 s $\leq T_y \leq$ 2.0 s and is larger than inelastic structures for $T_y \geq$ 2.5 s. For B/L=0.50 and $\Omega \geq$ 1.5, displacement amplification is larger for elastic structures than for moderately inelastic structures for $T_y \leq$ 1.0 s, while for δ_F/δ_{CM} of inelastic structures is larger than that of elastic structures in the period range 1.5 s $\leq T_y \leq$ 2.5 s. For B/L=0.50 and $T_y >$ 2.5 s, δ_F/δ_{CM} of elastic structures is larger than that of inelastic structures regardless of the period.

For B/L=1.0 (Fig. 4.4) the trends observed are similar to those of B/L=0.5, however, the differences between amplification values of all systems are narrower and, as previously identified in Fig. 4.2, δ_F/δ_{CM} is practically invariant with respect to Ω.

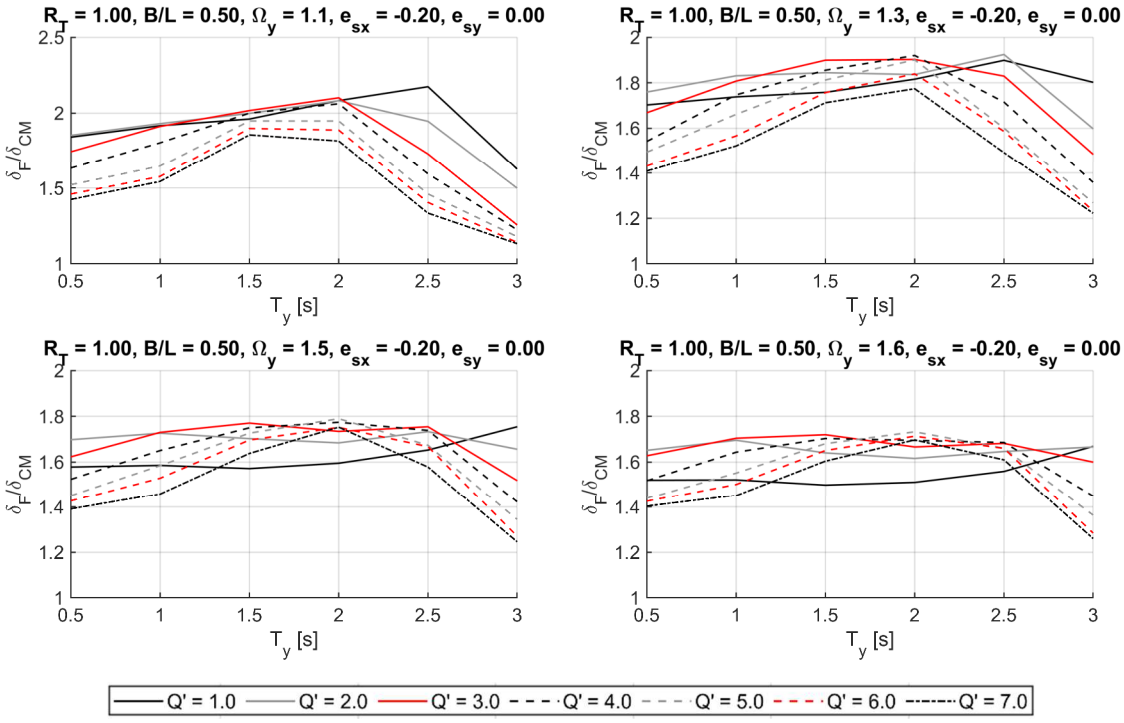

Fig. 4.3. Flexible side displacement amplification, δ_F/δ_{CM}, as a function of T_y, for B/L = 0.50

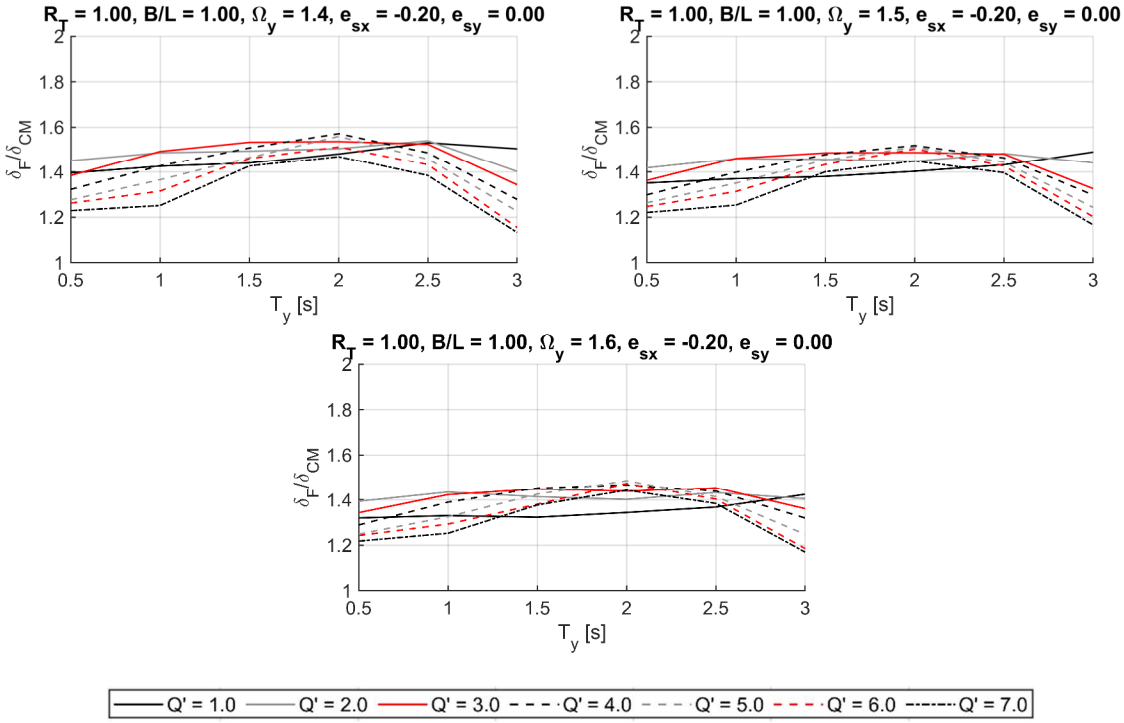

Fig. 4.4. Flexible side displacement amplification, δ_F/δ_{CM}, as a function of T_y, for B/L = 1.00

The influence of the stiffness eccentricity on the displacement amplification is shown in Figs. 4.5 to 4.8 for moderately torsionally rigid (Ω = 1.2) and high torsionally rigid structures (Ω = 1.6), respectively. It can be observed in such figures that as the eccentricity value is larger, the torsional moment and, consequently, the floor rotation increase, hence, the displacement on the flexible side is larger in all cases. Furthermore, it can be identified that the relation tends to be linear or bilinear depending on the combination of *B/L*, Ω and *Q'*.

For B/L= 0.50 and Ω=1.2 (Fig 4.5), δ_F/δ_{CM} of systems with $Q' \leq 2$ follows a linear increasing relation with respect to eccentricity up to e_{sx}=0.2 and is approximately constant for larger eccentricity values, except for period T_y =3 s, where the relationship tends to be linear in all the eccentricity range. On the other hand, the relationship between e_{sx} and δ_F/δ_{CM} of inelastic systems is different for distinct period values. For structures with T_y < 1 s and $Q' \leq 3$, δ_F/δ_{CM} follows an increasing linear variation with respect to eccentricity, however, the slope reduces for $e_{sx} \geq$ 0.3. Moreover, for such periods, δ_F/δ_{CM} increases linearly for systems with Q' > 3, although for T_y=1.0 s and Q'=7 the slope decreases for $e_{sx} \geq$ 0.2. Furthermore, it can be observed that δ_F/δ_{CM} is larger for systems with $Q' \leq 3$ than that corresponding to other values of Q'. It should be also noted that δ_F/δ_{CM} of elastic systems may be smaller than those corresponding to Q' values of 2 or 3. For systems with 1.5 s < T_y < 2 s, the variation of δ_F/δ_{CM} with respect to e_{sx} is approximately bilinear with a slope reduction in e_{sx}=0.2, although for $Q' \leq 3$ the second branch is horizontal, hence, the displacement amplification for elastic and moderately inelastic is virtually independent of e_{sx}. It is also observed that displacement amplification of elastic and moderately inelastic structures is

larger than that of highly inelastic systems for $e_{sx} \leq 0.2$; for $e_{sx} > 0.20$ the amplification is approximately the same for elastic and all inelastic systems in most cases. On the other hand, in the period range 1.5 s $< T_y <$ 2 s, the relation between e_{sx} and δ_F/δ_{CM} shifts from slightly bilinear to linear as Q' increases and displacement amplification decreases as Q' is larger.

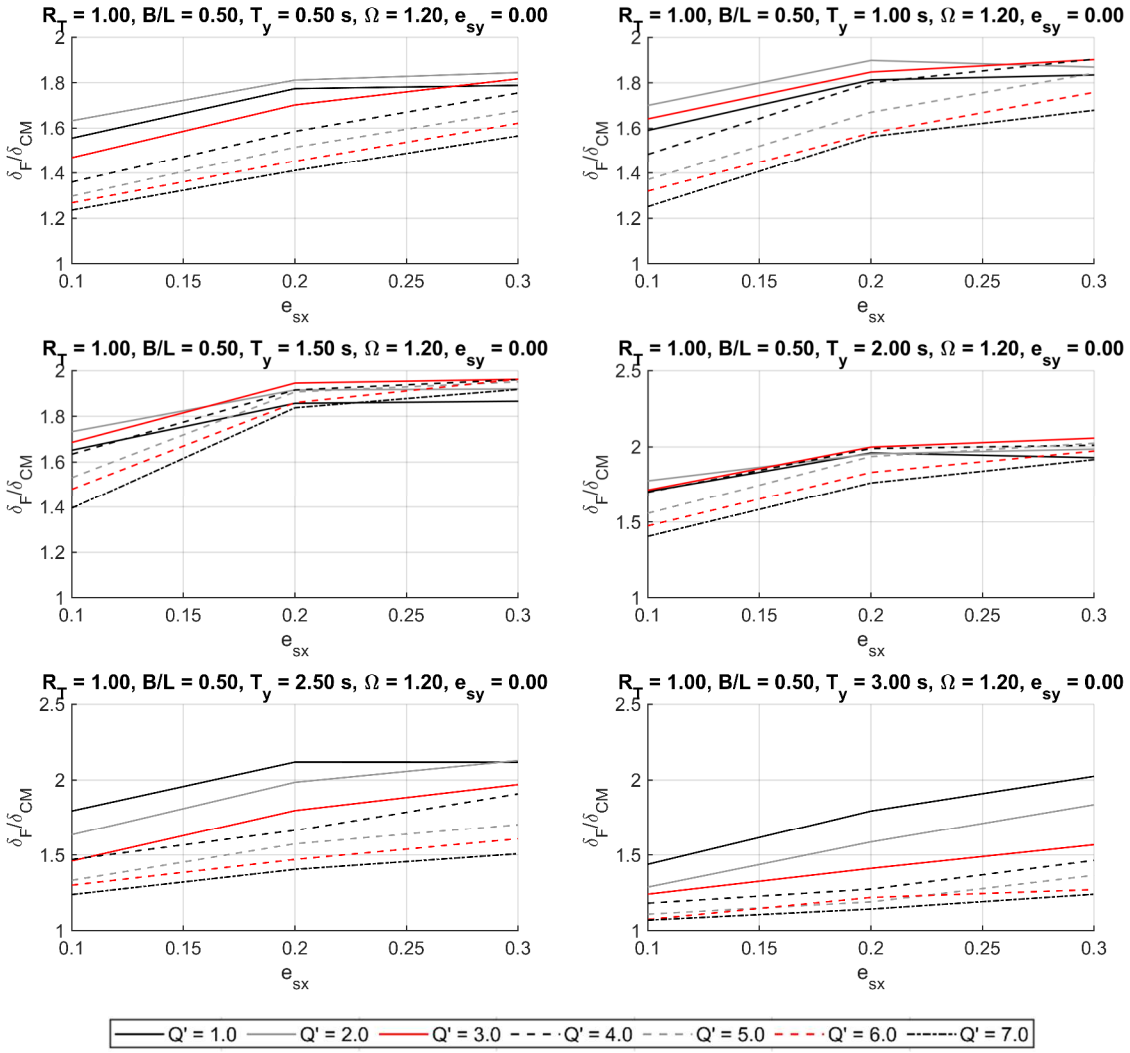

Fig. 4.5. Flexible side displacement amplification, δ_F/δ_{CM}, as a function of e_{sx}, for B/L = 0.50 and Ω = 1.2

A different trend of behavior can be seen for B/L= 0.50 and **Ω**=1.6 (Fig. 4.6), *i.e.*, rectangular-plan systems with extremely high torsional stiffness, δ_F/δ_{CM} shows a clear linear relation with respect to e_{sx} in the entire range considered. For $T_y <$ 1.0 s, systems with $2 \leq Q' \leq 4$ exhibit the larger displacement amplifications while structures with $Q' > 4$ present the lowest. A similar trend is identified in the period range 1.5 s $< T_y <$ 2.5 s; δ_F/δ_{CM} is larger for systems with $2 \leq Q' \leq 4$, however, displacement amplification of elastic systems is lower than that of inelastic ones for all

eccentricity values. For T_y = 3 s, the trend is significantly different than the former, as δ_F/δ_{CM} is larger for $1 \leq Q' \leq 3$ than that of systems with higher values of Q'.

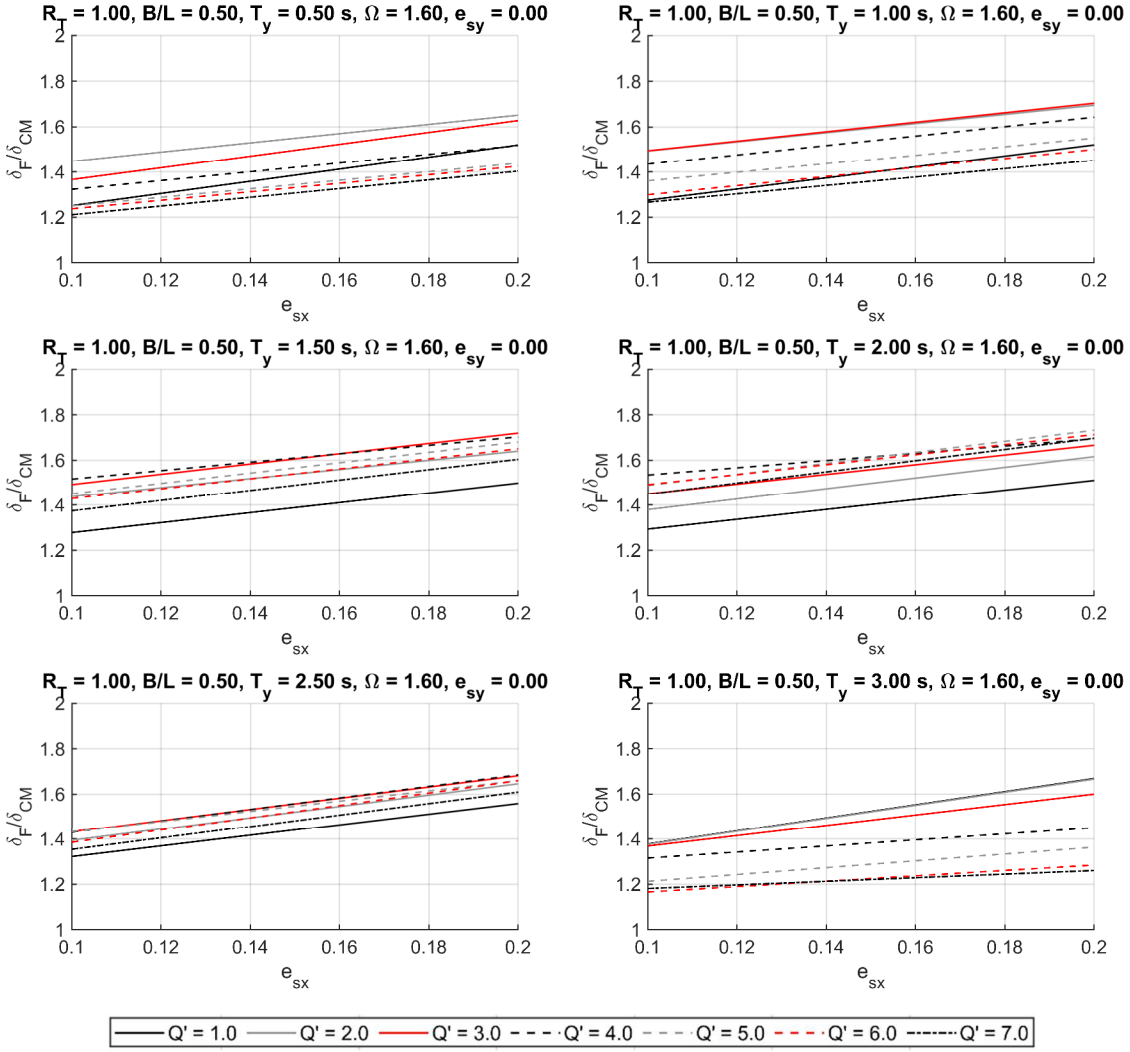

Fig. 4.6 Flexible side displacement amplification, δ_F/δ_{CM}, as a function of e_{sx}, for B/L = 0.50 and Ω = 1.6

For *B/L*= 1.0 and **Ω**=1.4 (Fig. 4.7), *i.e.*, square-plan structures with high torsional stiffness, δ_F/δ_{CM} of systems with $Q' \leq 2$ follow very similar trends to that of *B/L*= 0.50 and **Ω**=1.2 (Fig. 4.5), although the amplification level is lower for the former, which may be attributed to the fact that **Ω** is larger. In addition, the difference of displacement amplification between all systems appears to be narrower for *B/L*=1.0. It should be noted that it was not possible to compare the displacement amplification between systems with *B/L*=1.0 and 0.50 as the minimum possible value of **Ω** for a square building is 1.4.

For *B/L*=1.0 and **Ω**=1.6 (Fig. 4.8), *i.e.*, square-plan structures with extremely high torsional stiffness, the trends are also very similar to those for systems with *B/L*=0.50 and **Ω**=1.6 (Fig. 4.6),

however, δ_F/δ_{CM} is larger for the squared-building, even though both types share the same torsional stiffness values.

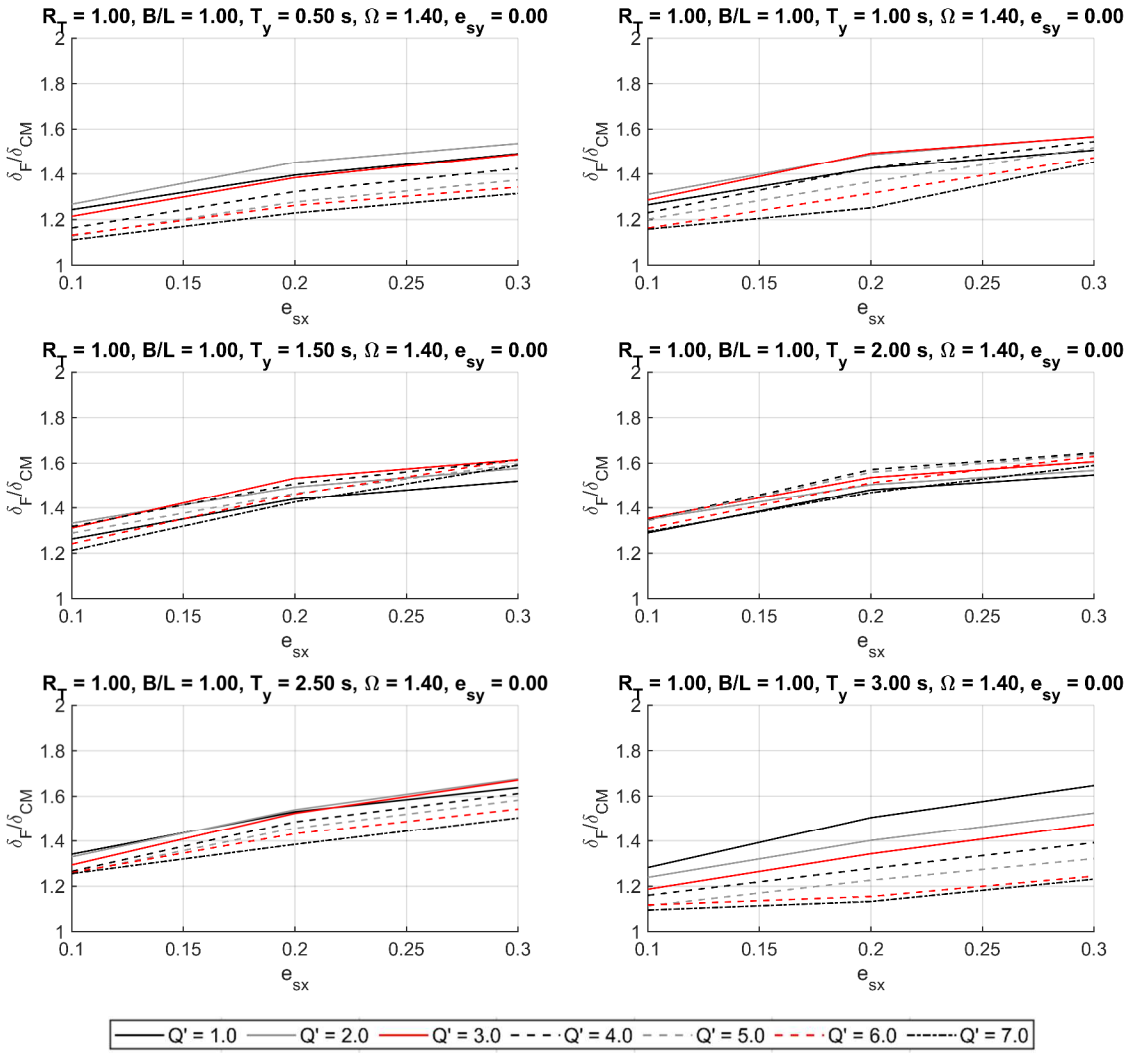

Fig. 4.7. Flexible side displacement amplification, δ_F/δ_{CM}, as a function of e_{sx}, for B/L = 1.00 Ω = 1.4

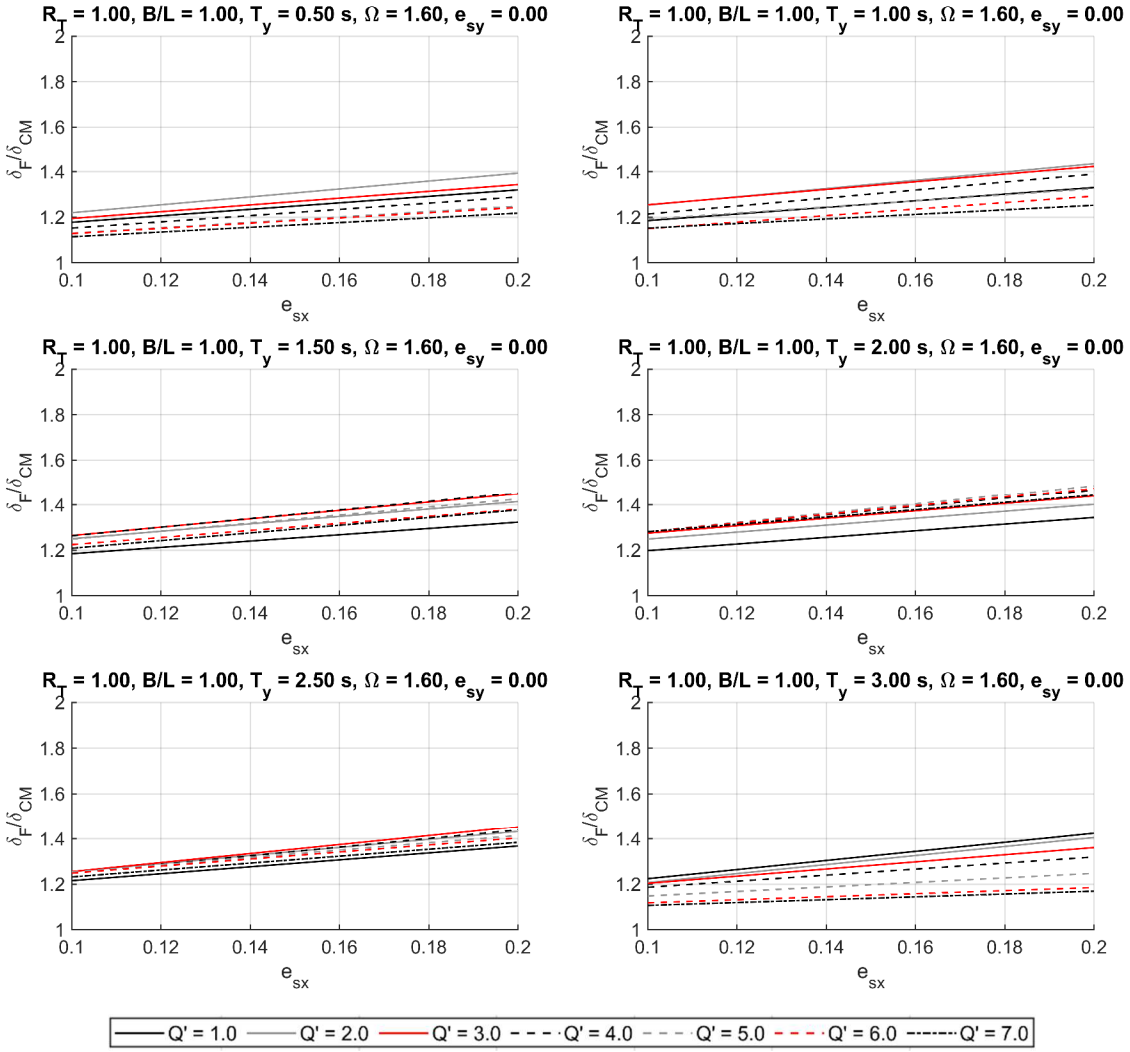

Fig. 4.8. Flexible side displacement amplification, δ_F/δ_{CM}, as a function of e_{sx}, for B/L = 1.00 Ω = 1.6

4.1.2. Dispersion of results

Figs. 4.9 and 4.10 show the normalized median absolute deviation of δ_F/δ_{CM} with respect to the median, denoted as $CV_{med} - \delta_F/\delta_{CM}$, for structures with B/L = 0.5 and 1.0 respectively, where it can be identified that the dispersion is significantly low. For B/L=0.5 (Fig. 4.9), CV_{med} - δ_F/δ_{CM} is smaller than 0.2 for all values of T_y. Particularly, for $T_y < 2.5$ s. the value of $CV_{med} - \delta_F/\delta_{CM}$ appears to be approximately constant and for $T_y \geq 2.5$ s. $CV_{med} - \delta_F/\delta_{CM}$ presents an ascending trend with respect to T_y; the largest $CV_{med} - \delta_F/\delta_{CM}$ values occur at T_y = 3.0 s regardless of **Ω**. Similar trend can also be observed for structures with B/L = 1.0 (Fig. 4.10).

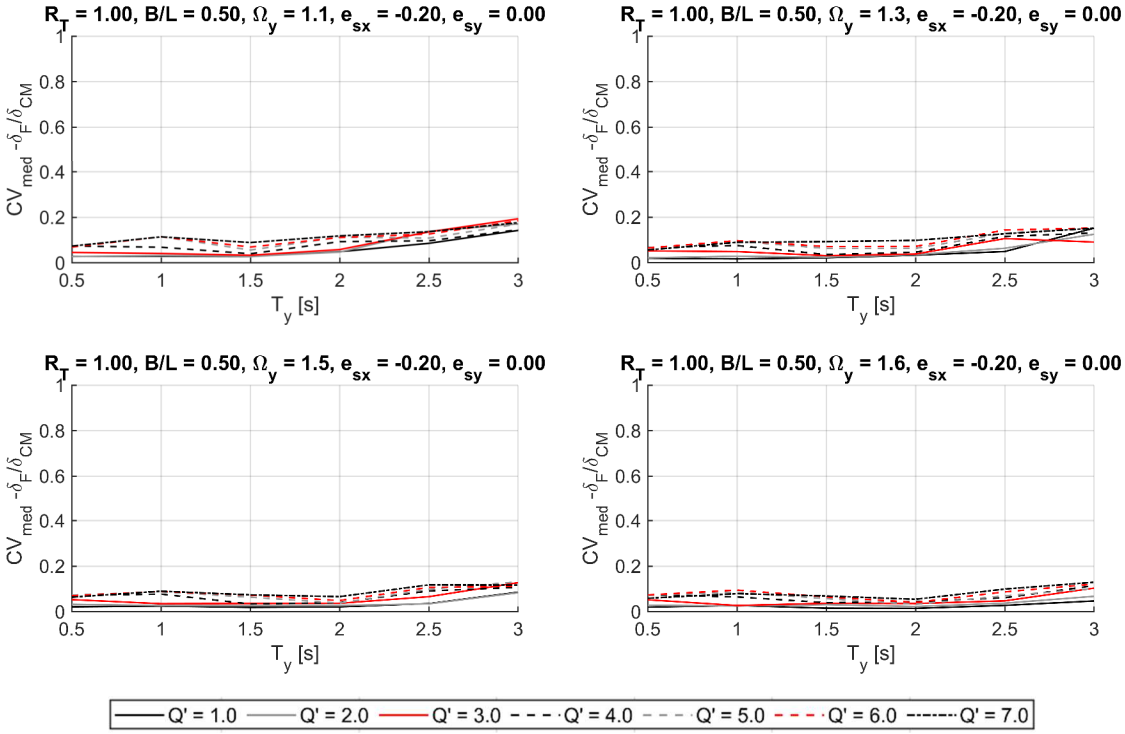

Fig. 4.9 Normalized median absolute deviation of δ_f/δ_{CM}, as a function of T_y, for B/L = 0.50

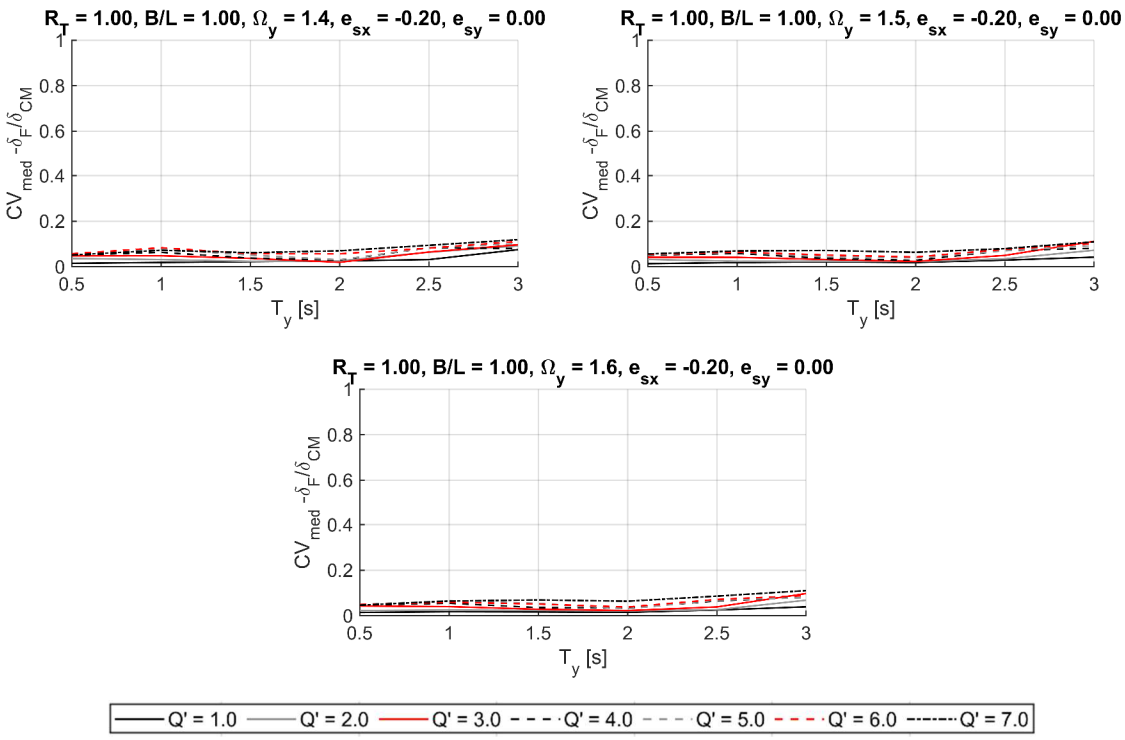

Fig. 4.10 Normalized median absolute deviation of δ_f/δ_{CM}, as a function of T_y, for B/L = 1.00

4.1.3. Comparison between elastic and inelastic displacement amplification

As mentioned earlier, the extended N2 method (Fajfar *et al.*, 2005) considers the torsional amplifications due to the dynamic load with a correction factor defined by the δ_F/δ_{CM} obtained from elastic modal analysis (eq. 2.15). However, the displacement amplification of the flexible side of asymmetric-plan buildings obtained from a non-linear dynamic analysis, with different levels of inelasticity, is not always smaller than the amplification of elastic structures with the same torsional parameters, hence, the use of the elastic deformed shape to estimate the maximum inelastic response of the flexible side may not provide conservative results in many cases.

The comparison of the values of δ_F/δ_{CM} obtained with a Q' = 1.0 and the one obtained with Q' ≠ 1.0, in terms of the relative error of the inelastic δ_F/δ_{CM} to the elastic δ_F/δ_{CM}, is shown in Fig. 4.11. According to eq. 4.1 a positive relative error indicates that the use of the elastic displacement amplification is conservative, conversely, a negative relative error indicates that the use of the elastic displacement amplification is non-conservative. As can be observed in Fig. 4.11, only 40% of the structures present a conservative result with respect to the elastic deformed shape, however, the M-System includes both moderate and high torsionally stiff structures.

$$\%RE = \frac{\left(\delta_F / \delta_{CM}\right)_{elastic} - \left(\delta_F / \delta_{CM}\right)_{inelastic}}{\left(\delta_F / \delta_{CM}\right)_{elastic}} \qquad 4.1$$

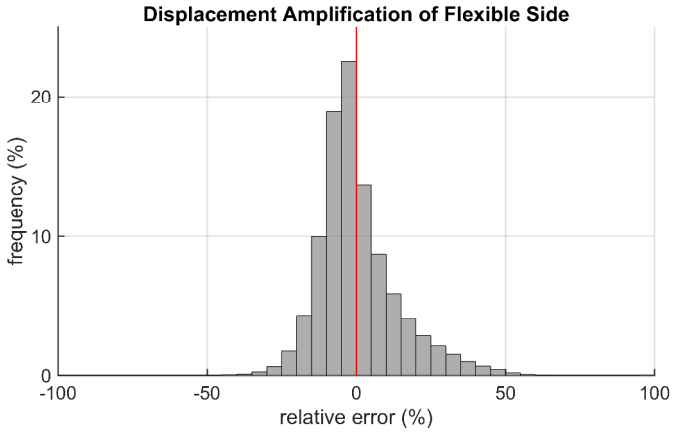

Fig. 4.11 Histogram of relative errors between elastic and inelastic δ_F/δ_{CM}

Fig. 4.12 shows the relative error of the inelastic δ_F/δ_{CM} with respect to the elastic δ_F/δ_{CM} for moderately and highly rotational stiff structures, *i.e.* with $\Omega < 1.4$ and $\Omega \geq 1.4$, respectively. For the case of moderately rotational stiff structures, 63% of the cases present a conservative result with respect to the inelastic deformed shape, conversely, for the case of highly rotational stiff structures only a 35% percent of the cases present a conservative result. This agrees with the conclusions made by De Stefano and Pintucchi (2010), however, this does not only depends on

the rotational stiffness, as the displacement amplification is also greatly affected by the period of the structure and the stiffness eccentricity.

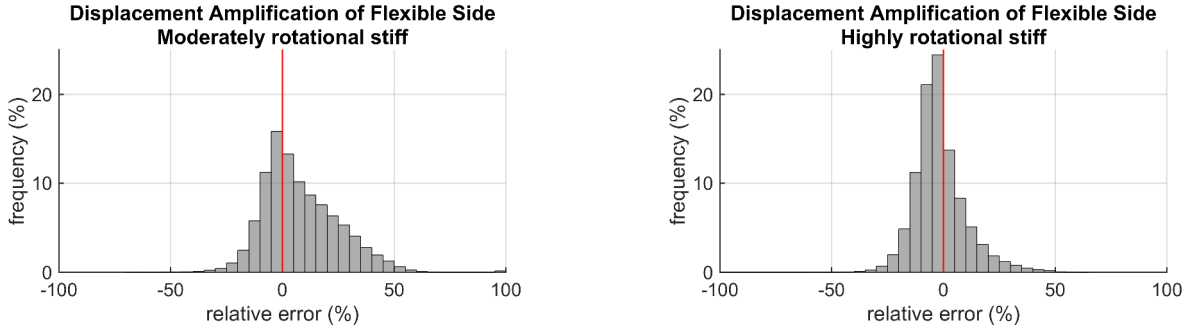

Fig. 4.12 Histogram of relative errors of inelastic to elastic δ_F/δ_{CM} for moderate and high rotationally stiff structures

4.2. Ductility demand

4.2.1. Median response

The ductility demand, μ, of the case studies was calculated as the ratio of the maximum displacement of the center of mass, obtained from the non-linear dynamic analyses, to the yield displacement at the same location defined from a bilinearized capacity curve attained from non-linear static analysis. Fig. 4.13 depict the relationship between μ and T_n for elastic and inelastic systems with moderately high and extremely high rotational stiffness, B/L=0.5 and B/L=1.0 and e_{sx}=0.20. These plots are shown in terms of the actual fundamental period of the system, T_n, instead of the uncoupled period, T_y, as shown for the other response parameters, for the purpose of comparing in a consistent manner the ductility demands of the 3DOF systems to those of SDOF systems.

As it can be identified in such, the ductility demand at the center of mass is a function of T_n and is virtually independent of B/L and Ω. Furthermore, it can be observed that ductility demand is significantly large for structures with short periods and is lower as the period decreases up to T_n = 2.0 s, from which it remains practically constant. The difference between ductility demands associated to different Q' values is significant for $T_n \leq$ 1.0 s and reduces as the period is larger; for $T_n \geq$ 2.0 s the difference in ductility demands amongst all elastic and inelastic systems is significantly smaller than for short periods. In fact, this trend is the same as that of SDOF systems in the entire period range considered. Fig. 4.14 shows the plot of T_n *vs* μ of SDOF systems with the same Q' values, where it can be identified that both 3DOF systems and SDOF systems follow identical trends.

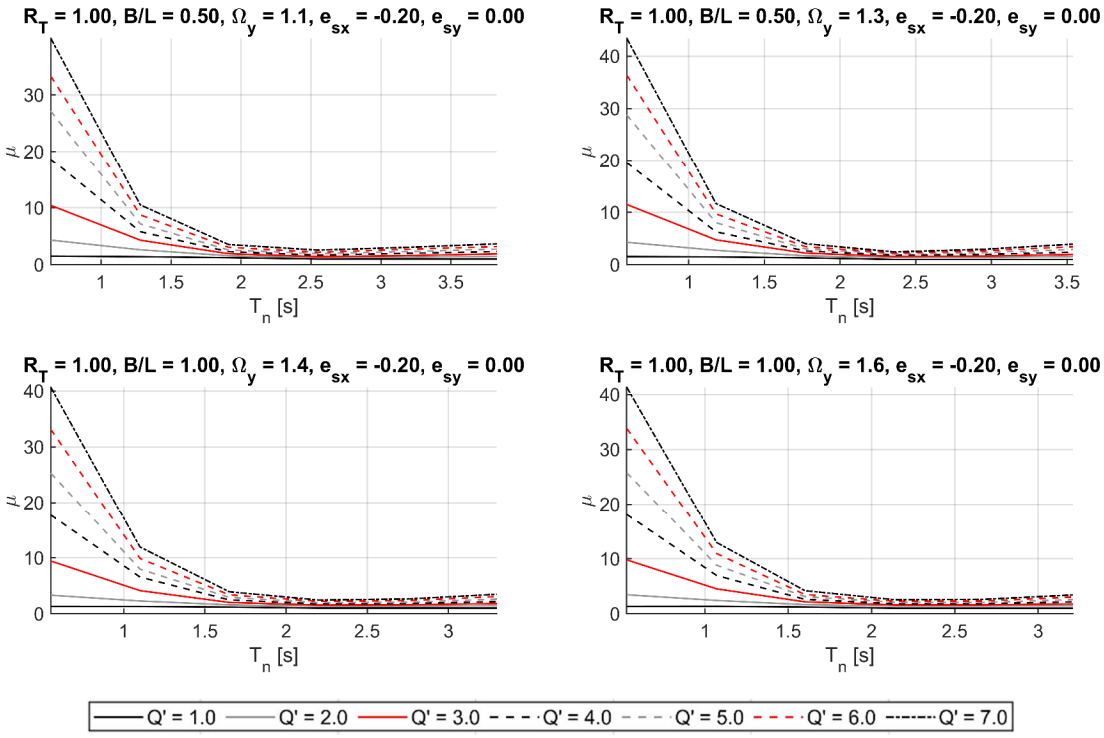

Fig. 4.13. Ductility demand, μ, as a function of T_n

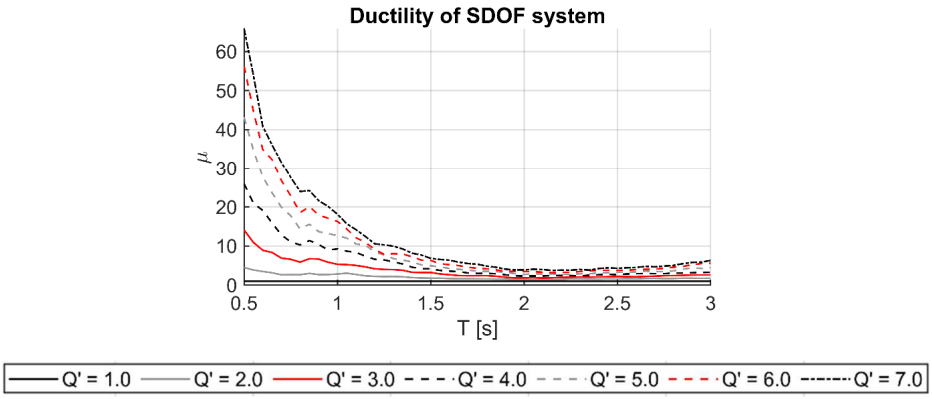

Fig. 4.14. Ductility demand, μ, as a function of T_n for SDOF systems

Nonetheless, although the trend of both 3DOF and SDOF systems are the same, their ductility demands differ in value. Fig. 4.15 depicts the ratio of ductility demand of 3DOF systems to that of SDOF systems, μ_{3DOF}/μ_{SDOF}, for the same parameters of Fig. 4.13, where it can be observed that, in general, such ratio is larger as the period is lower. Elastic structures exhibit the largest μ_{3DOF}/μ_{SDOF}, about 1.5 at T_n = 0.5 s for both the moderately and extremely torsionally stiff cases; the ratio decreases down to 1.0 at T_n = 2.0 s and remains constant for larger periods. In contrast, μ_{3DOF}/μ_{SDOF} of inelastic systems decrease with period in the entire range. The maximum and minimum values of μ_{3DOF}/μ_{SDOF} of inelastic structures at 0.5 s and 3 s, respectively, and the values of such ratio are higher as ductility is lower. For inelastic systems with *B/L*=0.50 and Ω=1.1, the

maximum ductility value, corresponding to Q' of 2.0 and 3.0, is approximately 1.3 and the lowest is 0.5 for $Q' \geq 5$; for all the other combinations of B/L and Ω, μ_{3DOF}/μ_{SDOF} varies between 1.0 and 0.5.

The differences in value of the ratio μ_{3DOF}/μ_{SDOF} can be attributed to the fact that SDOF systems are subjected to unidirectional loading whereas asymmetric 3DOF systems are subjected to bidirectional loading which induces additional lateral force demands that are not present in SDOF systems. Furthermore, the elements of 3DOF systems exhibit biaxial flexural interaction that also has an influence in their inelastic seismic response. These results suggest that the definition of ductility demands of asymmetric buildings comprised of moment-resisting frames (MRF) from SDOF systems may provide conservative results in most cases, except for the case of rectangular structures with B/L=0.5 and $T_n \leq 1.0$ s. Conversely, for inelastic structures, either square or rectangular in plan, with $T_n \geq 2.0$ s the results may be significantly conservative.

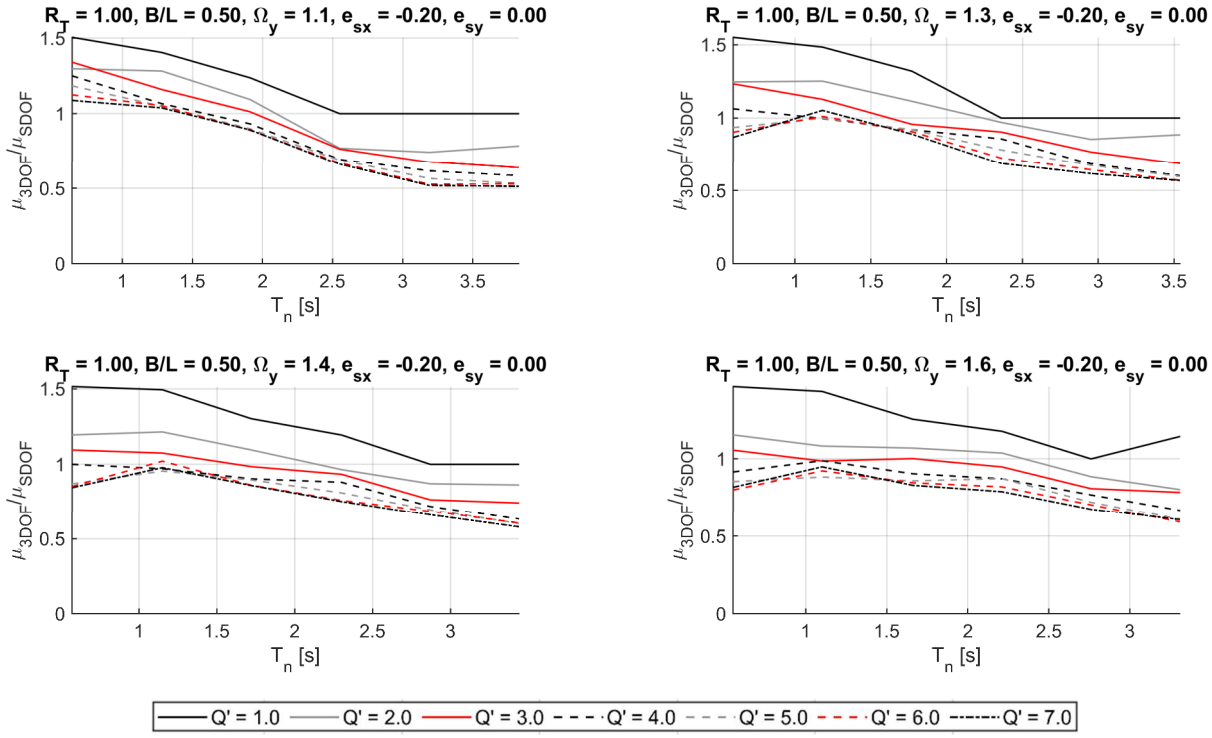

Fig. 4.15. Ductility demand ratio, μ, as a function of T_n for an SDOF system

Figs. 4.16 and 4.17 present the plots of μ *vs* e_{sx} for systems with different T_y values and B/L=0.5 and 1.0, respectively, for several values of Q'. As it can be observed in such figures, there is a certain degree of dependency between μ and e_{sx}, particularly for systems with high Q' values, which can also be attributed to the fact that 3DOF system is subjected to bidirectional demands while SDOF systems only to unidirectional demands; for distinct levels of eccentricity the demands of the structure differ. For B/L=0.5 (Fig. 4.16), μ for structures with $1.0 \leq T_y \leq 1.5$ s

follows an increasing trend for values of $Q' \leq 3.0$ and a decreasing trend for values of $Q' > 3.0$. For structures with $T_y > 2.0$ s. μ is larger as the eccentricity increases, with the exception of structures with $Q' \leq 3.0$, where the ductility demand remains approximately constant with respect to eccentricity. These same trends can be observed for B/L=1.0 (Fig. 4.17), however, for such structures the influence of e_{sx} on μ is less significant; μ can be considered constant for most values of Q' and T_y.

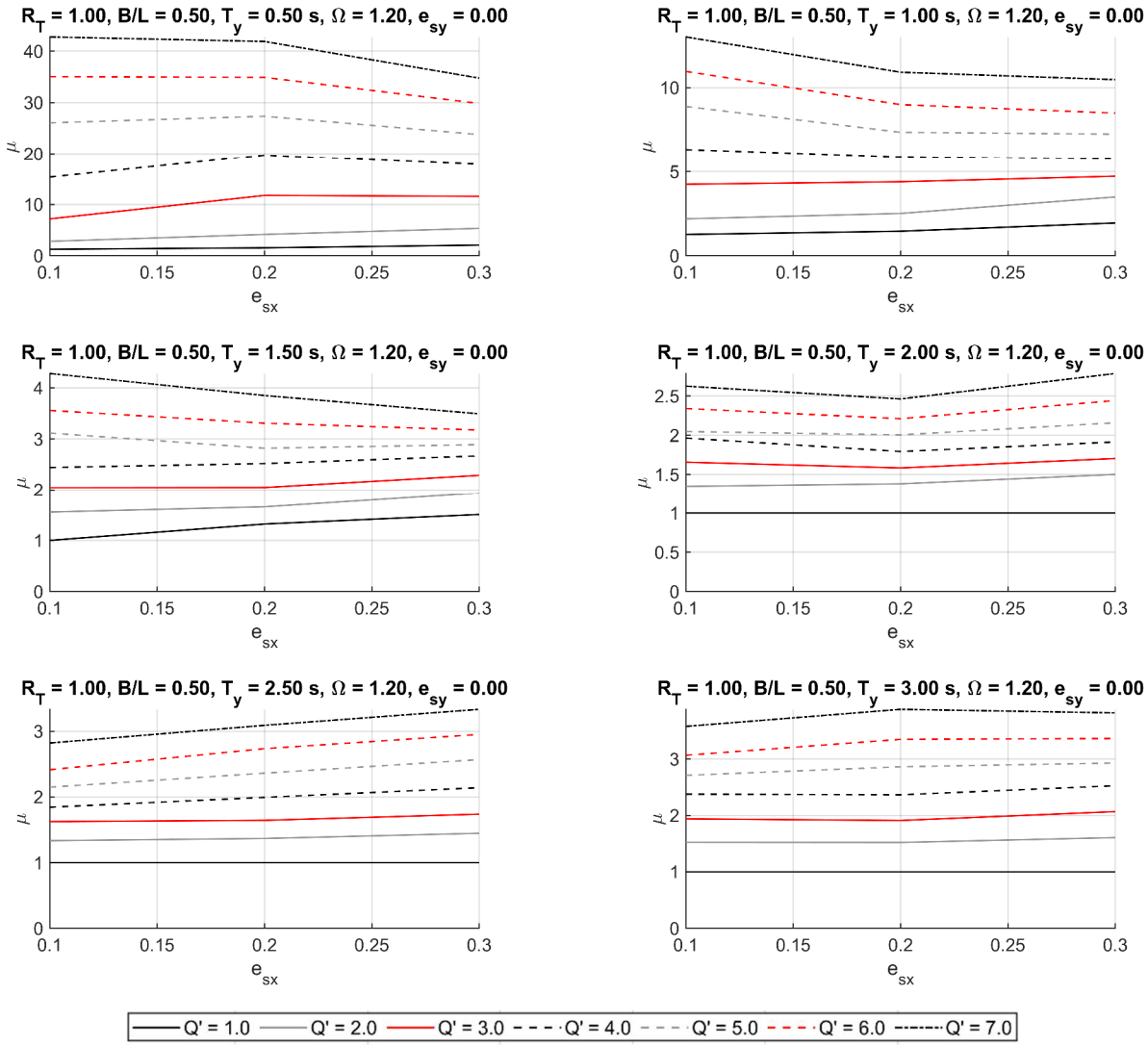

Fig. 4.16. Ductility demand, μ, as a function of e_{sx}, for B/L = 0.50 and Ω = 1.2

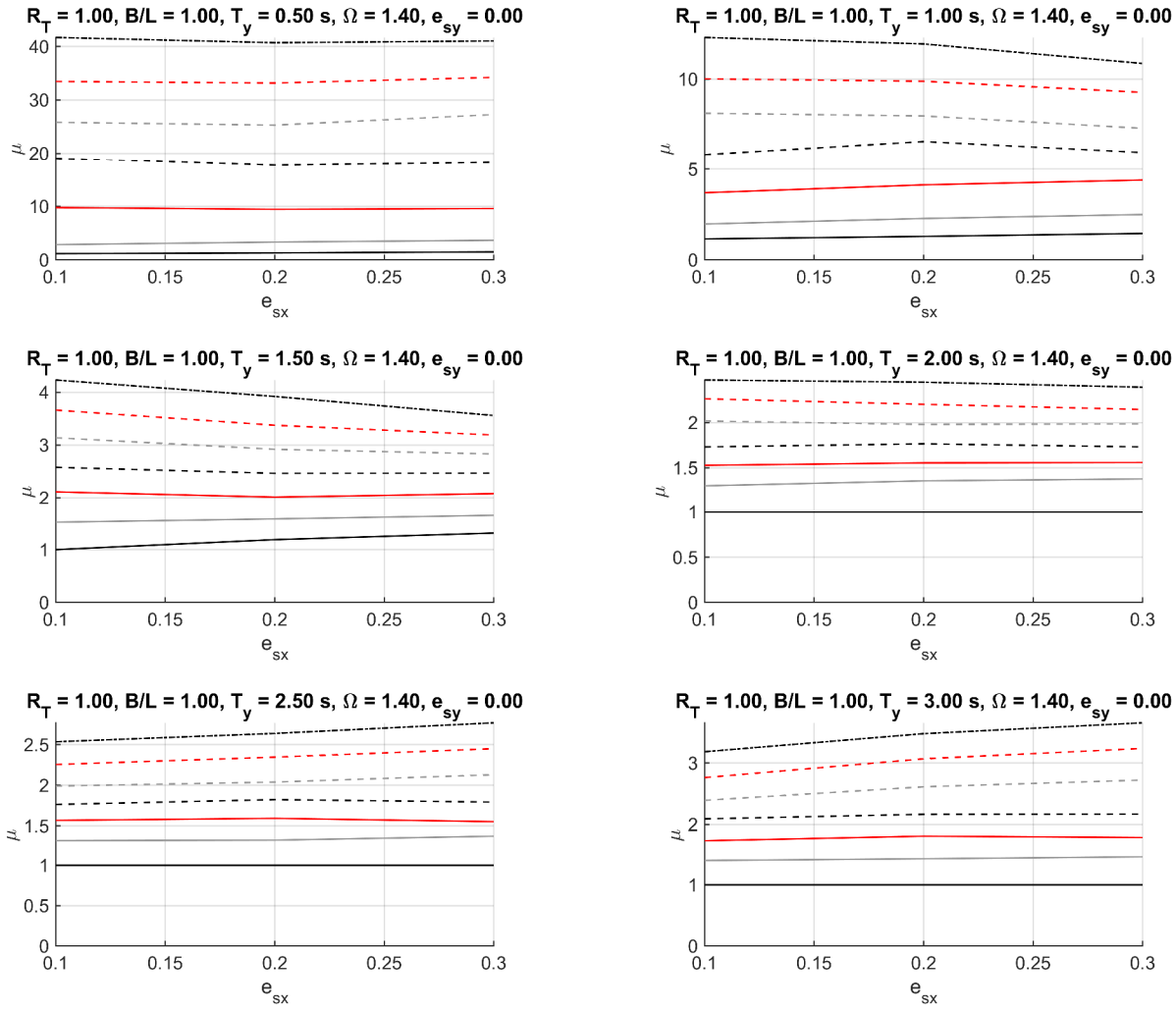

Fig. 4.17. Ductility demand, μ, as a function of e_{sx}, for B/L = 1.00 and Ω = 1.4

4.2.2. Dispersion of results

Figs. 4.18 and 4.19 show the normalized median absolute deviation of μ, denoted as $CV_{med} - \mu$, of structures with B/L = 0.50 and 1.0, respectively. As can be seen in Fig. 4.18 the value of CV_{med} - μ present a decreasing trend with respect to T_y, where the data present a larger variability for stiffer structures, *i.e.* $T_y \leq 1.0$ s. With respect to the inelastic behavior, the data presents the largest variability for $Q' = 2.0$ and $T_y \leq 1.0$ s and decreases for larger values of Q'; conversely for $T_y > 1.0$ s. the variability is smaller for $Q' = 2.0$ and increases as Q' is larger. A similar trend is found for structures with B/L = 1.0 (Fig. 4.19), however, the variability of the data increases slightly for T_y = 0.5 s, compared to that of structures with B/L = 0.50.

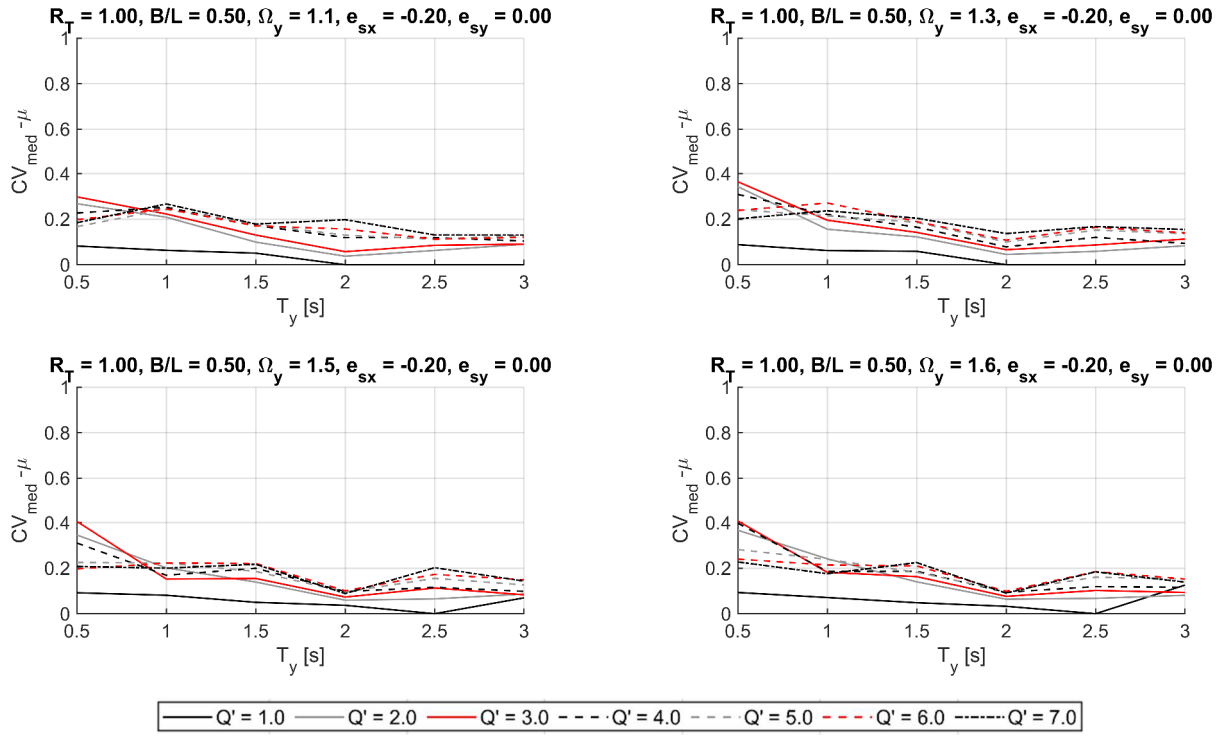

Fig. 4.18 Normalized median absolute deviation of μ, as a function of T_y, for B/L = 0.50

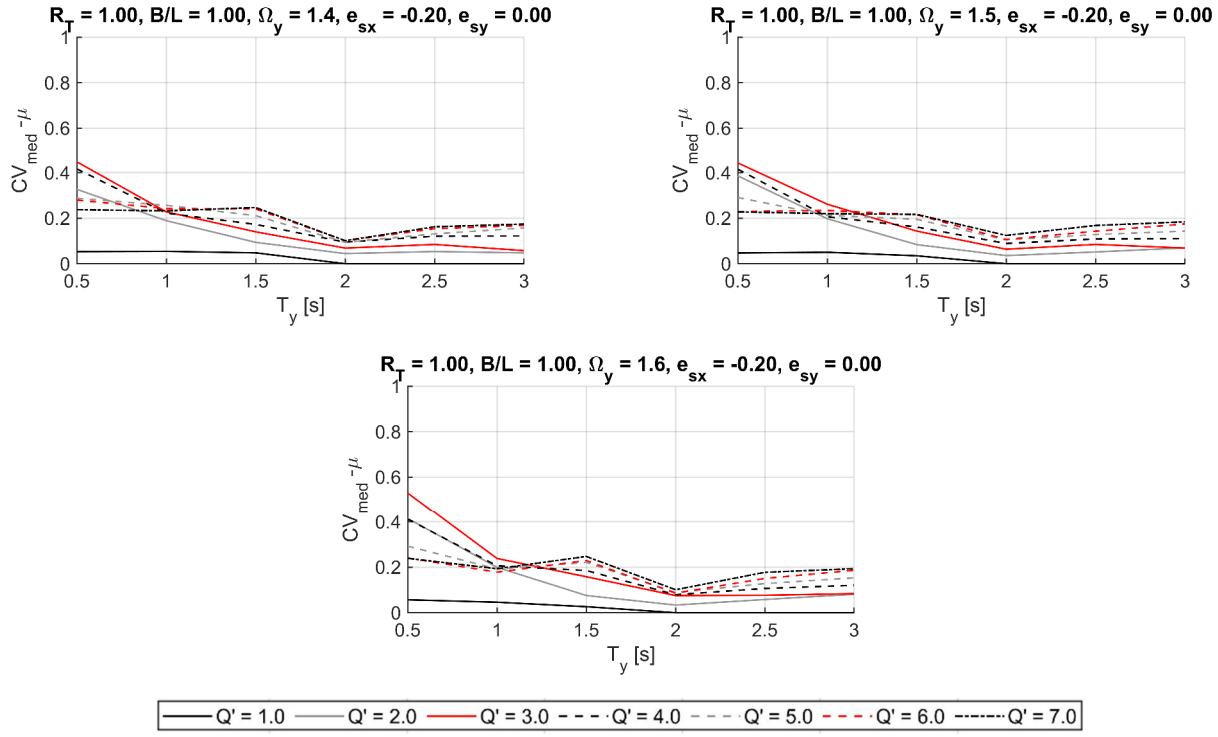

Fig. 4.19 Normalized median absolute deviation of μ, as a function of T_y, for B/L = 1.00

4.3. Combination factor of orthogonal demands

4.3.1. Median response

Figs. 4.20 and 4.21 show the plots of β *vs* Ω or e_{sx}=0.20 and several period values of systems with *B/L*=0.50 and 1.0, respectively. For *B/L*=0.5 (Fig. 4.20), elastic structures show the maximum β values among the whole set and exhibit different trends for different periods. For $T_y \leq 1.5$ s, β is approximately 0.17 in the entire range of Ω. In the period range 2.0 s $\leq T_y \leq$ 2.5 s, β values are maximum for low Ω values, around 0.5 and 0.6, and decrease as Ω is larger; for T_y = 2.0 s and 2.5 s, respectively, the minimum β values are 0.18 and 0.30. On the other hand, β is virtually constant for inelastic systems except for T_y= 1.5 s and $Q' \geq 3$ and T_y= 2.0 s and Q' = 2. Furthermore, β for inelastic systems is larger as Q' increases and the differences between their values reduces as period is larger; for T_y = 3.0 s, β is approximately 0.20 for all inelastic systems.

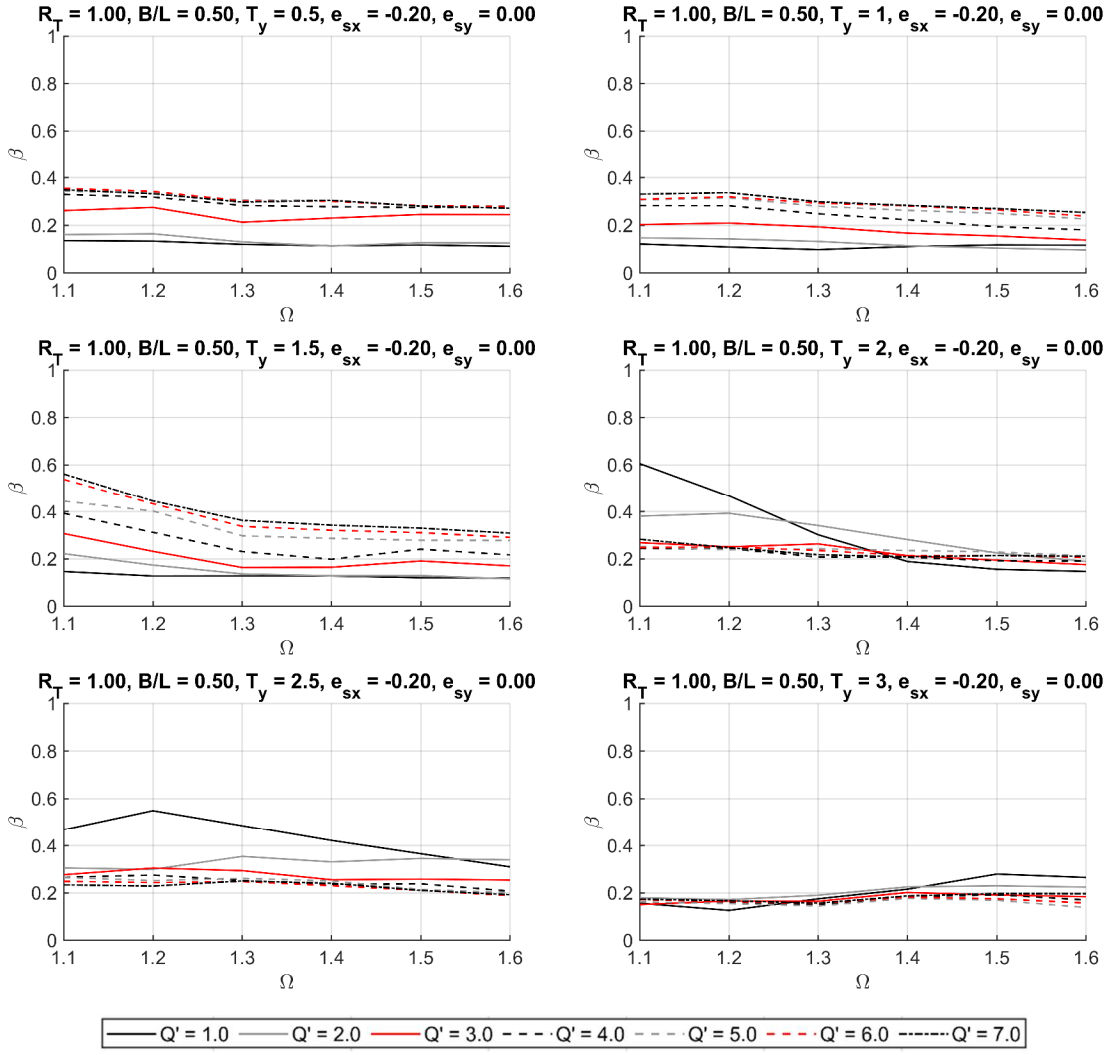

Fig. 4.20. Combination factor, β, as a function of Ω, for B/L = 0.50

Structures with *B/L*=1.0 (Fig. 4.21) exhibit β values which are virtually invariant with respect to period. Elastic systems exhibit the lowest combination factors among all structures, approximately 0.10, for $T_y \leq 1.5$ s, while for larger periods β of elastic systems is the largest, approximately 0.30. β for inelastic systems is larger as *Q'* increases for $T_y \leq 1.5$ and, as in rectangular structures, the differences between their values reduces as period is larger; for T_y = 2.5 s and 3 s, β is approximately 0.25 and 0.20 for all inelastic systems.

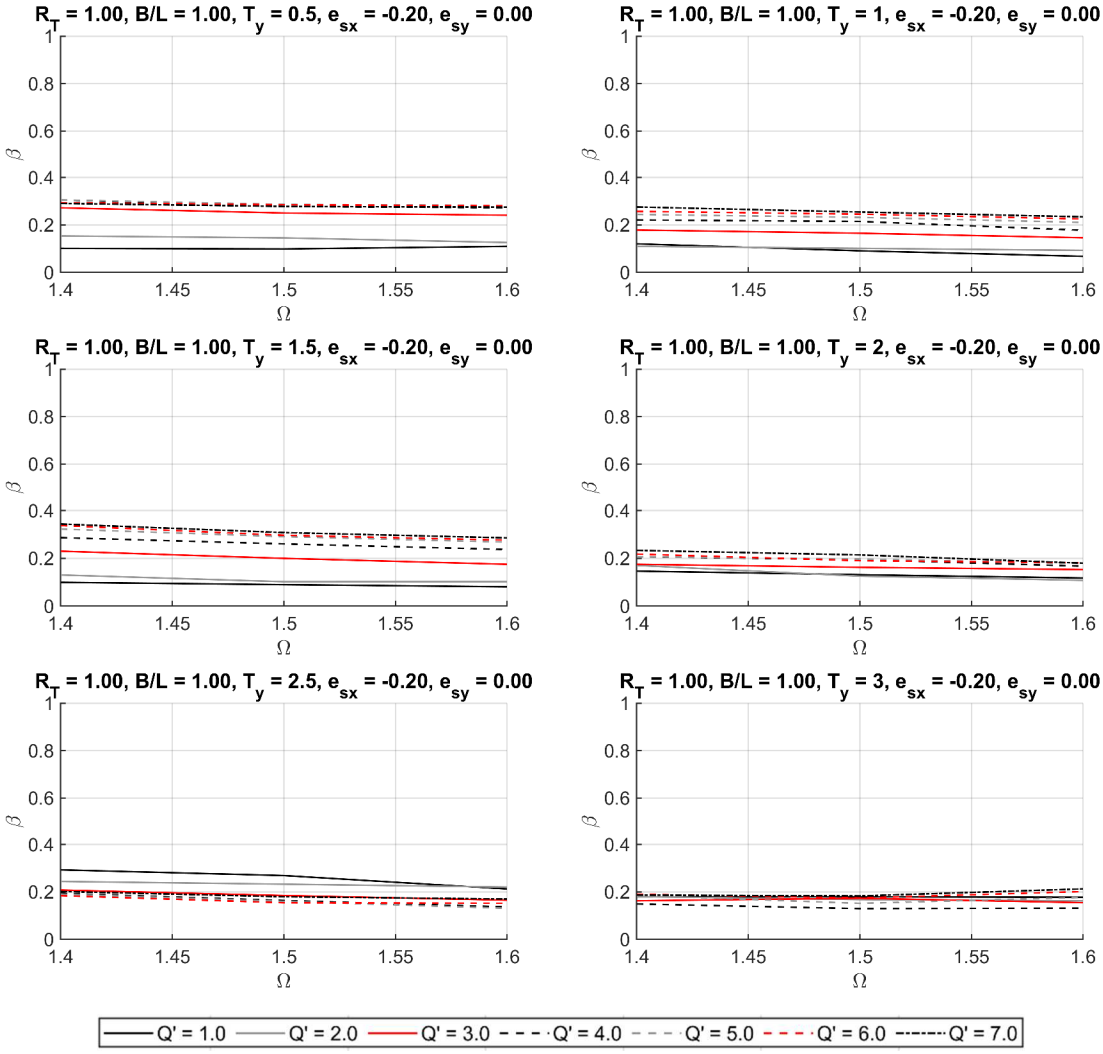

Fig. 4.21. Combination factor, β, as a function of Ω, for B/L = 1.00

Figs. 4.22 and 4.23 depict the relationship between the combination factor and T_y for e_{sx} = 0.20 and moderately and extremely torsionally stiff structures. In general, β values are larger for inelastic systems than elastic systems for $T_y < 2$ s; in such period range β increases as *Q'* is larger. For larger periods β is higher for elastic systems than inelastic ones. Furthermore, it can be identified that β is smaller for moderately torsionally stiff systems than less flexible ones.

For *B/L*=0.50 (Fig. 4.22), elastic systems show the larger variations of β with respect to period. For moderately torsional structures with $T_y \leq 1.5$ s, β is approximately constant and it increases up to its maximum value, 0.6 at $T_y = 2$ s and 0.5 s for **Ω**=1.1 at $T_y = 2.5$ **Ω** = 1.3, respectively. From such maximum values, β decreases to a value close to 0.2 at $T_y = 3$ s. Elastic systems with extremely high torsional stiffness exhibit a similar trend, however, β is about 0.10 up to $T_y = 2.5$ s, increases to values around 0.35 at $T_y = 2.5$ s and decreases to approximately 0.20. Structures with *B/L* = 0.50 with *Q'* = 2 follow the same trend than elastic systems although the maximum amplification is approximately 0.35. Furthermore, β of moderately torsionally stiff systems with *B/L* = 0.50 is approximately constant for all *Q'* values and $T_y \leq 1.0$ s, from which it increases to its maximum value, 0.55 and 0.35 for **Ω**=1.1 and 1.3, respectively, at T_y=1.5 s From such period, β decreases to approximately 0.2 at $T_y = 2.0$ s and remains approximately constant. For extremely torsionally stiff inelastic systems with *B/L* = 0.50, β remains approximately constant for all *Q'* values in the entire period range with values between 0.15 and 0.30.

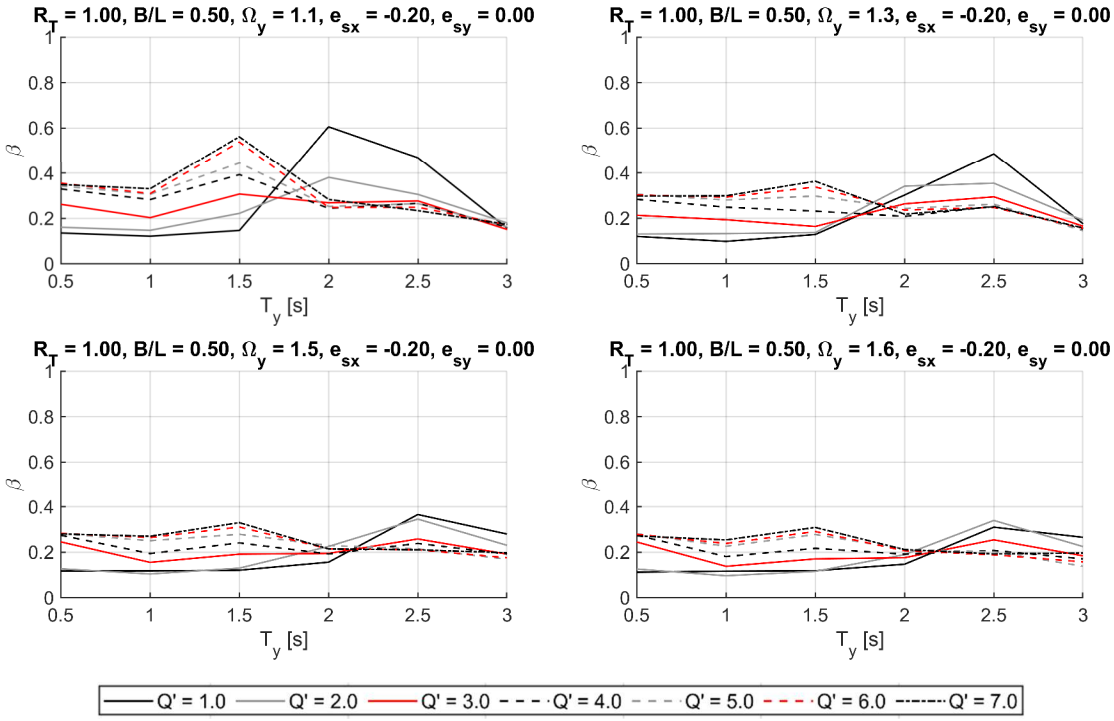

Fig. 4.22. Combination factor, β, as a function of T_y, for B/L = 0.50

Squared buildings, *B/L* = 1.0 (Fig. 4.23), exhibit similar trends than those previously described for rectangular structures, however, β values are smaller and their relationship with T_y is smoother. Moreover, the differences between β values for the distinct *Q'* values are smaller than those corresponding to *B/L*=0.5. β varies approximately from 0.1 to 0.3 for elastic systems and from 0.10 to 0.30 for inelastic systems.

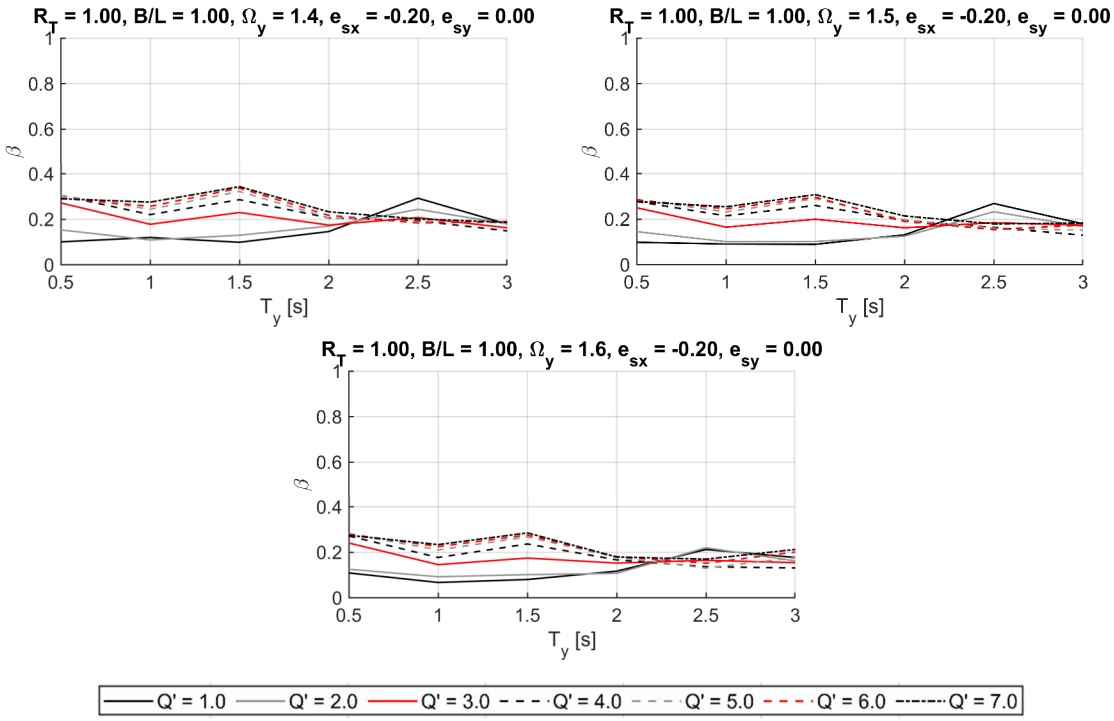

Fig. 4.23. Combination factor, β, as a function of T_y, for B/L = 1.00

Figs. 4.24 and 4.25 depict plots of β *vs* e_{sx} for several periods and *B/L* = 0.5 and 1.0, respectively, where it can be observed that β of elastic structures follow an irregular trend with respect to period. For *B/L*=0.5 (Fig. 4.24), elastic systems with $T_y \leq 1.5$ s exhibit an approximately linear or bilinear trend with respect to e_{sx}, being smoother as the period is larger; β varies from about 0.05 at $e_{sx} = 0.1$ to about 0.2 at $e_{sx} = 0.30$. For 1.5 s $\leq T_y >$ 2.5 s it follows a significantly different trend, as β varies from about 0.10 to 0.75. However, for $T_y = 3.0$ s the variation smoothens, β is approximately 0.10 at e_{sx}=0.1 and increases up to 0.25 at e_{sx}=0.3. On the contrary, for inelastic systems β does not vary significantly, in fact it is approximately constant for most period values. For $T_y \leq 1.5$ s, β is larger as *Q'* increases and its values range from 0.20 for 0.30. For $T_y = 2.0$ s, β is constant, approximately 0.2 for $Q' > 2$ up to $e_{sx} = 0.2$, point from which it shows an increasing relation with e_{sx} being the less ductile systems the ones that exhibit the larger β values; β of systems with $T_y = 2.0$ s and *Q'*=2.0 follow an increasing relation with respect to e_{sx} similar to that of elastic systems with the same period; β is about 0.15 at $e_{sx} = 0.10$ and increases up to 0.6 at $e_{sx} = 0.30$. For $T_y = 2.5$ s, β of inelastic structures is slightly linear for $Q' \geq 3$, being larger as *Q'* increases; the range of β values is about 0.20 to 0.30 for $T_y = 2.5$ s. For systems with such period and $Q' = 2$, β is approximately 0.25 up to $e_{sx} = 0.2$ and increases again to 0.5 at $e_{sx} = 0.3$. Inelastic structures with $T_y = 3.0$ s exhibit practically the same β value, 0.2, regardless of e_{sx}.

In structures with *B/L* = 1.0 the relationship between β and e_{sx} is smoother and less complex than that of systems with *B/L* = 0.50 for all *Q'* values, as can be observed in Fig. 4.25. β is approximately constant for all eccentricity values for $T_y < 1.5$ with values ranging from 0.10 to 0.15, and its values

are smaller than those of inelastic systems. For 2.0 s $\leq T_y \leq$ 2.5 s, β shows and increase as eccentricity is larger, with values varying between 0.10 and 0.35 for T_y=2.0 s, and 0.2 to 0.55 for T_y = 2.5 s. For elastic structures with T_y=3.0 s, β exhibits a constant value of 0.2 and is very similar to that of inelastic systems in all the eccentricity range considered. On the other hand, β of inelastic systems with *B/L* = 1.0 exhibit small variations with respect to eccentricity value. For $T_y \leq$ 2.0 s, β follows a slightly linear trend, and in some cases virtually constant, for all *Q'* values with values between 0.15 and 0.4, being larger as *Q'* increases. However, the difference of β values reduces as the period is larger. For T_y = 2.5 s β increases linearly with respect to e_{sx}; the values range between 0.10 to 0.25 for systems with $Q' \geq$ 3.0 and vary from 0.2 to 0.35 for systems with *Q'*=2.0; for the latter, the trend is similar to that to the elastic system. Furthermore, for this period, β is larger for the less ductile systems. On the contrary, for T_y = 3.0 s β decreases slightly with respect to eccentricity with values ranging between 0.15 and 0.25 for al *Q'* values.

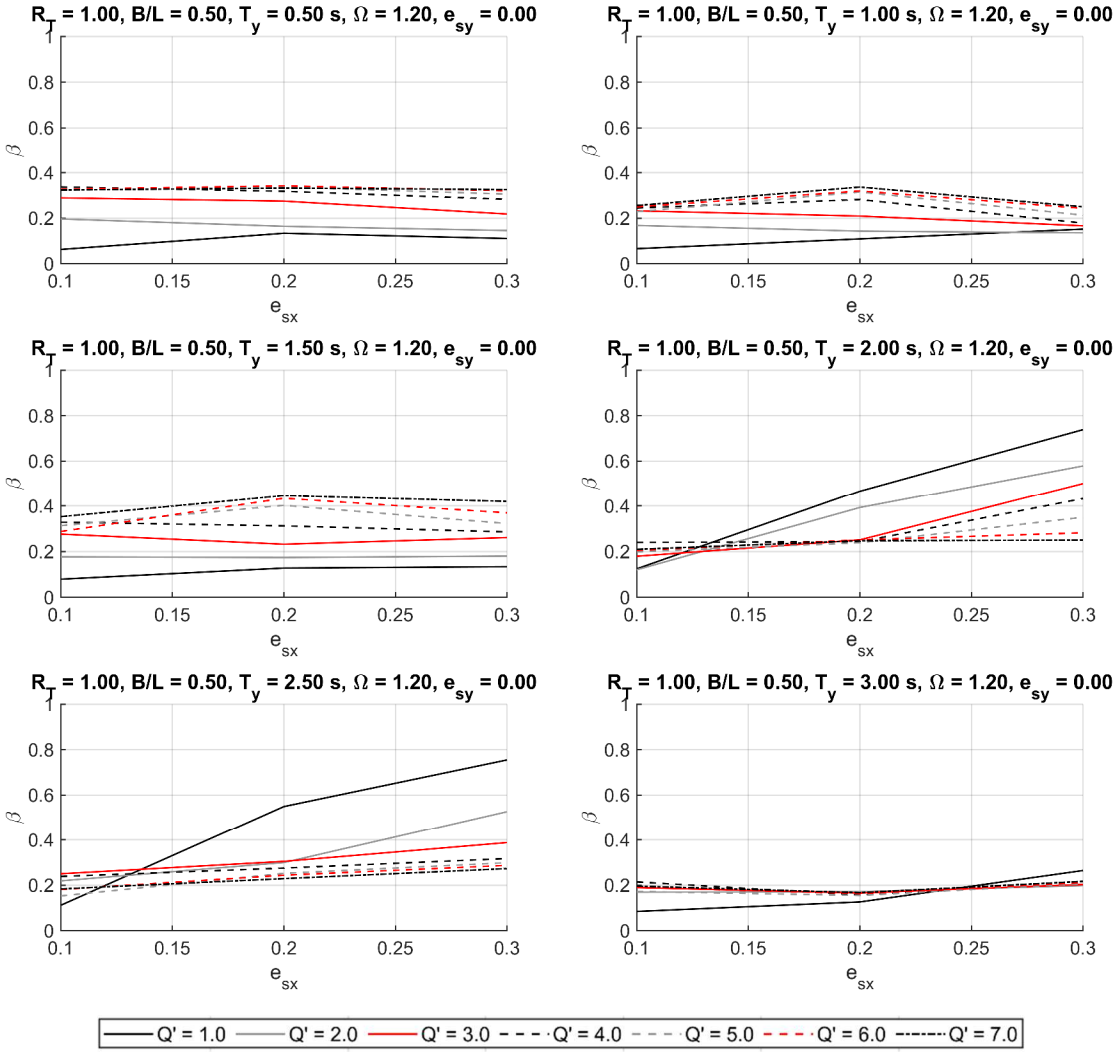

Fig. 4.24. Combination factor, β, as a function of e_{sx}, for B/L = 0.50 and Ω = 1.2

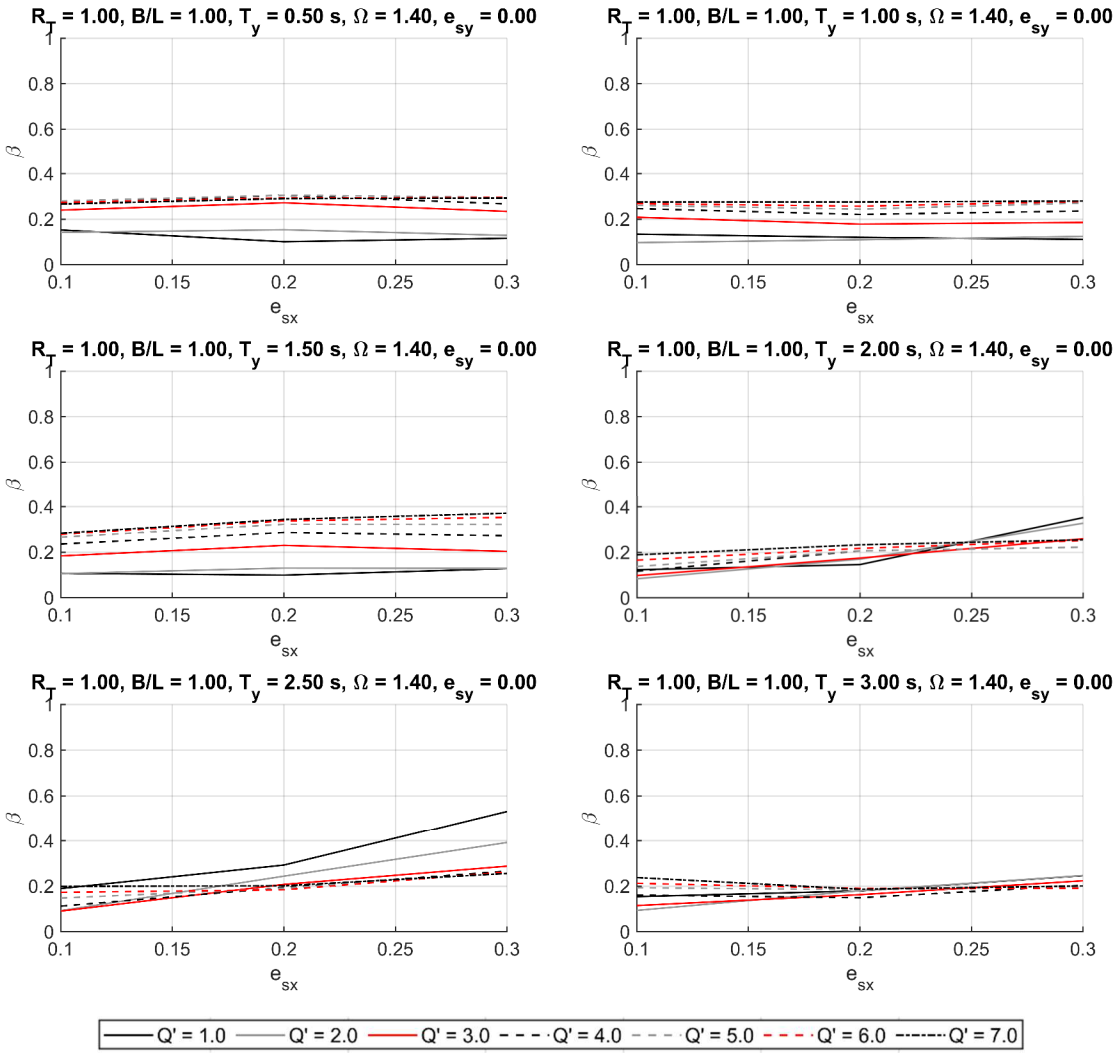

Fig. 4.25. Combination factor, β, as a function of e_{sx}, for B/L = 1.00 and Ω = 1.4

4.3.2. Dispersion of results

Figs. 4.26 and 4.27 show the normalized median absolute deviation with respect to median of β, $CV_{med} - \beta$, of structures with B/L = 0.50 and 1.0 respectively. As can be seen in such figures, the dispersions are extremely high in elastic systems and moderate to small in inelastic systems. For systems with B/L=0.50 (Fig. 4.26), CV_{med} - β presents an increasing trend for a moderately torsionally stiff structure, *i.e.* $\Omega \leq 1.3$, and Q' ≥ 3.0, conversely, for structures with $\Omega > 1.3$ the $CV_{med} - \beta$ appears to remain approximately constant for all values of T_y. For $Q' \leq 2.0$ the variability of the data is higher than the one obtained for $Q' > 2.0$. A similar trend can be observed in structures with B/L = 1.0 (Fig. 4.27).

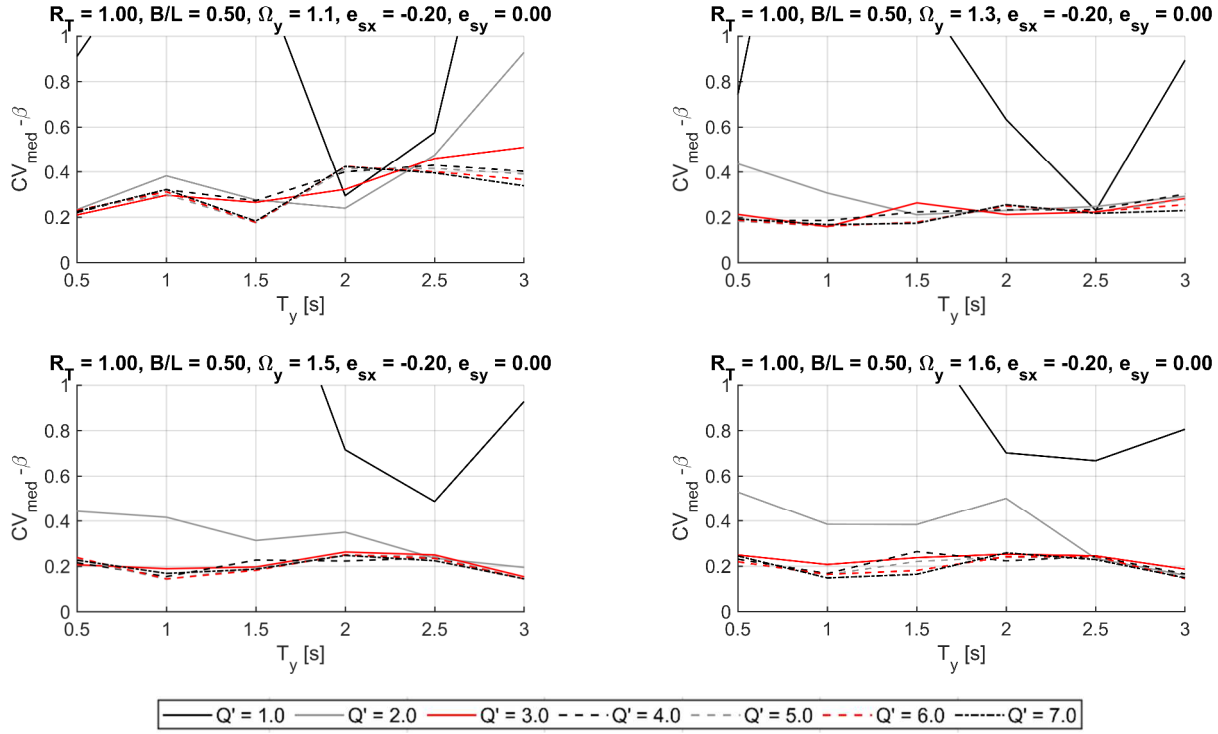

Fig. 4.26 Normalized median absolute deviation of β, as a function of T_y, for B/L = 0.50

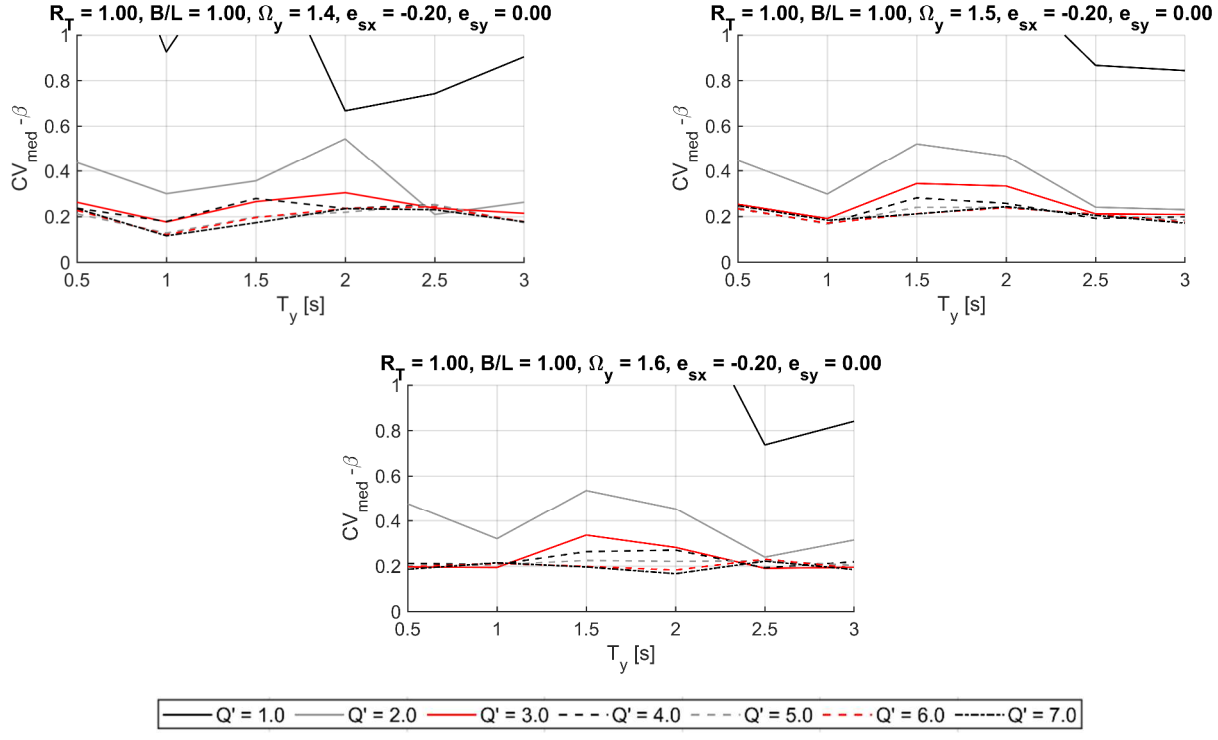

Fig. 4.27 Normalized median absolute deviation of β, as a function of T_y, for B/L = 1.00

4.3.3. Comparison with the Mexico City's Building Code combination factor

The comparison between the values of β obtained from the non-linear dynamic analysis and the combination factor prescribed on the Mexico City's Building Code (*NTC-DS*, 2017a), $\beta_{norm} = 0.3$, in terms of the relative error of β to the value of β_{norm}, is shown in Fig. 4.28. According to eq. 4.2, a positive relative error indicates that the calculated β is smaller than β_{norm}, conversely a negative relative error indicates that the calculated β is larger than the normative β_{norm}.

As can be observed in Fig. 4.28a, 76% of the cases present a value of β that is larger than β_{norm}. This implies that for these cases, the forces in the orthogonal direction, and consequently the displacements, are being underestimated.

$$\%RE = \frac{0.3 - \beta}{0.3} \tag{4.2}$$

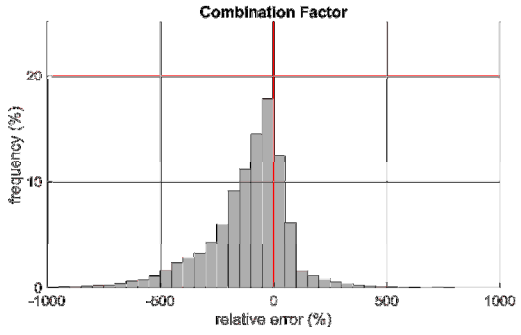

Fig. 4.28 Histogram of relative error of β to β_{norm}

Chapter 5. SEISMIC BEHAVIOR OF X-SYSTEM

5.1. Displacement amplification due to torsional effects, δ_F/δ_{CM}

5.1.1. Median response

Figs. 5.10 and 5.20 shows the groups of plots of δ_F/δ_{CM} *vs* Ω for different T_y and Q' values and B/L=0.50 and 1.00, respectively. It should be noted that for X-System e_{sx} is not independent from Ω, hence, the points of the curves correspond to structures with different eccentricity values. As can be observed in such figures for X-System the displacement amplification is larger as omega decreases for every period value, as it is expected in structures with rigid diaphragm. However, as shown in Chapter 3, flexible M systems with T_y > 2.5 s, particularly inelastic ones, exhibited an increasing relation of δ_F/δ_{CM} with respect to Ω. Furthermore, the behavioral trends of δ_F/δ_{CM} of X-System do not change as significantly as for M-System. These differences in trends can be attributed to the fact that the elements of such M-System are subjected to bidirectional flexural demands which may lead to a more complex dynamic behavior as the stiffness of the elements is affected by the bidirectional loading. On the contrary, X-System are comprised of uniaxial elements, hence, the behavior is less complex.

δ_F/δ_{CM} of rectangular structures with B/L=0.5 (Fig. 5.1) exhibit a bilinear trend with respect to Ω, regardless of the period; the change in slope occurs at Ω=1.6 for all cases. For $T_y \leq$ 2.0 s the amplification is about the same for all elastic systems; approximately 1.75 at Ω=1.45 from which it decreases to 1.6 at Ω=1.6 and to 1.3 at Ω=1.7. Furthermore, δ_F/δ_{CM} of elastic systems is smaller than that of inelastic systems for 1.0 s $\leq T_y \leq$ 2.0 s for all Ω values considered. For T_y = 0.5 s the larger δ_F/δ_{CM} values correspond to systems with Q'=2 and 3; approximately 1.95 at Ω=1.45 from which it decreases to 1.75 at Ω=1.6 and to 1.45 at Ω=1.7. The smallest amplifications are associated with Q' = 7 for which δ_F/δ_{CM} is about 1.8 at Ω=1.45 from which it decreases to 1.6 at Ω=1.6 and to 1.3 at Ω=1.7. For the period range 1.0 s $\leq T_y \leq$ 2.5 s the largest amplifications occur for Q′=7.0 for almost all Ω values. For T_y = 2.5 s. the largest δ_F/δ_{CM} values are associated also with systems with Q'=3 and the smaller for Q' = 7 in a similar fashion to systems with T_y = 0.5 s. For T_y = 3.0 s, δ_F/δ_{CM} of elastic systems are the largest in the entire Ω range considered, about 1.9 at Ω=1.45 and 1.37 at Ω=1.7, while the smaller amplifications are those of systems with Q'=1.7, about 1.23 for all Ω values.

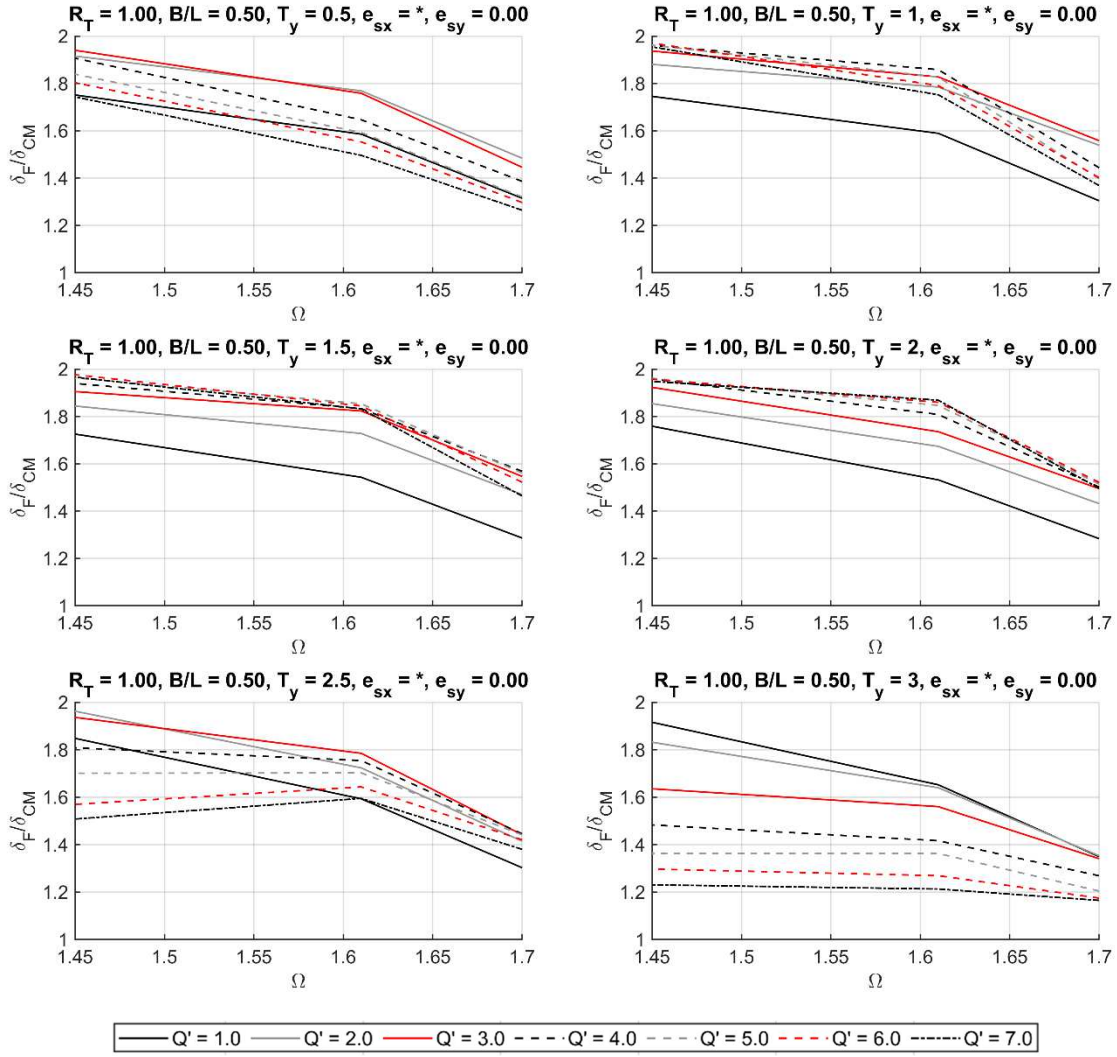

Fig. 5.1. Flexible side displacement amplification, δ_F/δ_{CM}, as a function of Ω, for B/L = 0.50

For square-plan buildings B/L=1.0, the decrease of δ_F/δ_{CM} as a function of the period is smoother than for buildings with B/L=0.5 and is virtually is in many cases virtually bilinear since the change in slope at Ω=1.6 is not as pronounced. Furthermore, the differences between the δ_F/δ_{CM} values between the different ductility values and periods is not as different as in the rectangular plan case studies. For $T_y \leq 2.0$ s the amplification is about the same for all elastic systems; approximately 1.4 at Ω=1.56 from which it decreases to 1.15 at Ω=1.8. Furthermore, for $T_y \leq 2.5$ s the largest δ_F/δ_{CM} values correspond to systems with $Q' = 3$ in most cases.

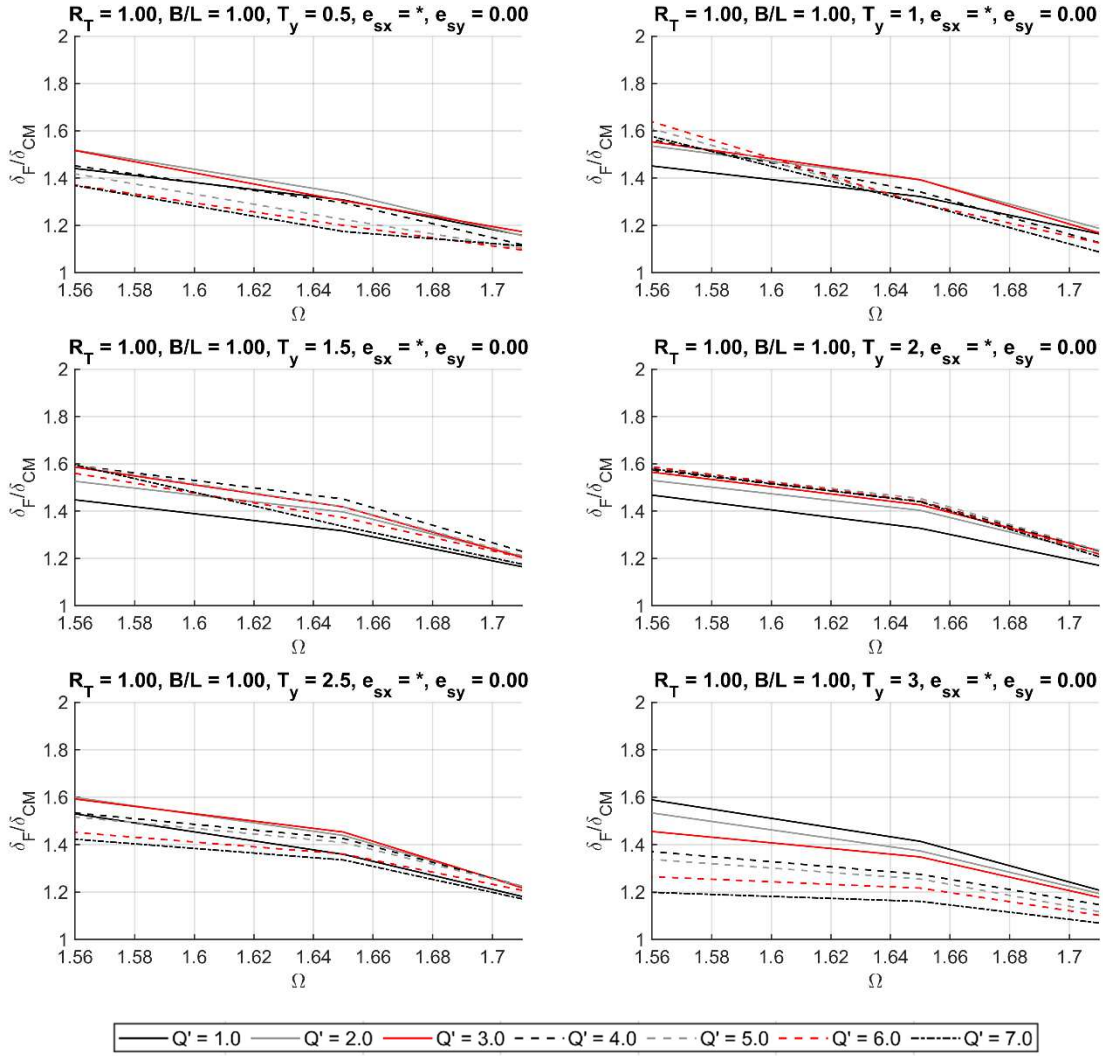

Fig. 5.2. Flexible side displacement amplification, δ_F/δ_{CM}, as a function of Ω, for B/L = 0.50

The relationship between the displacement amplification factor and T_y is shown in Figs. 5.3 and 5.4. As can be observed in such figures, δ_F/δ_{CM} of elastic structures does not vary significantly with respect to period. On the contrary, δ_F/δ_{CM} of inelastic systems follows an increasing trend for $T_y \leq 1.0$ s, it is virtually invariant from such point up to T_y=2.5 s and decreases for larger periods. Furthermore, δ_F/δ_{CM} of elastic structures is smaller than that of inelastic systems for most period values, trend that coincides with those identified in De Stefano and Pintucchi (2010) for structures with high rotational stiffness.

For B/L=0.5 (Fig. 5.3), δ_F/δ_{CM} of elastic structures is approximately 1.6, 1.2 in the entire period range for Ω=1.61 and 1.7, respectively, while for Ω=1.45 is approximately 1.75 up to T_y = 2.0 s and it increases to about 1.9 at T_y = 3.0 s. For the same aspect ratio, the largest amplification values correspond to inelastic structures with Q'=3.0 and 4.0, approximately, 1.95, 1.85 and 1.55, for Ω

values of 1.45, 1.61 and 1.7, respectively. The smallest values of δ_F/δ_{CM} are associated to inelastic structures with T_y = 3.0 s and Q'=7; δ_F/δ_{CM} is around 1.2 for Ω=1.56 and 1.65 and 1.71.

For systems with B/L=1.0 (Fig. 5.4) the trends are similar to those of structures with B/L=0.50, however, the curves of δ_F/δ_{CM} *vs* T_y are smoother and the differences amongst the δ_F/δ_{CM} values corresponding to the different Q' values considered are smaller. δ_F/δ_{CM} of elastic structures with Ω=1.56 is about 1.45 up to T_y = 2.0 s and increases to 1.6 at T_y = 3 s, whereas for Ω=1.56 δ_F/δ_{CM} is about 1.3 up to T_y = 2.0 s and increases to 1.45 at T_y = 3 s; δ_F/δ_{CM} elastic structures with Ω=1.56 is about 1.2 for all period values. The largest amplification values correspond to inelastic structures with Q'=5 and 6; δ_F/δ_{CM} is approximately, 1.65, 1.45 and 1.25, for Ω values of 1.56, 1.65 and 1.71, respectively. The smallest values of δ_F/δ_{CM} are associated to inelastic structures with T_y = 3.0 s and Q'=7; δ_F/δ_{CM} is around 1.2 for Ω=1.56 and 1.65 and 1.1 for Ω=1.71.

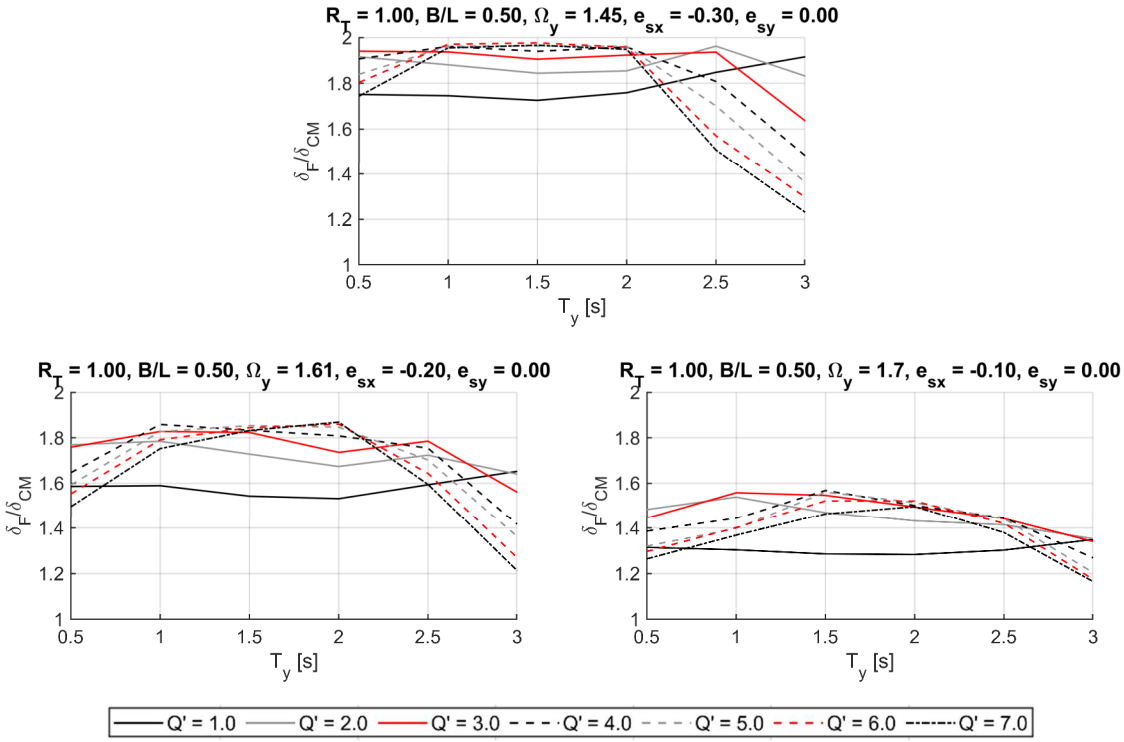

Fig. 5.3. Flexible side displacement amplification, δ_F/δ_{CM}, as a function of T_y, for B/L = 0.50

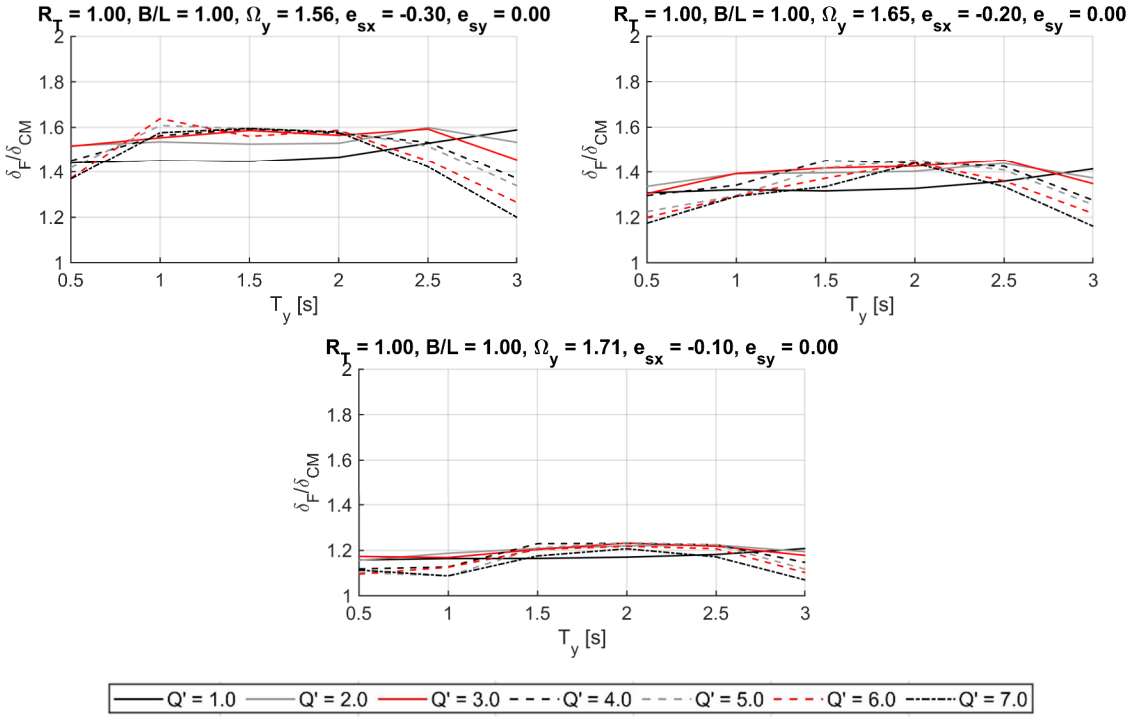

Fig. 5.4. Flexible side displacement amplification, δ_F/δ_{CM}, as a function of T_y, for B/L = 1.00

Figs. 5.5 and 5.6 shows the curves of δ_F/δ_{CM} *vs* e_{sx}. where it is observed that the amplification factor has an increasing linear or bilinear relationship with e_{sx}. This trend is evident since the stiffness eccentricity is larger as the floor rotation increase. For B/L= 0.50 (Fig. 5.5), δ_F/δ_{CM} of systems with $Q' \leq 2$ follows a bilinear increasing relation with respect to eccentricity with a change in slope at e_{sx}=0.2, except elastic systems with periods 2.0 s $\leq T_y \leq$ 3.0 s, where the relationship tends to be linear in all the eccentricity range. For structures with T_y < 1.0 s, δ_F/δ_{CM} is larger for moderately inelastic systems (Q' = 2 and 3) than that corresponding to other values of Q'; δ_F/δ_{CM} varies from 1.45 to 1.9 and 1.55 to 1.95 for T_y = 0.50 s and 1.0 s, respectively. For systems with 1.5 s < T_y < 2.0 s, the largest δ_F/δ_{CM} values correspond to $Q' \geq 5$; the range of values are 1.6 to 1.95 and 1.4 to 1.9 for T_y = 1.5 s and 2.0 s, respectively. For inelastic systems with $T_y \geq$ 2.5 s, the largest δ_F/δ_{CM} values are those of Q' = 2.0 and 3.0, about 1.4 to 1.9 in the entire range of eccentricity values considered. Furthermore, for inelastic systems with $T_y \geq$ 2.5 s and $Q' \geq 5$, δ_F/δ_{CM} is virtually constant for e_{sx} > 0.20.

For rectangular-plan systems with B/L=1.0 (Fig. 5.6), as was the case for M-System the relation between δ_F/δ_{CM} and eccentricity is similar but smoother than for squared-plan buildings. δ_F/δ_{CM} of systems with $Q' \leq 2$ is virtually linear with respect to eccentricity while inelastic systems with larger Q' values exhibit a bilinear relationship. For T_y < 1.0 s, δ_F/δ_{CM} is larger for moderately inelastic systems (Q' = 2 and 3) than that corresponding to other values of Q'; δ_F/δ_{CM} varies from approximately 1.2 to 1.55. The exception to this trend are systems with $Q' \geq 5$ with e_{sx}=0.3 for whom δ_F/δ_{CM} is larger than for the other systems as its value is about 1.65. For systems with

1.5 s < T_y < 2.0 s, the largest δ_F/δ_{CM} values correspond to $Q' \geq 5$; about 1.2 to 1.6. For systems with T_y = 2.5 s, the largest δ_F/δ_{CM} values are those of Q' = 2 and 3, approximately 1.2 to 1.6 in the entire range of eccentricity values considered. For T_y = 3.0 s, the largest δ_F/δ_{CM} values of T_y = 3.0 s correspond to elastic structures, about 1.2 to 1.6.

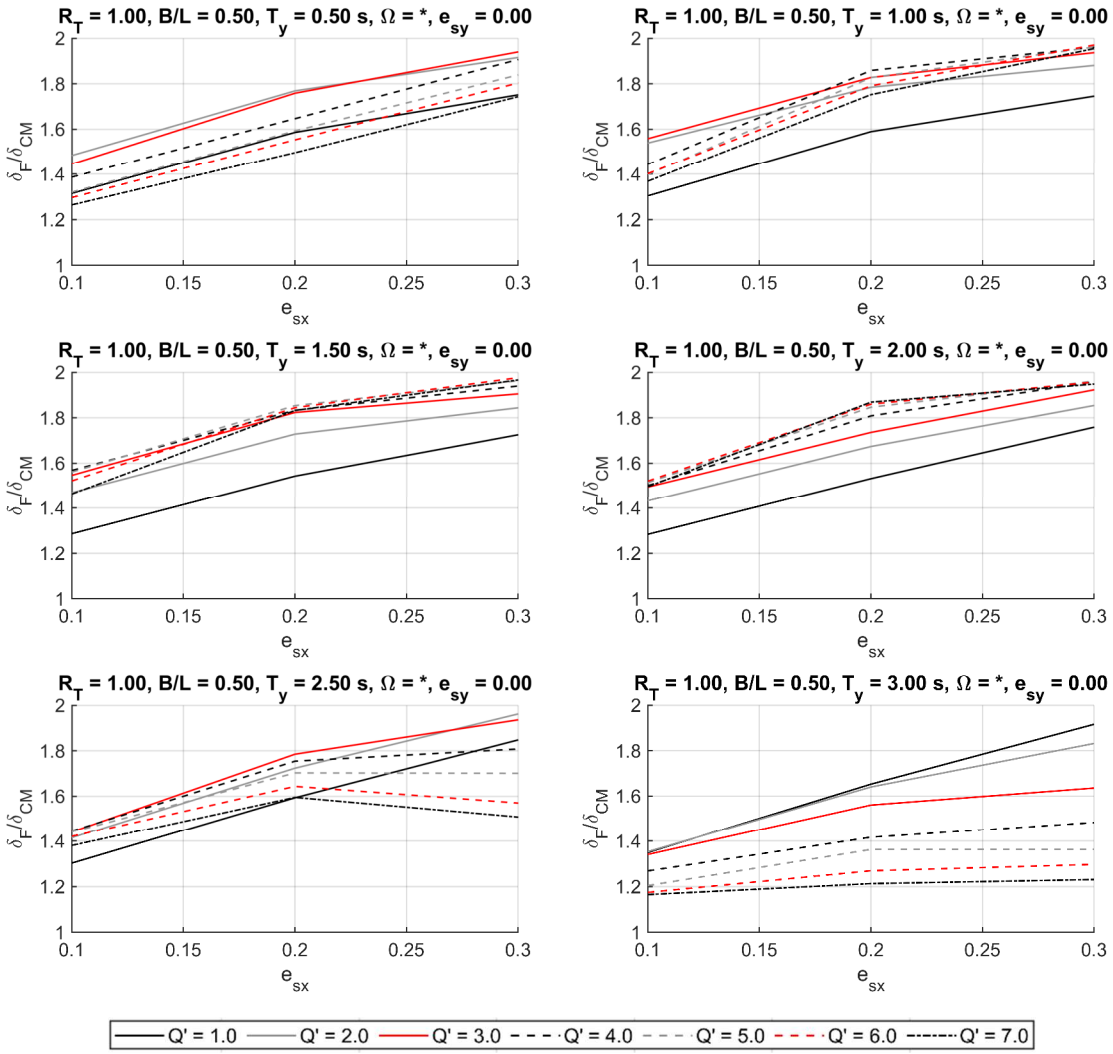

Fig. 5.5. Flexible side displacement amplification, δ_F/δ_{CM}, as a function of e_{sx}, for B/L = 0.50

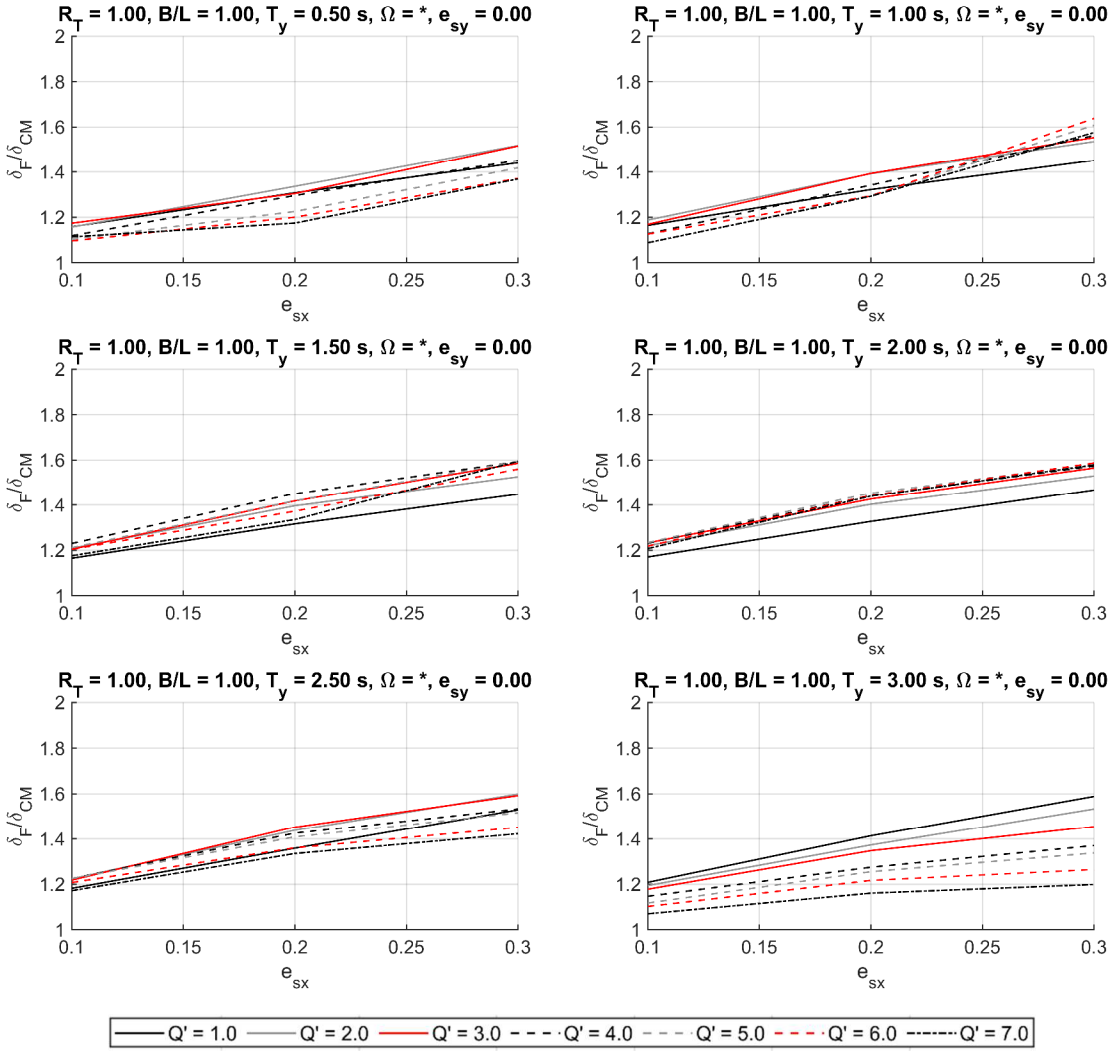

Fig. 5.6. Flexible side displacement amplification, δ_F/δ_{CM}, as a function of e_{sx}, for B/L = 1.00

5.1.2. Dispersion of results

Figs. 5.7 and 5.8 show the normalized median absolute deviation of δ_F/δ_{CM}, $CV_{med} - \delta_F/\delta_{CM}$, of structures with B/L = 0.50 and 1.0 respectively. As can be seen in both figures the variation of the data is very small for all periods, having a slight increase for $T_y \geq 2.0$ s. Comparing with the results obtained with the M-System (Figs. 4.9 and 4.10), it can be observed that the variability for the X-System is lower, particularly for short periods ($T_y \leq 2.0$ s), this can be attributed to the fact that the torsional effects for this system are smaller due to its high rotational stiffness.

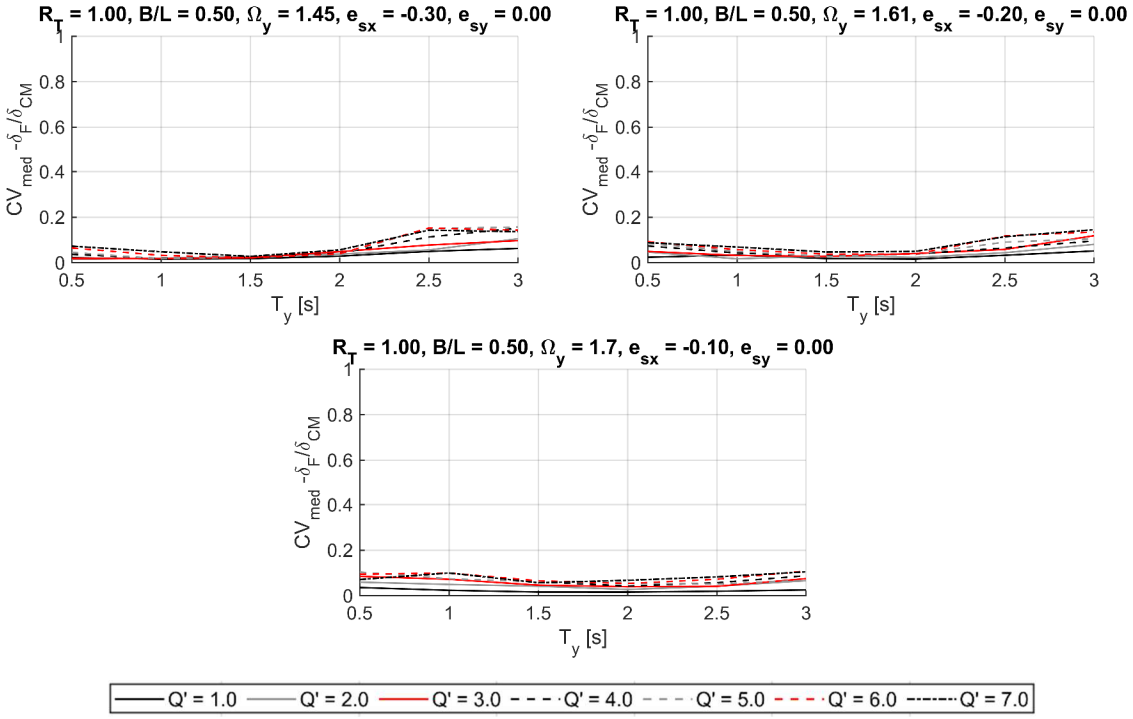

Fig. 5.7 Normalized median absolute deviation of δ_F/δ_{CM}, as a function of T_y, for B/L = 0.50

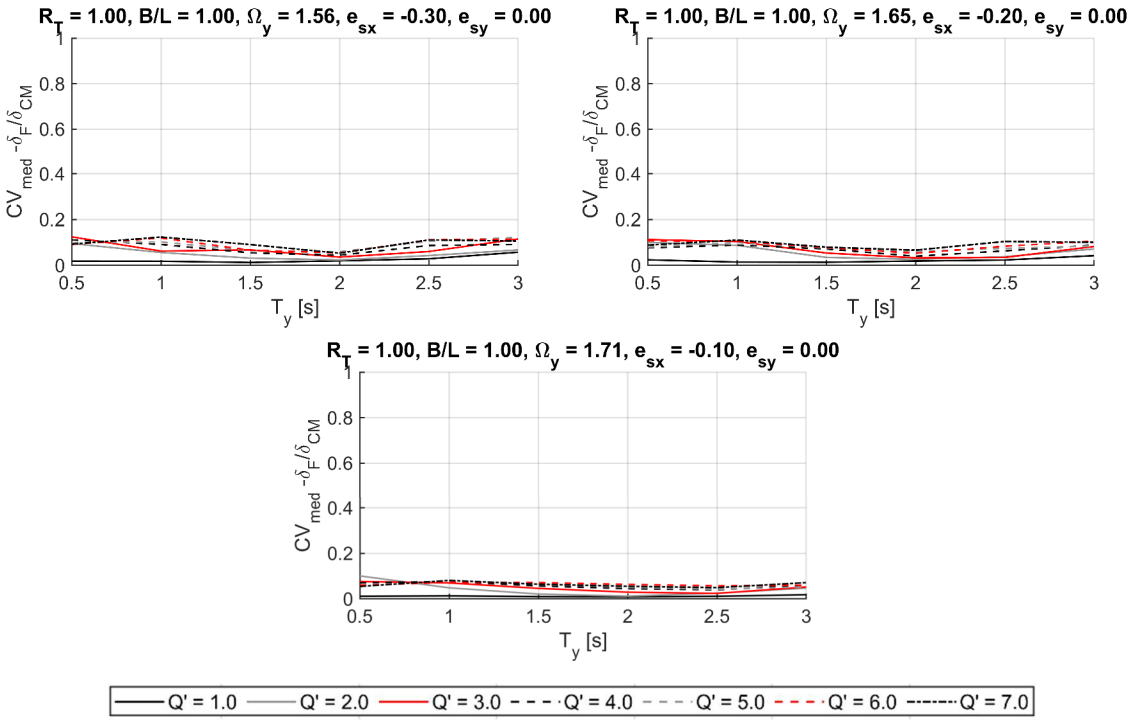

Fig. 5.8 Normalized median absolute deviation of δ_F/δ_{CM}, as a function of T_y, for B/L = 1.00

5.1.3. Comparison between elastic and inelastic torsional effects

The comparison of the values of δ_F/δ_{CM} obtained with a $Q' = 1.0$ and the one obtained with $Q' \neq 1.0$, in terms of the relative error of the inelastic δ_F/δ_{CM} to the elastic δ_F/δ_{CM}, is shown in Fig. 5.9. According to eq. 5.1 a positive relative error indicates that the elastic amplification is larger than the inelastic, conversely, a negative relative error indicates that the elastic displacement amplification is smaller than the inelastic.

$$\%RE = \frac{\left(\delta_F / \delta_{CM}\right)_{elastic} - \left(\delta_F / \delta_{CM}\right)_{inelastic}}{\left(\delta_F / \delta_{CM}\right)_{elastic}} \quad 5.1$$

As can be observed in Fig. 5.9, for 25% of the structures the use of the elastic floor displacement shape to estimate the inelastic maximum displacement of the flexible side would provide a conservative result with respect to the elastic deformed shape. This is consistent with the results obtained for M-System with high rotational stiffness (Fig. 4.12), as it is expected that most of the X-System present a non-conservative result with respect to the elastic deformed shape due to its inherent significantly high rotational stiffness, once again confirming the conclusions made by De Stefano and Pintucchi (2010). Nonetheless, other parameters such as T_y have an effect on the displacement amplification of the structure; it can be observed in Figs. 5.3 and 5.4 that elastic systems that exhibit larger flexible side amplification than inelastic systems are those with $T_y > 2.5$ s.

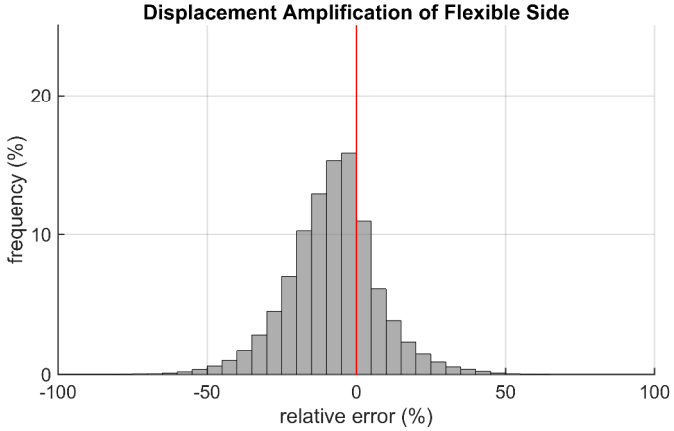

Fig. 5.9 Histogram of relative errors of inelastic to elastic δ_F/δ_{CM}

5.2. Ductility demand

5.2.1. Median response

Fig. 5.10 depicts the relationship between μ and T_n for elastic and inelastic systems with moderately high and extremely high rotational stiffness and B/L=0.5 and B/L=1.0. As it can be

observed in such figure, the ductility demand at the center of mass is a function of T_n and exhibits some level of dependency on e_{sx}, which, as explained in the preceding chapter, can be attributed to the fact that the demands of a structure are different for distinct e_{sx} values.

The trends of ductility demand with respect to period are the same as for M-System and SDOF systems. μ is significantly large for structures with short periods and is lower as the period decreases up to $T_n = 2.0$ s, from which it remains practically constant. μ corresponding to distinct Q' values are significantly different for $T_n \leq 1.0$ s, however, such difference reduces as the period increases. For $T_n \geq 2.0$ s, the differences between the μ values of the distinct systems are not as pronounced.

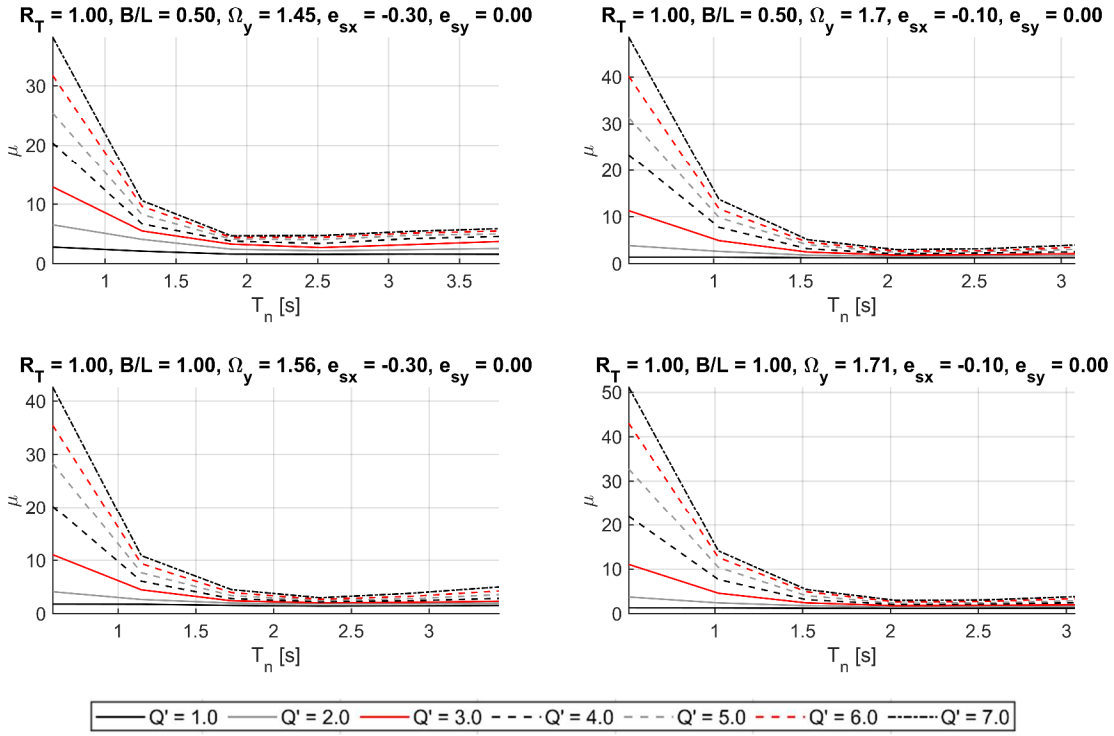

Fig. 5.10. Ductility demand, μ, as a function of T_n for B/L = 0.50

Fig. 5.11 depicts the ratio of ductility demand of 3DOF systems to that of SDOF systems, μ_{3DOF}/μ_{SDOF}, for the same parameters of Fig. 5.10, where it can be observed that, as for M-System, the demands of X-System are different than those of 3DOF structures, however, the trends are different. Elastic structures with $B/L = 0.5$ exhibit the largest μ_{3DOF}/μ_{SDOF}, about 2.3 for $e_{sx} = 0.30$, from which it decreases to about 1.5 at $T_n = 2.0$ s and remains constant for the larger periods. For elastic systems with $B/L = 0.5$ and e_{sx}=0.10, μ_{3DOF}/μ_{SDOF} is 2.0 and decreases to approximately 1.75 at $T_n = 1.5$ s and fluctuates around that value for larger periods. For $B/L = 1.0$ and $e_{sx} = 0.30$, μ_{3DOF}/μ_{SDOF} of elastic structures is about 1.75 for $T_n = 0.5$ s and 1.0 s and decreases to approximately 1.5 at $T_n = 2.0$ s and remains constant for the larger periods. For elastic systems $B/L = 1.0$ and $e_{sx} = 0.10$, μ_{3DOF}/μ_{SDOF} fluctuates around a value of 1.75 in the period range shown.

For inelastic systems, $\mu_{3DOF}/\ \mu_{SDOF}$ does not vary significantly with respect to T_n and its values decrease as Q' increases, hence, the larger values are associated with Q'=2 and the smaller to Q' = 7. Furthermore, $\mu_{3DOF}/\ \mu_{SDOF}$ of the distinct Q' values are not significantly different. For B/L = 0.5 and e_{sx} = 0.30, μ_{3DOF}/μ_{SDOF} of structures with Q' = 2 is 2 at T_n = 0.5 s and decreases to approximately 1.5 at T_n = 2.5 s, point from which it remains constant; $\mu_{3DOF}/\ \mu_{SDOF}$ of structures with Q' = 7 fluctuates around a value of 1.0 in the entire period range. For B/L = 0.5 and e_{sx} = 0.10, μ_{3DOF}/μ_{SDOF} of structures with Q' = 2 fluctuates around 1.05 in the entire period range, while for Q' = 7.0, $\mu_{3DOF}/\ \mu_{SDOF}$ is about 0.8 for all periods. For systems with B/L = 1.0 and e_{sx} = 0.30, $\mu_{3DOF}/\ \mu_{SDOF}$ associated to Q' = 2.0 is about 1.10 at T_n = 0.5 s, point from which it increases up to approximately 1.25 at T_n = 1.7 and decreases up to 1.10 at T_n = 3.4 s.; for Q'=7.0, $\mu_{3DOF}/\ \mu_{SDOF}$ decreases from 0.90 at T_n = 0.5 s to approximately 0.80 at T_n = 3.4 s. For systems with B/L = 1.0 and e_{sx} = 0.10, $\mu_{3DOF}/\ \mu_{SDOF}$ fluctuates in the entire period range around values of 1.0 and 0.85, for Q' values of 2 and 7, respectively.

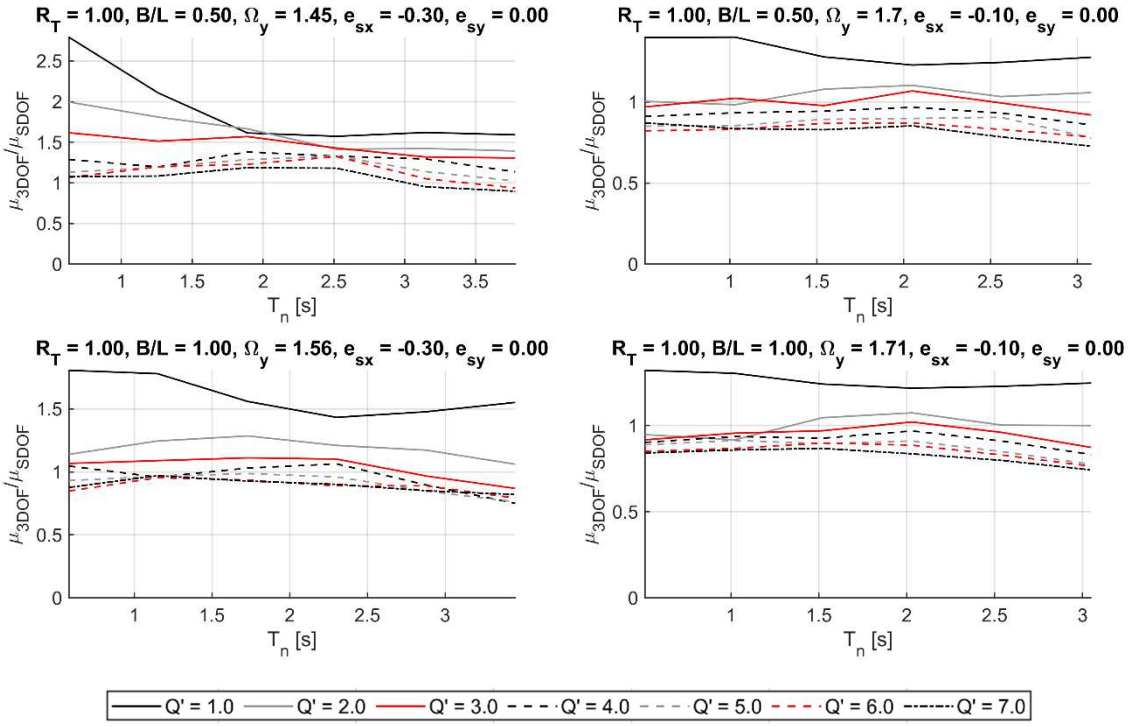

Fig. 5.11. Ductility ratio, $\mu_{3DOF}/$, μ_{3DOF}, as a function of T_n

As previously discussed for M-System, the differences in value between the ductility demands of 3DOF systems and SDOF system arise from the fact that the former are subjected to bidirectional demand, however, such differences are smaller for X-System than those of M-System. Furthermore, the $\mu_{3DOF}/\ \mu_{SDOF}$ *vs* T_n plots also show that the ductility demand at the center of mass, μ, depends of e_{sx}, as discussed in a preceding paragraph.

Figs. 5.12 and 5.13 present the plots of μ *vs* e_{sx} for systems with different ratios and B/L = 0.5 and 1.0, respectively, for systems with distinct values of T_y and Q'. In all cases structures with Q' = 1.0

exhibit constant ductility demands slightly larger than 1.0, which is due to the fact of the difference between demands of SDOF systems and MDOF systems. For B/L = 0.5 (Fig. 5.12), μ of inelastic structures with 0.5 s ≤ T_y ≤ 1.5 s follows an increasing linear or bilinear trend for values of $Q' \leq 3$ and a decreasing trend for values of $Q' > 3$. For structures with $T_y \geq 2.0$ s. μ is larger as the eccentricity increases. These same trends can be observed for B/L = 1.0 (Fig. 5.13), with the exception that the constant values for structures with $Q' \leq 4$ is present for all values of T_y.

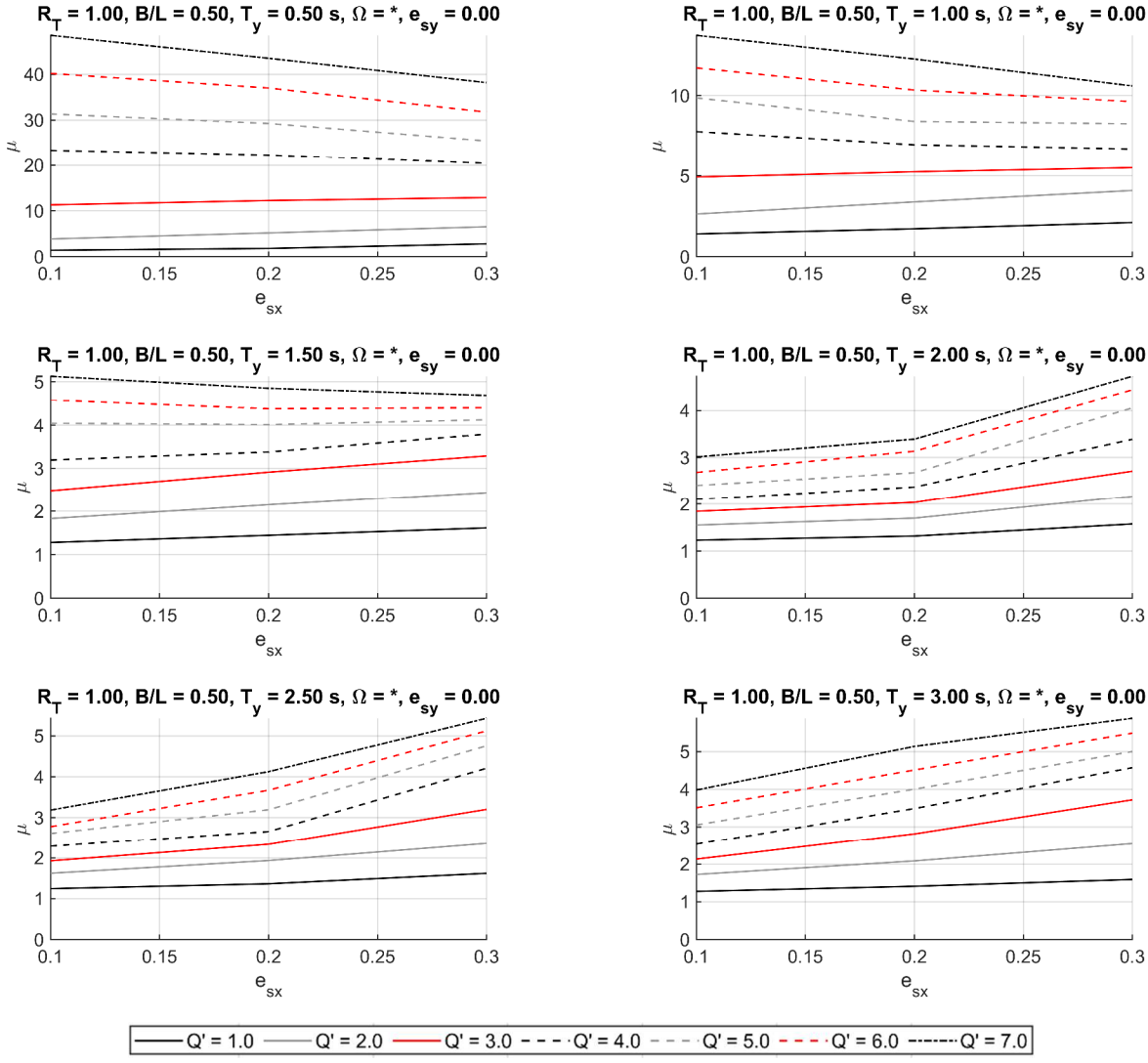

Fig. 5.12. Ductility demand, μ, as a function of e_{sx}, for B/L = 0.50

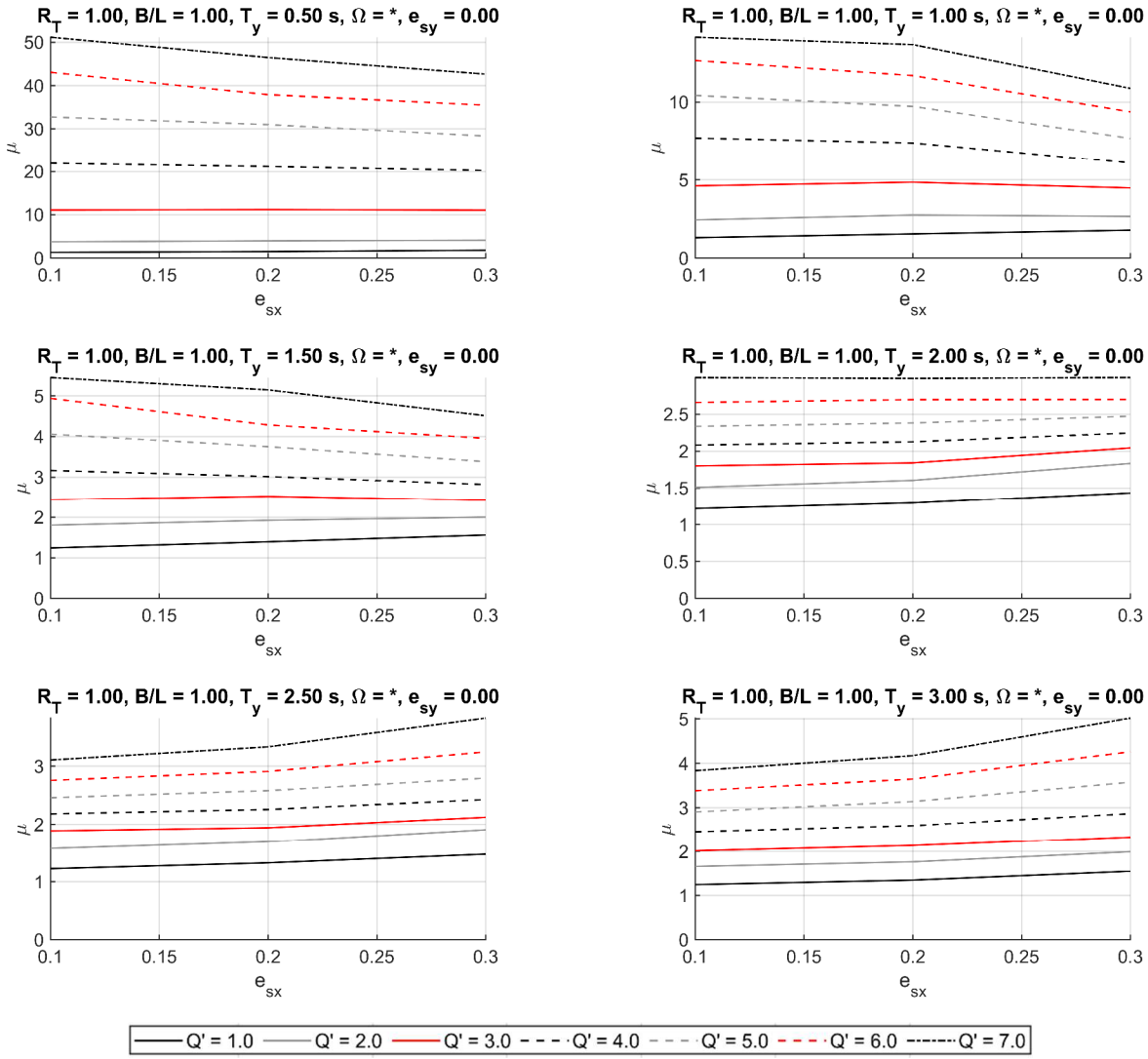

Fig. 5.13. Ductility demand, μ, as a function of e_{sx}, for B/L = 1.00

5.2.2. Dispersion of results

Figs. 5.14 and 5.15 show the normalized median absolute deviation of μ, $CV_{med} - \mu$, of structures with B/L = 0.50 and 1.0 respectively. In general, the dispersion of μ is moderate to low for all cases. For B/L = 0.50 (Fig. 5.14), the value of CV_{med} - μ present a decreasing trend with respect to T_y, where the data exhibits a higher variability for stiffer structures, *i.e.* $T_y \leq 1.0$ s. For inelastic systems with the same B/L value, the data presents the largest variability for $Q' = 2$ and $T_y \leq 1.0$ s and decreases for larger values of Q'; conversely, for $T_y > 1.0$ s the variability is smaller for $Q' = 2$ and increases as Q' is larger. A similar trend is found for structures with B/L = 1.0 (Fig. 5.15), however, the variability of the data increases for $T_y = 0.5$ s, compared to that of structures with B/L = 0.50.

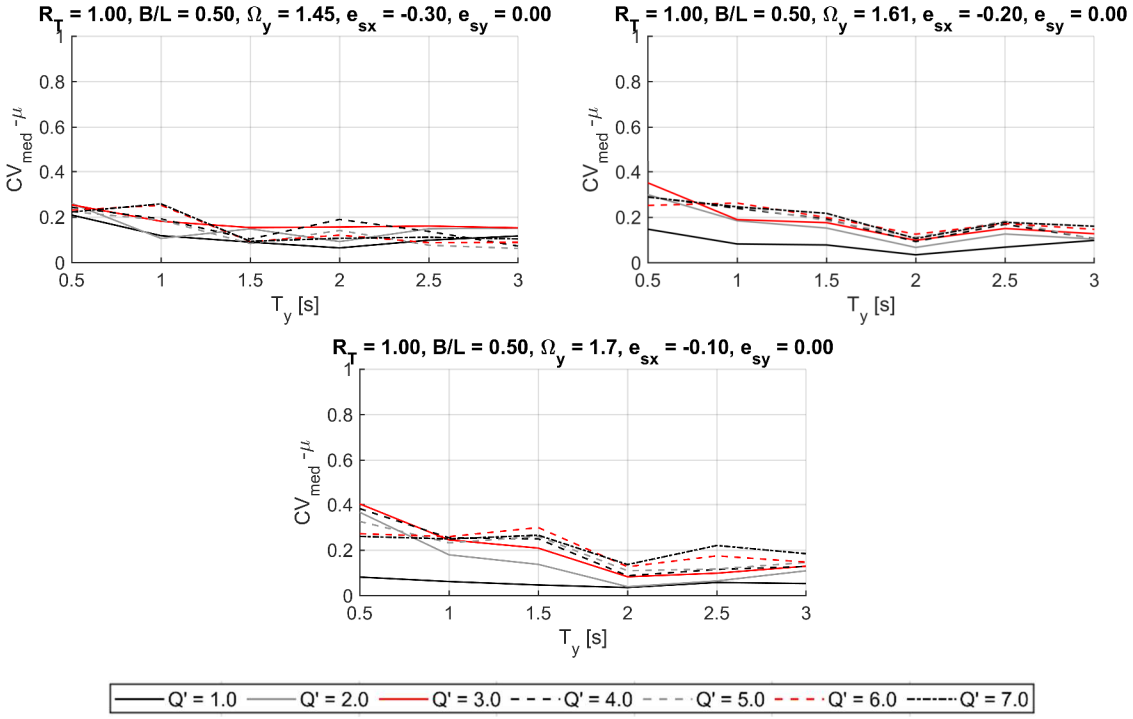

Fig. 5.14 Normalized median absolute deviation of μ, as a function of T_y, for B/L = 0.50

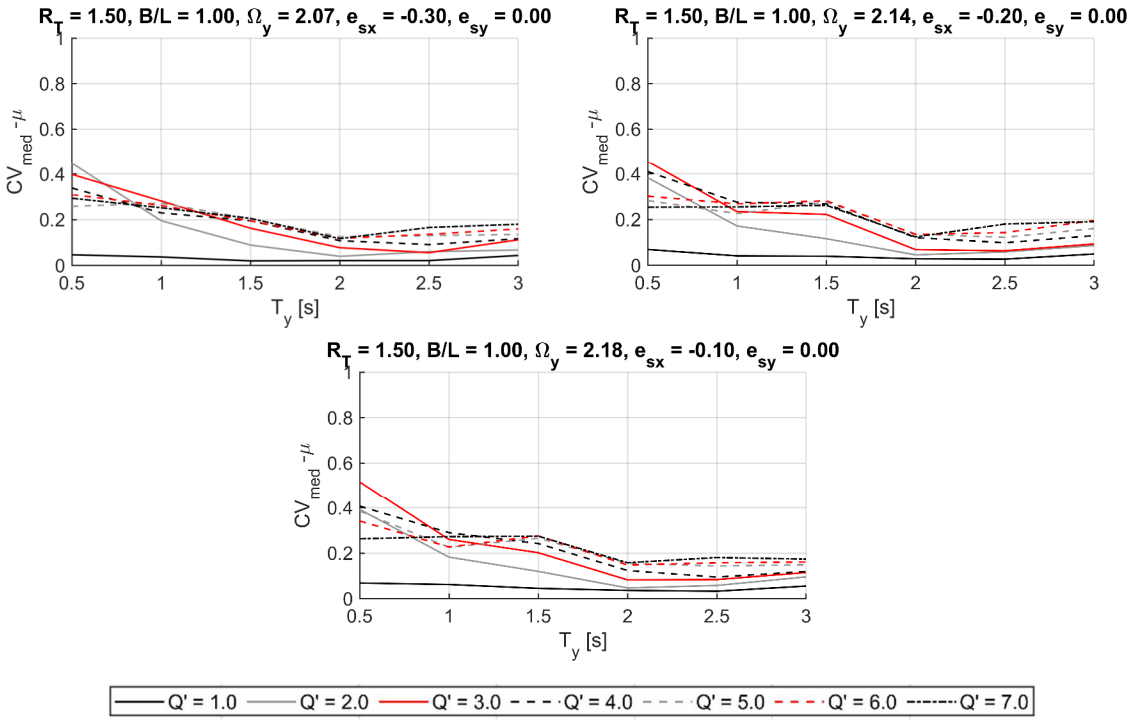

Fig. 5.15 Normalized median absolute deviation of μ, as a function of T_y, for B/L = 1.00

5.3. Combination factor of orthogonal demands

5.3.1. Median response

The combination factors, β, of X-System were calculated in the same manner as for M-System. Figs. 5.16 and 5.17 present the plots of combination factor, β *vs* Ω, for systems with different T_y and Q' values and B/L=0.5 and 1.0, respectively. As can be seen in such figures, the β values attained for X-System are considerable lower than those of M-System (see Figs. 4.20 and 4.21), Furthermore, β is larger as Q′ increases and, consequently, the largest values correspond to structures with $Q' \geq 5$ and the smaller values to elastic systems.

For B/L=0.5 (Fig. 5.16), the trends of β with respect to Ω change for different periods. For $T_y \leq 1.0$ s, β of elastic systems follows an approximately linear behavior with respect to Ω, with values around 0.05 and 0.10, while for inelastic systems β is virtually constant in the entire omega range considered and does not show a significant variation between the different levels of inelasticity; their values are around 0.20 and 0.10, for T_y = 0.5 s and 1.0 s, respectively. For T_y = 1.5 s, β of elastic systems increases linearly from 0.05 at Ω=1.45 to 0.10 at Ω=1.7. For T_y = 2.0 s, β of elastic structures decreases as Ω increases, it varies from 0.2 at Ω=1.45 to 0.05 at Ω=1.7. In the period range 2.0 s $\leq T_y \leq$ 2.5 s, β of elastic systems decreases bilinearly, from about 0.2 to 0.05 and 0.35 to 0.10, for Ω =2.0 s and 2.5 s, respectively. For T_y = 3.0 s, elastic structures exhibit a constant β value of about 0.2 in the entire range of Ω values considered. β of inelastic structures with $T_y \leq$ 1.0 is approximately constant for all Ω values shown and the difference between the values corresponding to the different Q' values is small; their values are approximately 0.2 for T_y = 0.5 s and 0.10 for T_y = 1.0 s. For T_y = 1.5 s, β of inelastic structures decrease linearly in the Ω range shown; the largest values correspond to Q'=7, which vary from about 0.3 at Ω=1.45 and 0.10 at Ω=1.7. In the period range 2.0 s $\leq T_y \leq$ 2.5 s, β of inelastic structures follow a bilinear decreasing relation with respect to Ω, where the largest values are also those associated with Q'=7. Such values vary in the entire Ω range shown from about 0.50 to 0.05 for T_y = 2.0 s, 0.45 to 0.10 for T_y = 2.5 s and 0.55 to 0.10.

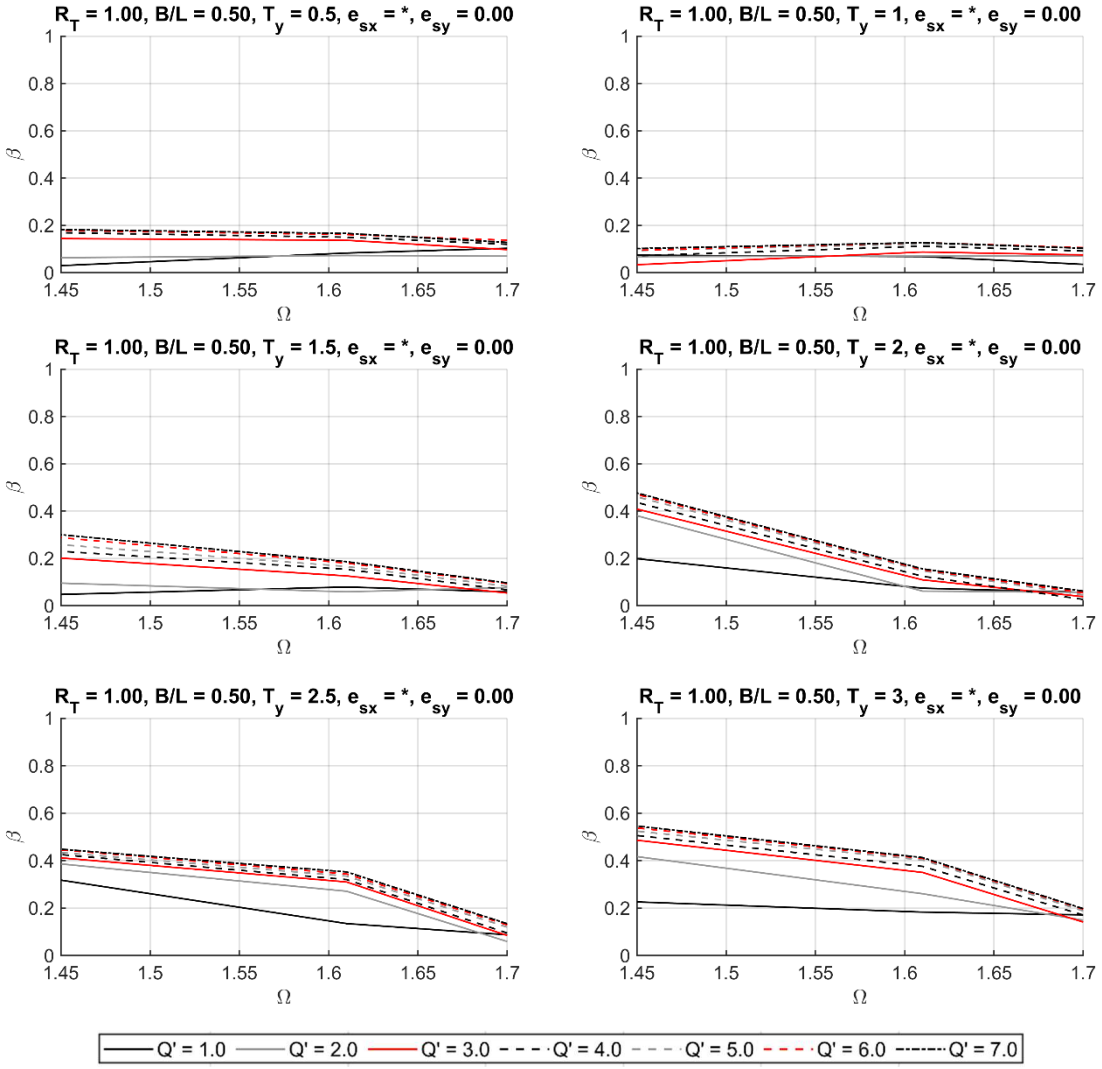

Fig. 5.16. Combination factor, β, as a function of Ω, for B/L = 0.50

For squared-plan structures, B/L = 1.0 (Fig. 5.17) the relationship between β and Ω is smoother than for systems with B/L = 1.0. In the period range $T_y \leq 1.5$, β of elastic structures is virtually independent from Ω, approximately 0.10, 0.05 and 0.05 for T_y = 0.5 s, 1.0 s and 1.5 s, respectively. For 2.0 s $\leq T_y \leq$ 2.5 s, β of elastic systems decreases bilinearly from 0.10 to 0.05 for T_y=2.0 s and from 0.2 to 0.10 for T_y = 2.5 s in the range of Ω shown. For T_y = 3.0 s, elastic structures exhibit a practically constant value of 0.20 for all Ω values. For inelastic structures, the largest β values are associated with Q'=7, although there is not much difference with the values corresponding to the other systems. For $T_y \leq$ 1.0 and Q' = 7 β is virtually constant for all Ω values, about 0.2 and 0.10 for T_y = 0.5 s and 1.0 s, respectively. For T_y = 1.5 s and Q' = 7, β of inelastic structures decreases linearly from 0.2 to about 0.05 in the range of Ω shown. For $T_y \geq$ 2.0 s and Q' = 7, β decreases bilinearly with a change in slope around Ω = 1.64, their values vary from about 0.3 to 0.05, 0.4 to 0.1 and 0.45 to 0.2 in the Ω range shown for T_y = 2.0 s, 2.5 s and 3.0 s, respectively.

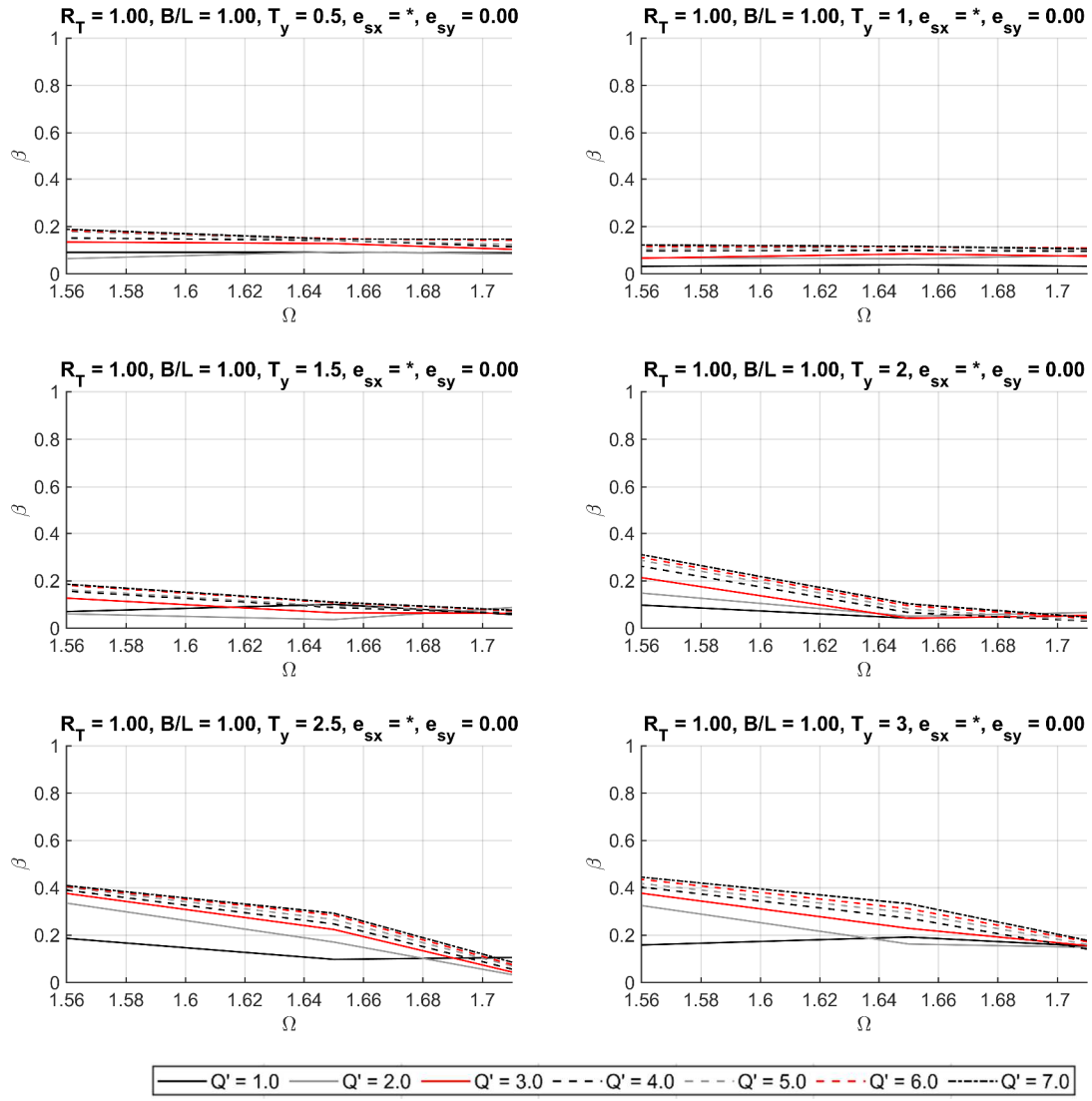

Fig. 5.17. Combination factor, β, as a function of Ω, for B/L = 1.0

Figs. 5.18 and 5.19 show the plots of β *vs* T_y for several **Ω** and *Q'* values of systems with *B/L*=0.50 and 1.0, respectively. X-System exhibit smoother and more regular trends of β with respect to period than M-System, particularly, the curves of β *vs* T_y of elastic systems are similar (see Figs. 4.22 and 4.23) to those of inelastic systems. Moreover, it can also be identified in such figures that the smallest β values are associated with elastic systems. Furthermore, β increases as *Q'* is larger, hence, the largest values correspond to structures with *Q'*=7.

For *B/L*=0.5 (Fig. 5.18), the difference between β values of elastic and inelastic systems decreases as **Ω** increases. For **Ω** = 1.45, β of elastic structures is approximately constant, 0.05, up to T_y = 1.5 s and increases to about 0.35 at T_y = 2.5 s, point from which it decreases to about 0.20; β of systems with *Q'*=7 and the same **Ω** value is 0.2 at T_y = 0.5 s, point from which it decreases to approximately 0.10 at T_y = 1.0 s, from where it increases to about 0.55 at T_y = 3.0 s. For **Ω**=1.61, elastic systems

with $T_y \leq 2$ s present a constant β value with respect to period of 0.10 s, point from which it increases to 0.2 at $T_y = 3$ s. β of inelastic systems with **Ω**=1.61 and Q'=7 fluctuates around a value of 0.2 for $T_y < 2.0$ s, point from which it increases up to 0.4 at $T_y = 3.0$ s. For structures with **Ω**=1.7, β of elastic and inelastic systems are similar; for Q'=7, β decreases from about 0.12 at $T_y = 0.5$ s to 0.05 at $T_y = 2.0$ s, from which it increases to 0.2 at $T_y = 3.0$ s.

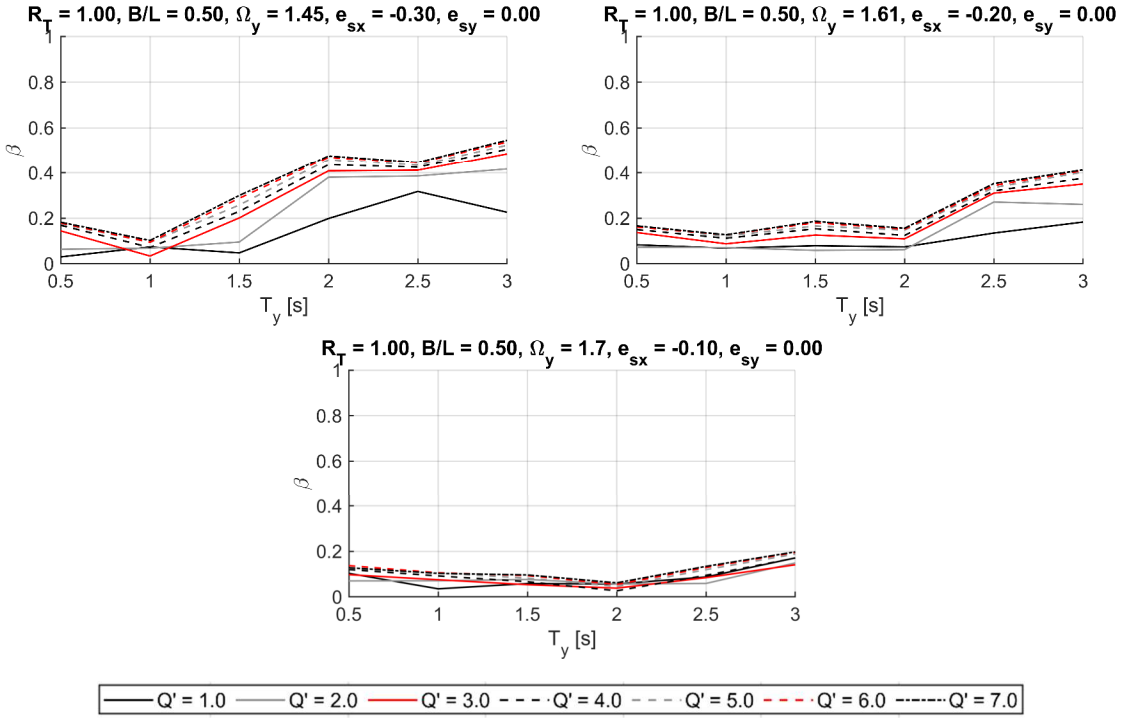

Fig. 5.18. Combination factor, β, as a function of T_y, for B/L = 0.50

Structures with *B/L*=1.0 (Fig. 5.19), exhibit the same trends as those with *B/L*=0.5, although the relationships between β and T_y are smoother. For **Ω**=1.56, β of elastic systems fluctuates around 0.10 for $T_y \leq 2.0$ s, and increases up to 0.2 at T_y =2.5, whereas for inelastic systems with Q'=7, β is 0.2 at T_y =0.5 s, decreases to about 0.10 at T_y =1.5 s and increases to 0.4 at T_y =2.5 s. For **Ω**=1.65, elastic systems exhibit a β that fluctuates around 0.05 for $T_y < 2.0$ s and it increases up to about 0.22 at $T_y = 3.0$ s, while for structures with Q'=7 β is approximately constant, 0.15, for $T_y \leq 2.0$ s and it increases to about 0.30 at $T_y = 3.0$ s. For **Ω**=1.71, β of elastic and inelastic systems fluctuate around 0.10 for $T_y \leq 2.0$ s and increases up to about 0.2 at $T_y = 3.0$ s.

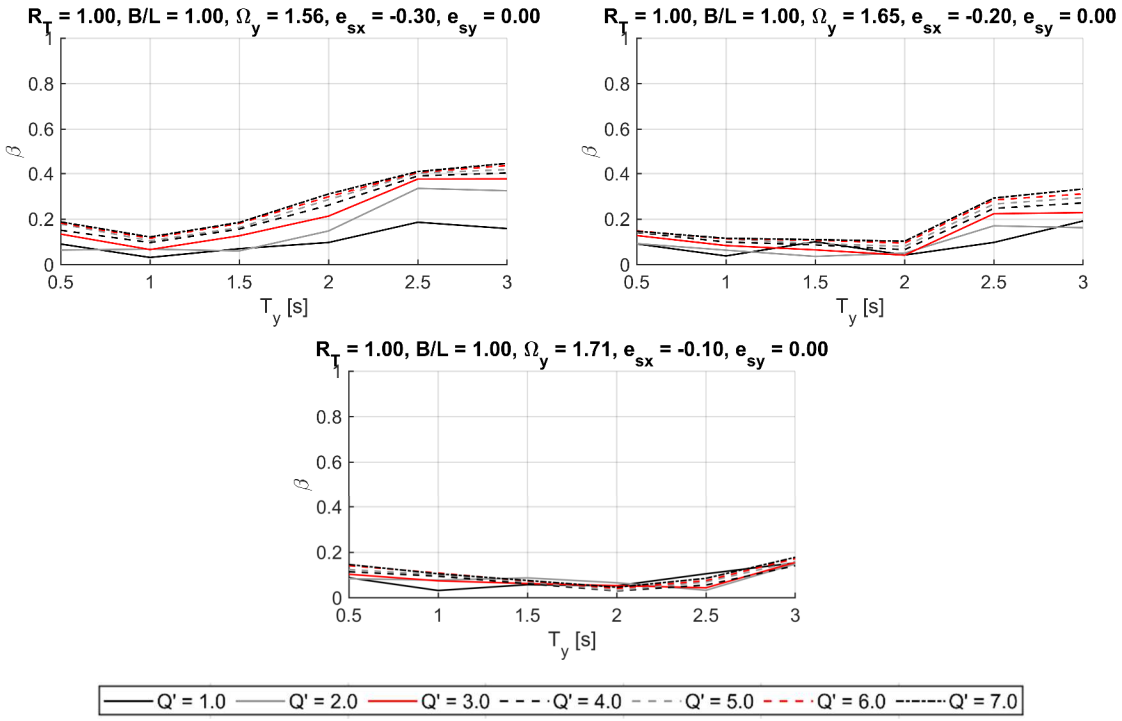

Fig. 5.19. Combination factor, β, as a function of T_y, for B/L = 1.00

Figs. 5.20 and 5.21, depict the plots of β *vs* e_{sx} of systems with *B/L*=0.5 and 1.0, respectively, for different values of T_y and *Q'*. As for M-System the relationship between β and e_{sx} in X-System is linear or bilinear in most cases for both elastic and inelastic system, being constant in some cases. Moreover, the smallest β values correspond to elastic systems for practically all e_{sx} values and the largest values are associated with inelastic structures *Q'*=7.

For *B/L*=0.5 (Fig. 5.20), elastic systems with T_y = 0.5 s present β values that decrease from about 0.10 at e_{sx} = 0.10 to 0.02 at e_{sx} = 0.05. For T_y = 1.0 s and 1.5 s, β of elastic systems fluctuates around values of 0.05 for all eccentricity values. Elastic systems with T_y = 2.0 s and 2.5 s exhibit an increasing bilinear relationship with respect to e_{sx} ranging from about 0.05 to 0.2 and 0.10 to 0.3, respectively. For T_y = 3.0 s, β is virtually constant, 0.2, in the entire e_{sx} range shown. For inelastic structures with *Q'*=7 and 0.5 ≤ T_y ≤ 1.0 s, β fluctuates around constant values of 0.15 and 0.10 for T_y =0.5 s and 1.0 s, respectively. For T_y =1.5 s, β of systems with *Q'* = 7 increases linearly from about 0.05 to 0.3 in the e_{sx} range shown. For systems with *Q'* = 7 and 2.0 s ≤ T_y ≤ 3.0 s, β follows an increasing bilinear relation with respect to e_{sx}, with values ranging from about 0.05 to 0.45, 0.15 to 0.4 and 0.2 to 0.55, for T_y = 2.0 s, 2.5 s and 3.0 s, respectively, in the e_{sx} range shown.

The same trends are identified for *B/L*=1.0 (Fig. 5.21), although the relationship between β and e_{sx} is smoother and the values of the former are smaller than those of *B/L*=0.05. For T_y ≤ 1.5 s, β of elastic systems is virtually constant, about 0.10, 0.02 and 0.05, for T_y values of 0.5 s and 1.0 s,

respectively, in the e_{sx} range shown. For T_y = 2.0 s and 2.5 s, β of elastic systems increases bilinearly from about 0.05 to 0.10 and 0.10 to 0.20, respectively. Elastic systems with T_y = 3.0 s exhibit an approximately constant value of 0.2. For inelastic systems with $T_y \leq$ 1.0 s β fluctuates around a constant value in the e_{sx} range shown; for Q'=7, β is around 0.15 and 0.10 for T_y = 0.5 s and 1.0 s, respectively. For inelastic structures with T_y = 1.5 s, β increases linearly with respect to e_{sx}; for Q'=7, its values range between about 0.05 to 0.2 in the e_{sx} range shown. β of inelastic systems with $T_y \geq$ 2.0 s increase bilinearly with respect to e_{sx}; for Q'=7, its values range from about 0.05 to 0.3, 0.10 to 0.4 and 0.2 to 0.45, for T_y = 2.0 s, 2.5 s and 3.0 s, respectively.

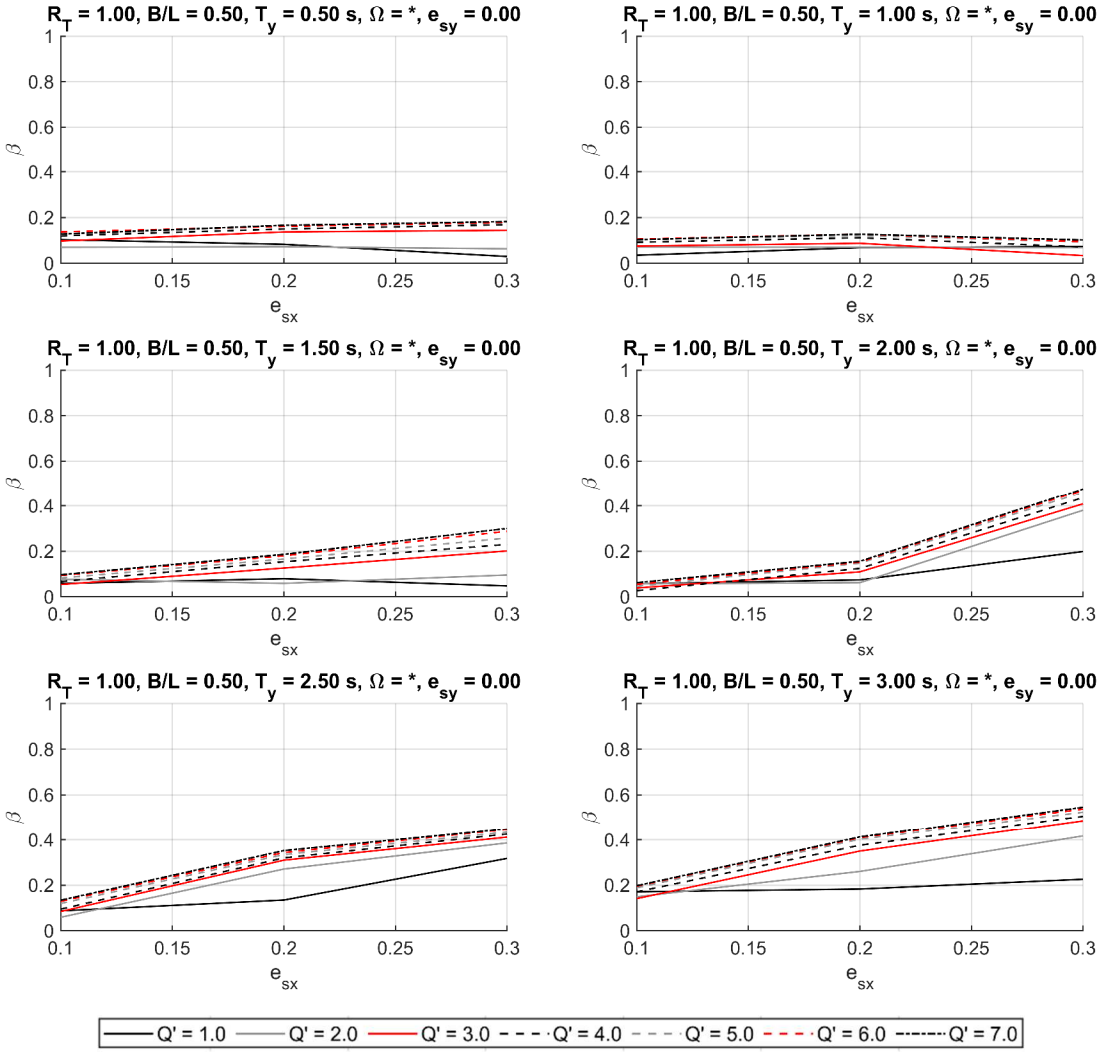

Fig. 5.20. Combination factor, β, as a function of e_{sx}, for B/L = 0.50

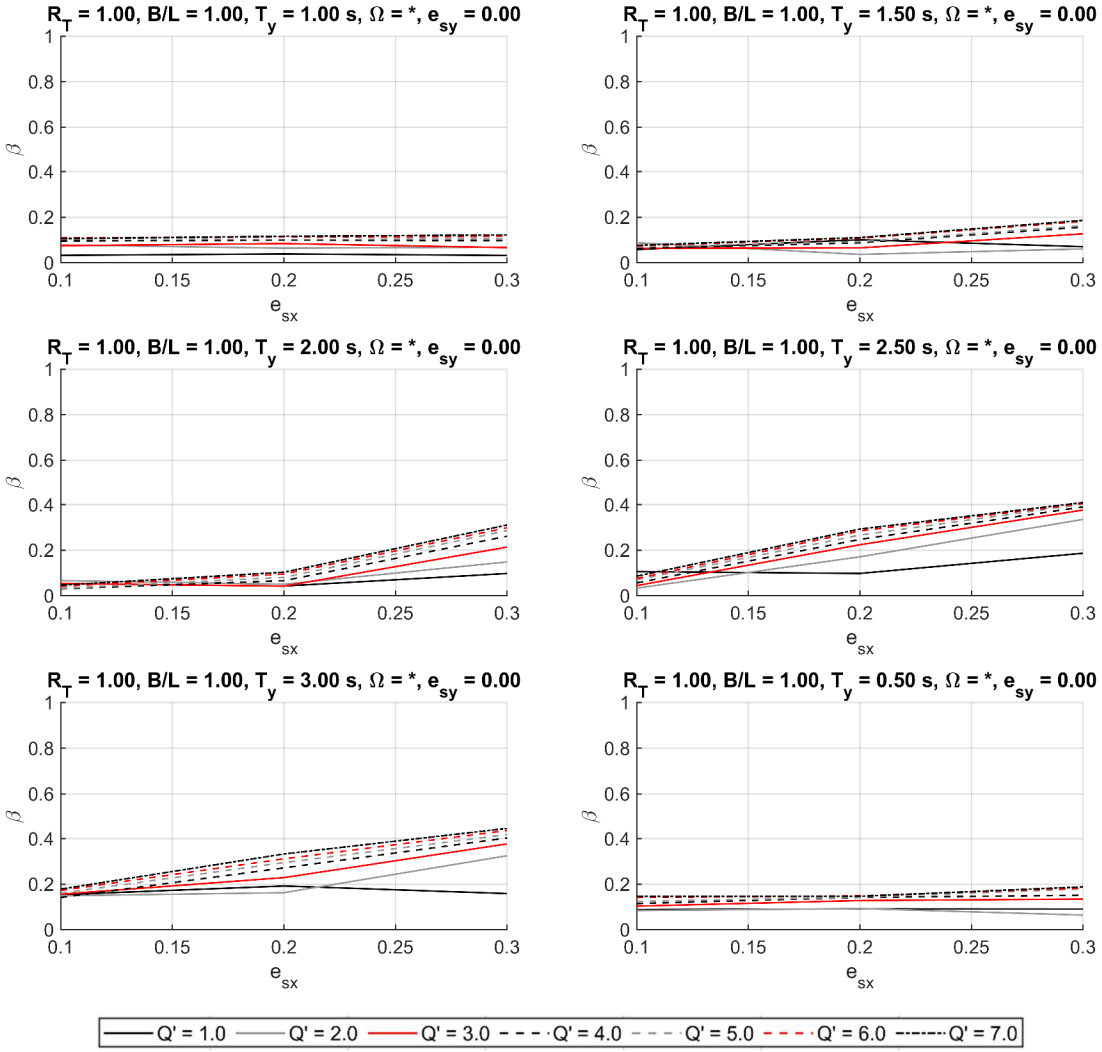

Fig. 5.21. Combination factor, β, as a function of e_{sx}, for B/L = 1.00

5.3.2. Dispersion of results

Figs. 5.22 and 5.23 depict the normalized median absolute deviation of β, CV_{med} - β, of structures with B/L = 0.50 and 1.0, respectively. It can be observed that the dispersion is significantly high for several case studies, particularly for elastic systems. For B/L=0.5 (Fig. 5.22), CV_{med} - β presents an increasing trend for a moderately torsionally stiff structure, *i.e.* $\Omega \leq 1.3$, and $Q' \geq 3.0$, conversely, for structures with $\Omega > 1.3$, CV_{med} - β appears to remain approximately constant for all values of T_y. For $Q' \leq 2.0$ the variability of the data is higher than the one obtained for Q' > 2.0, especially the variation of elastic structures. A similar trend is found for structures with B/L = 1.0 (Fig. 5.23).

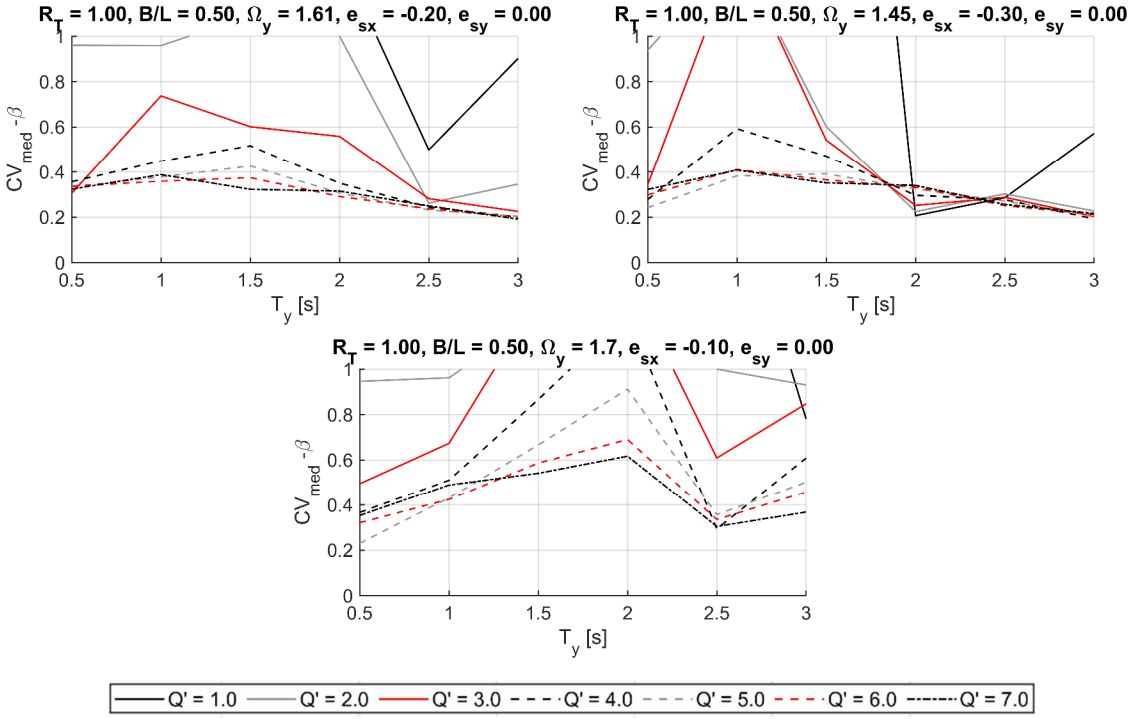

Fig. 5.22 Normalized median absolute deviation of β, as a function of T_y, for B/L = 0.50

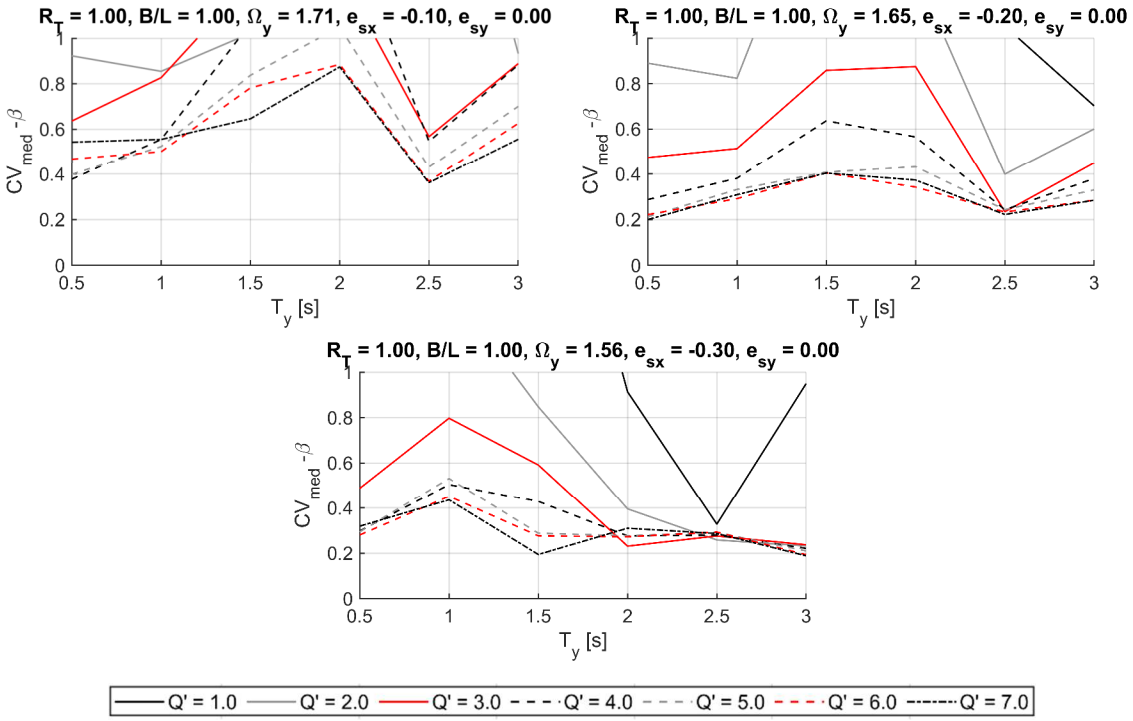

Fig. 5.23 Normalized median absolute deviation of β, as a function of T_y, for B/L = 1.00

5.3.3. Comparison with the Mexico City's Building Code combination factor

The comparison of the values of β obtained from the non-linear dynamic analysis and the combination factor prescribed by the Mexico City's Building Code (*NTC-DS*, 2017a), $\beta_{norm} = 0.3$, in terms of the relative error of β to the value of β_{norm}, is shown in Fig. 5.24. According to eq. 5.2, a positive relative error indicates that the calculated β is smaller than β_{norm}, conversely, a negative relative error indicates that the calculated β is greater than β_{norm}.

As can be observed in Fig. 5.24, 65% of the cases present a value of β that is smaller than β_{norm}. This implies that for the X-System, the forces in the orthogonal direction are being overestimated in most of the cases.

$$\%RE = \frac{0.3 - \beta}{0.3} \qquad 5.2$$

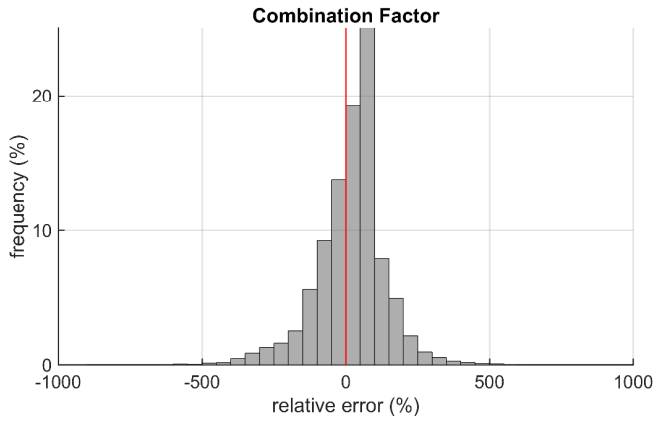

Fig. 5.24 Histogram of relative error of β ton β_{norm}

Chapter 6. REGRESSION ANALYSIS OF RESPONSE PARAMETERS

To estimate rational seismic demands for design and assessment of asymmetric-plan buildings, a set of equations dependent on the structural parameters involved in torsional response were derived from regression analyses of the median demands attained from non-linear dynamic analyses. The regression analysis was performed via the artificial neural fitting network programmed in the software MATLAB (The Mathworks, 2019). Such neural network consists of a two-layer feedforward network (Fig. 6.1), with a logarithmic sigmoid transfer function in the hidden layer and a linear function in the output layer. The neural network training was done using 70% of the results obtained from the parametric analysis, in which a Levenberg-Marquardt backpropagation function was used as training function; 15% were used for the validation of the neural network, where the mean squared error was used for the validation of performance; and the remaining 15% were used for testing the neural network.

In order to have a good approximation of the data, the size of the hidden layer was set so that the coefficient of determination, R^2, of the linear regression between the target values and the outputs of the neural network, was greater or equal to 90%. The parameters used as the input layer of the neural network were chosen in accordance to their influence in each of the seismic demands considered in this work.

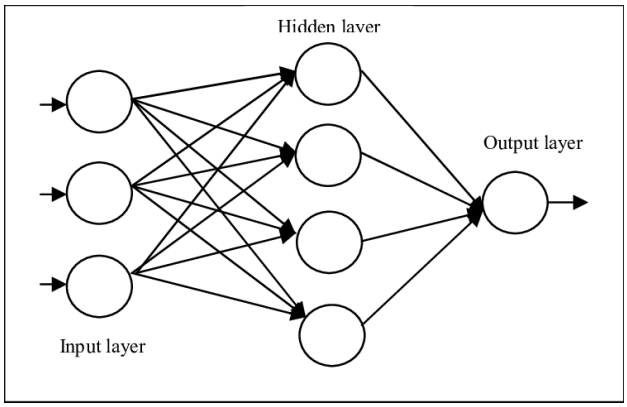

Fig. 6.1 Artificial neural network architecture (Sim Vui et al., 2013)

6.1. Flexible side displacement amplification

The fitting of the displacement amplification factor, δ_F/δ_{CM}, was performed using as input parameters the plan aspect ratio, B/L; the stiffness eccentricity, e_{sx}; the rotational stiffness factor, Ω; the seismic reduction factor, Q'; and the fundamental period of the structure, T_n. The equation derived from this non-linear regression is the following:

$$\frac{\delta_F}{\delta_{CM}} = \frac{7.22}{14.27e^{\alpha_1}+1} + \frac{8.20}{0.076e^{\alpha_2}+1} - 6.17$$
$$\alpha_1 = -1.110B/L + 9.264e_{sx} - 0.981\Omega - 0.203Q' - 1.287T_n \qquad 6.1$$
$$\alpha_2 = 1.186B/L - 8.695e_{sx} + 1.059\Omega + 0.183Q' + 1.063T_n$$

The displacement amplification of the flexible side was calculated using eq. 6.1, for all the case studies and was compared to the actual one. Fig. 6.2 shows such comparison. The coefficient of determination of eq. 6.1. is $R^2 = 0.94$, which indicates a good approximation to the actual displacement amplification of the flexible side.

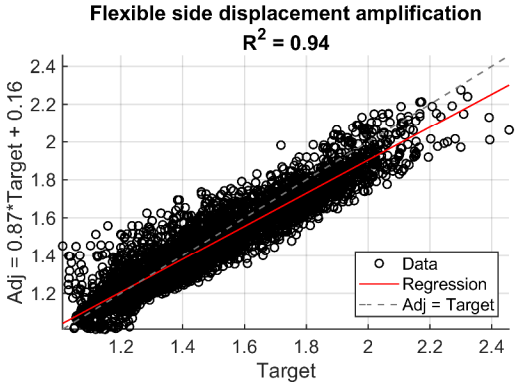

Fig. 6.2 Regression adjustment of δ_F/δ_{CM}

Additionally, the cumulative probability of error of eq. 6.1, was obtained to further assess its goodness of fit. As can be observed in Fig. 6.3, for 30% of the cases the value of δ_F/δ_{CM} obtained with eq. 6.1 is equal or greater than the real seismic demand, which implies that using this equation will give conservative results for these cases. For the non-conservative results, it can be observed that the largest relative error is about 10%, hence, this indicates that the δ_F/δ_{CM} obtained with eq. 6.1 provides a good estimation of the seismic response.

$$e_r = \frac{(\delta_F/\delta_{CM})_{adj} - (\delta_F/\delta_{CM})_{NLD}}{(\delta_F/\delta_{CM})_{NLD}} \qquad 6.2$$

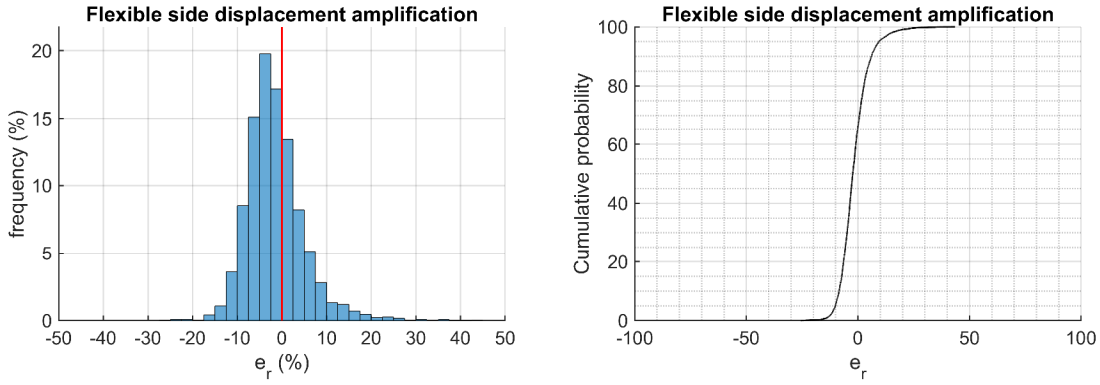

Fig. 6.3 Histogram of relative error and cumulative probability of error for δ_F/δ_{CM}

6.2. Ductility demand

Regression analysis of the ductility demand, μ, was carried out using as input parameters the plan aspect ratio, B/L; the seismic reduction factor, Q'; and the fundamental period of the structure, T_n. The equation derived is the following:

$$\mu = -\frac{54.59}{0.25e^{\beta_1}+1} + 56.526$$
$$\beta_1 = -0.243B/L + 0.686Q' - 3.878T_n \qquad 6.3$$

Fig. 6.2 shows the relationship between the actual μ and that calculated with eq. 6.3. The coefficient of determination obtained from the fitting is $R^2 = 0.97$, which indicates a good approximation of the real demands. However, it can be observed that the results obtained via such equation may provide significant differences in some cases.

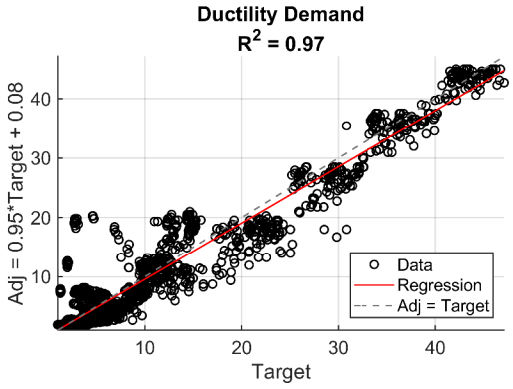

Fig. 6.4 Regression adjustment of μ

Fig. 6.5 presents the histogram and cumulative probability of error of eq. 6.3. As can be observed in such figure, for almost 60% of the cases the value of μ obtained with eq. 6.3 is equal to or greater than the actual ductility demand, thus, the equation provides conservative results. Conversely, for the other 40% of the data the estimated ductility is smaller than the actual ductility developed by

the structure, hence, the inelastic displacement of the structure would be underestimated. For these non-conservative cases, it can be observed in Fig. 6.5, that 75% of the cases present a relative error that is smaller than 20%, hence, eq. 6.3provides results that are conservative or with a low relative error for most cases.

$$e_r = \frac{\mu_{adj} - \mu_{NLD}}{\mu_{NLD}} \tag{6.4}$$

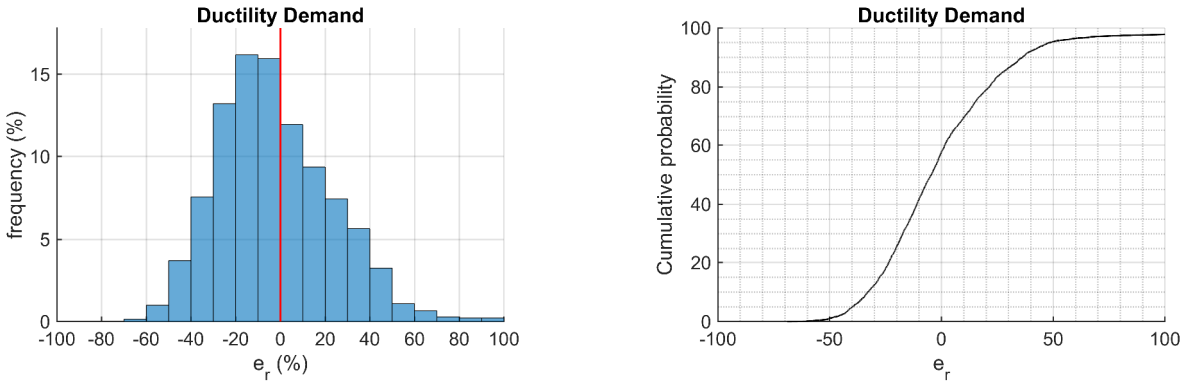

Fig. 6.5 Histogram of relative error and cumulative probability of error for μ

6.3. Combination factor of orthogonal demands

Regression analysis for the combination factor, β, was carried out using as input parameters the uncoupled translational periods ratio, $R_T = T_y/T_x$; the plan aspect ratio, B/L; the seismic reduction factor, Q'; and the fundamental period of the structure, T_n. The equation derived is the following:

$$\begin{aligned} \beta &= -\frac{42.707}{0.0069e^{\gamma_1}+1} - \frac{3.529}{13.188e^{\gamma_2}+1} + 42.60 \\ \gamma_1 &= 1.039R_T - 0.1892B/L - 0.088T_n \\ \gamma_2 &= -1.80R_T + 0.3017B/L + 0.652Q' + 0.302T_n \end{aligned} \tag{6.5}$$

Fig. 6.6 shows the relationship between the real β and that obtained with eq. 6.5. The coefficient of determination of the equation is $R^2 = 0.90$. It can be observed in this figure that eq. 6.5 provides a good approximation of β, however for values of β > 1.5 eq. 6.5 does not give a good approximation, however, β values given by building codes are less than one, thus eq. 6.5 may be used for design purposes.

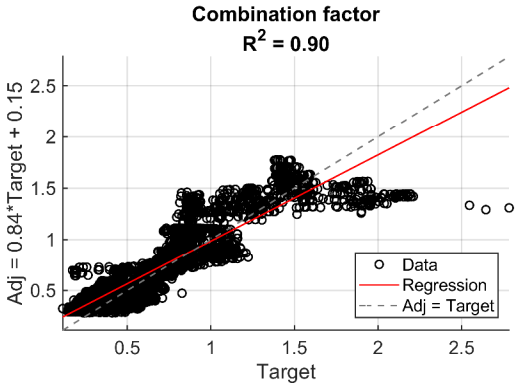

Fig. 6.6 Regression adjustment of β

As can be observed in Fig. 6.7, for 40% of the cases the value of β obtained with eq. 6.5 is equal or lower than the combination factor, which implies that using this equation will provide non-conservative forces when considered in a modal-spectral analysis, however, 90% of the cases present a relative error that is smaller than 10%, hence, eq. 6.5 provides results that are conservative or with a low relative error for most cases.

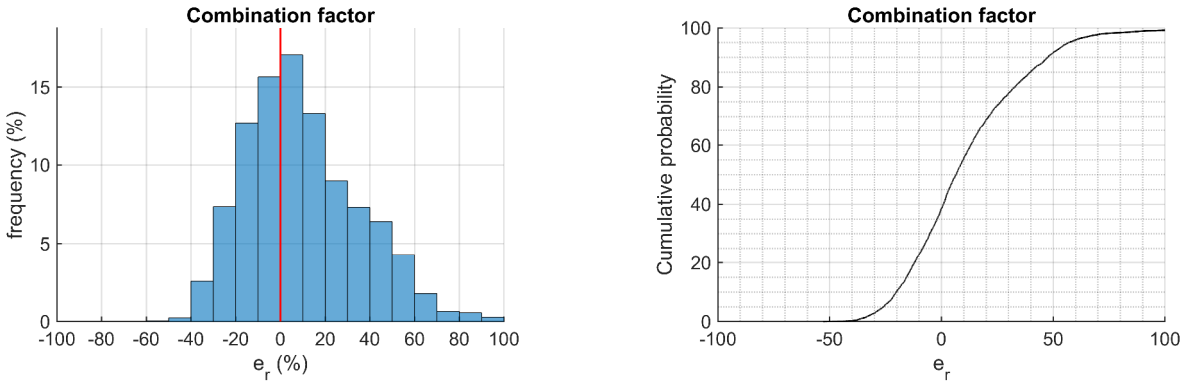

Fig. 6.7 Histogram of relative error and cumulative probability of error for β

Chapter 7. CONCLUSIONS

In this study, a parametric analysis was performed to assess the inelastic response of plan-asymmetric buildings subjected to seismic excitations at soft soil sites of the Valley of Mexico. The torsional parameters of the buildings considered in this study were the uncoupled period, T_y, the stiffness eccentricity, e_s; the rotational stiffness factor, **Ω**; the seismic reduction factor, *Q'*; the plan-aspect ratio, *B/L*; and the uncoupled translational periods ratio, T_y/T_x. Three demand parameters that are essential in the seismic design of plan asymmetric buildings were obtained from the parametric analysis and assessed in detail: 1) displacement amplification factor of the flexible side of the plan with respect to the center of mass; 2) ductility demand developed in the center of mass and 3) combination factor, β, of the bidirectional demands in terms of the design spectrum. Furthermore, equations to estimate such demand parameters that may be used in seismic assessment and design applications were derived from regression analysis. From the results of this study, the following conclusions are withdrawn.

7.1. Displacement amplification due to torsional effects

The rotational stiffness factor, **Ω**, and the seismic reduction factor, *Q'*, have a significant influence in the displacement demand of the flexible side. The displacement amplification factor obtained for inelastic structures was compared with that of elastic structures, with the same dynamic properties. It was observed that, in most cases, in structures with moderate rotational stiffness, the displacement amplification of the flexible side is larger for elastic systems than inelastic ones. Conversely, for structures with a high rotational stiffness, most of the cases present smaller displacement amplification in the elastic range.

This implies that the use of modal response spectrum analysis to estimate the maximum inelastic response of plan-asymmetric buildings built at soft soil sites, which is the common approach used in modern building codes and displacement-based design methods, *e.g.* the N2 extended method (Fajfar *et al.*, 2005); may provide unconservative results, particularly for structures with high rotational stiffness. For this reason, the seismic design provisions for such type of buildings should consider the effect of both rotational stiffness and the level of inelastic behavior, in terms of *Q',* in the estimation of displacement demands of the flexible side of the plan. The equation proposed in this study provides a reasonable approximation of a median displacement amplification of the flexible side of plan-asymmetric buildings built at soft soil sites of the Valley of Mexico as a function of their plan aspect ratio, the stiffness eccentricity, the rotational stiffness factor, the seismic reduction factor and the fundamental period of the structure.

7.2. Ductility demand

The ductility demand developed at the center of mass, μ, was obtained considering the maximum displacement of the non-linear dynamic analysis and the yield displacement obtained from a non-linear static analysis. It was observed that the ductility demand is mainly affected by the fundamental period of the structure, T_n, and the seismic reduction factor, Q'. As for the stiffness eccentricity, e_{sx}, and the rotational stiffness factor, **Ω**, it was observed that their influence can be neglected, as the ductility demand remains nearly constant with respect to these two parameters.

As modern building codes consider a ductility demand derived from SDOF systems, a comparison was carried out between the ductility demand obtained from an SDOF system and the one obtained from a non-linear dynamic analysis of a 3DOF structure. It was observed that for short period structures, *i.e.* $T_n < 1.0$ s, the ductility demand of the 3DOF system is approximately equal to the ductility of an SDOF system. However, for structures with larger periods, particularly for structures with a moderate rotational stiffness, *i.e.* $\Omega < 1.3$, the ductility developed for a 3DOF system is 20% to 50% smaller than the ductility developed by an SDOF structure. Thus, a correction factor of the ductility demand should be considered for the design of buildings, particularly for flexible buildings with a moderate rotational stiffness. For this reason, an equation that provides a reasonable estimation of a median design ductility demand for buildings located at soft soil sites at the Mexico Valley is proposed in this study. Such equation is a function of the plan aspect ratio, the seismic reduction factor, and the natural period.

7.3. Combination factor of orthogonal demands

The combination factor of the orthogonal demands, β, was defined in this study as that for which the seismic base shear obtained from modal-spectral analysis using the given design spectrum in its natural scale in the critical direction with the same spectrum scaled by β in the horizontal orthogonal direction, provides a reasonable approximation of the base shear demands attained from non-linear dynamic analysis of the set of records considered. The design spectra employed was the median response spectrum of such set. From the results attained from these analyses, it was observed that the combination factor is strongly correlated to the seismic behavior factor, Q', and the fundamental period of the structure, T_n. Moreover, it is observed that β is virtually independent of e_{sx}, except for structures with periods $1.5 \text{ s} < T_y \leq 2.5$ s.

Furthermore, a comparison was carried out between the combination factor (median value) obtained in this study via non-linear dynamic analyses and the combination factor stipulated in most modern building codes, $\beta = 0.3$. It was observed that for most cases the median combination factor is larger than such value, which implies that the design forces obtained from applications of the conventional design method may be unconservative for buildings located at soft soil sites. Therefore, in this study, an equation is proposed which allows a reasonable estimation of a median combination factor for use in the seismic design of plan- asymmetric buildings built at soft soil

sites of the Mexico Valley, in terms of the uncoupled translational period ratio, the plan aspect ratio, the seismic reduction factor, and the fundamental period of the structure.

REFERENCES

"Accelerographic record database of the RAII-UNAM." (2018). <http://aplicaciones.iingen.unam.mx/AcelerogramasRSM/Inicio.aspx>.

Anagnostopoulos, S. A., Alexopoulou, C., and Stathopoulos, K. G. (2008). "Are results for inelastic torsion in buildings based on simplified, one-storey, shear beam models, applicable to actual multistory buildings?" *Proceedings of the 5th European Workshop on the Seismic behaviour of irregular and complex structures*, Catania, Italy.

Anagnostopoulos, S. A., Kyrkos, M. T., and Stathopoulos, K. G. (2015). "Earthquake induced torsion in buildings: critical review and state of the art." *Earthquakes and Structures*, 8(2), 305–377.

Anagnostopoulos, S., Alexopoulou, C., and Stathopoulos, K. (2010). "An answer to an important controversy and the need for caution when using simple models to predict inelastic earthquake response of buildings with torsion." *Earthq. Eng. Struct. Dyn.*, 39, 521–540.

Anastassiadis, K., Athanatopoulou, A., and Makarios, T. (1998). "Equivalent Static Eccentricities in the Simplified Methods of Seismic Analysis of Buildings." *Earthquake Spectra*, 14(1), 1–34.

Bazán, E., and Meli, R. (1985). *Manual de diseño sísmico de edificios: de acuerdo con el Reglamento de construcciones para el Distrito Federal*. Limusa, México.

Bensalah, M. D., Bensaibi, M., and Modaressi, A. (2012). "Assessment of the torsional effect in asymmetric buildings under seismic load." *Proceedings of the 15th World Conference, Earthq. Eng.*

Bresler, B. (1960). "Design Criteria for Reinforced Columns under Axial Load and Biaxial Bending." *Journal of the American Concrete Institute*, 57(11), 481–490.

Construction Code for Mexic City and Complementary Technical Standards or Seismic Desing. (2017a). Oficial Gazette, Mexico City's Government, Mexico.

De Stefano, M., and Pintucchi, B. (2002). "A model for analyzing inelastic seismic response of plan-irregular building structures." *Proceedings of the 15th ASCE Engineering Mechanics Conference*.

De Stefano, M., and Pintucchi, B. (2010). "Predicting torsion-induced lateral displacements for pushover analysis: Influence of torsional system characteristics." *Earthq. Eng. Struct. Dyn.*, 39, 1369–1394.

De Stefano, M., and Rutenberg, A. (1999). "Seismic stability and the force reduction factor of code designed one storey asymmetric structures." *Earthq. Eng. Struct. Dyn.*, 28, 785–103.

De Stefano, M., Tanganelli, M., and Viti, S. (2013). "Effect of the variability in plan of concrete mechanical properties on the seismic response of existing RC framed structures." *Bull Earthquake Eng*, 11(4), 1049–1060.

Eurocode 8: Design of structures for earthquake resistance - Part 1: General rules, seismic actions and rules for buildings. (2004). European Commitee for Standarization, Brussels.

Fajfar, P., Marusic, D., and Perus, I. (2005). "The Extension of the N2 Method to Asymmetric Buildings." *Proceedings of the 4th European workshop on the seismic behaviour of irregular and complex structures*, Thessaloniki, Greece.

Ghersi, A., and Rossi, P. P. (2000). "Formulation of design eccentricity to reduce ductility demand in asymmetric buildings." *Eng. Struct*, 22, 857–871.

Jeong, S., and Elnashai, A. S. (2004). "Analytical and Experimental Seismic Assessment of Irregular Buildings." *13th World Conference on Earthquake Engineering*, Vancouver, B.C., Canada.

Lucchini, A., Monti, G., and Kunnath, S. (2011). "Nonlinear response of two-way asymmetric single-story building under biaxial excitation." *J. Struct. Eng*, 137(1), 34–40.

Marusic, D., and Fajfar, P. (2005). "On the inelastic seismic response of assymetric buildings under bi-axial excitation." *Earthq. Eng. Struct. Dyn.*, 34(8), 943–963.

McKenna, F., Fenves, G. L., and Filippou, F. C. (2016). *Open System for Earthquake Engineering Simulations*. Pacific Earthquake Engineering Research, University of California, Berkeley.

Minimum Design Loads and Associated Criteria for Buildings and other Structures. (2016). Virginia, USA.

Moehle, J. P. (1984). "Seismic Response of Vertically Irregular Structures." *Journal of Structural Engineering*, 110(9), 2002–2014.

Moehle, J. P. (1992). "Displacement-Based Design of RC Structures Subjected to Earthquakes." *Earthquake Spectra*, 8(3), 403–428.

Myslimaj, B., and Tso, W. K. (2002). "A strength distribution criterion for minimizing torsional response of asymmetric wall-type systems." *Earthq. Eng. Struct. Dyn.*, 31(1), 99–120.

Newmark, N. M. (1959). "A Method of Computation for Structural Dynamics." *Journal of the Engineering Mechanics Division*, 85(3), 67–94.

Norma Chilena Oficial: Diseño sísmico de edificios. (2012). Instituto Nacional de Normalización, Chile.

Normas Técnicas Complementarias para Diseño por Sismo. (2017b). Gaceta Oficial del Gobierno de la Ciudad de México, Ciudad de México, México.

Paulay, T. (2001). "Some Design Principles Relevant to Torsional Phenomena in Ductile Buildings." *J. Earth. Eng.*, 5(3), 273–308.

Priestley, M. J. N. (2003). *Myths and Fallacies in Earthquake Engineering, Revisited. The Ninth Mallet Milne Lecture*. Rose School, Collegio Alessandro Volta, Pavia, Italy.

Priestley, M. J. N., Calvi, G. M., and Kowalsky, M. J. (2007). *Displacement-Based Seismic Design of Structures*. IUSS Press, Pavia, Italy.

Rosemblueth, E., and Contreras, H. (1977). "Approximate Design for multi-component earthquakes." *International Journal of Engineering Mechanincs Division ASCE*, 103, 895–911.

Ruiz, S. E., Rosemblueth, E., and Diederich, R. (1989). "The Mexico Earthquake of September 19, 1985 - Seismic Response of Asymmetrically Yielding Structures." *Earthquake Spectra*, 5(1), 103–111.

Ruiz-Garcia, J., and Miranda, E. (2004). "Inelastic Displacement Ratios for Design of Structures on Sot Soil Sites." *J. Struct. Eng*, 130(12), 2051–2061.

Rutenberg, A., and De Stefano, M. (1997). "On the seismic performance of yielding asymmetric multistorey buildings: A review and a case study." *Seismic Design Methodologies for the Next Generation of Codes*, P. Fajfar and H. Krawinkler, eds., Rotterdam, Netherlands.

Sim Vui, C., Kim Soon, G., Jim On, C., Rayner, A., and Anthony, P. (2013). "A Review of Stock Market Prediction with Artificial Neural Network (ANN)." Penang, Malaysia, 477–482.

Stathopoulos, K. G., and Anagnostopoulos, S. A. (2007). "Inelastic seismic response of asymmetric one-story steel buildings." *ECCOMAS Thematic Conference Composition Methods Struct. Dyn. Earthq. Eng.*

The Mathworks. (2019). *MATLAB and Deep Learning Toolbox Release 2019b*. The MathWorks, Inc., Natick, Massachusetss, United States.

Wilson, E. L., Suharwardy, I., and Habibullah, A. (1995). "A Clarification of the orthogonal effects in a three-dimensional seismic analysis." *Earthquake Spectra*, 11(4), 659–666.

Appendix A. EQUATIONS FOR THE RESISTING ELEMENTS DIMENSIONS

The dimensions of the vertical resisting elements were changed, in order to obtain the desired mechanic and dynamic properties for the parametric analysis. The following expressions were used to determine the dimensions of the resisting elements, as a function of the different parameters used in this work, for each case study described in Chapter 3.

A.1 Moderate to large torsionally stiff system

The M-system's vertical resisting elements are column-type elements, with ratio $h/b = R_T$. The height of the elements has been normalized with respect to the height of the element C1, which is the upper left element as shown in Fig. A.1. The height of each column, which is the dimension along the x-direction, can be obtained with the equations A.1 to A.3 for the elements C1 to C3, respectively. The width of each column is obtained from the element dimensions ratio, $b_i = h_i / R_T$

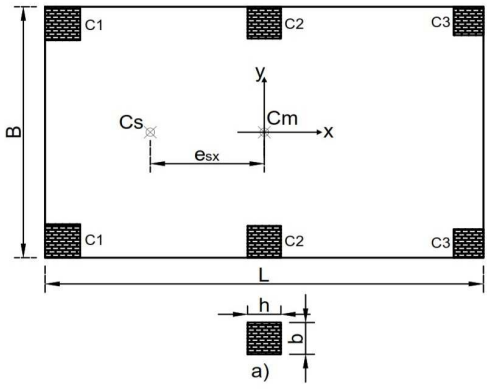

Fig. A.1. M-System*, element distribution and dimensions*

$$\left(h_1\right)^4 = \frac{2H^3 m_T}{E}\left(\frac{\pi}{T_y}\right)^2 \left(R_T\right)^3 \frac{1}{\left[1+\left(h_2^*\right)^4+\left(h_3^*\right)^4\right]} \qquad \text{A.1}$$

$$\left(h_2^*\right)^4 = \left(h_3^*\right)^4 \left(\frac{1-2e_x}{2e_x}\right) - \left(\frac{1+2e_x}{2e_x}\right) \qquad \text{A.2}$$

$$\left(h_3^*\right)^4 = \frac{4e_{sx}^2 + 2e_{sx} + 4\left(\Omega\rho\right)^2 - \left(\frac{B}{L}\right)^2 \left(R_T\right)^2}{4e_{sx}^2 - 2e_{sx} + 4\left(\Omega\rho\right)^2 - \left(\frac{B}{L}\right)^2 \left(R_T\right)^2} \qquad \text{A.3}$$

where:

h_i^* is the dimension along the x-direction of Ci, normalized with respect to h_1.

b_i^* is the dimension along the y-direction of Ci, normalized with respect to h_1.

R_T is the uncoupled periods ratio. $R_T = T_y / T_x$

B / L is the plan dimensions ratio.

e_{sx} is the stiffness eccentricity along the x-direction, normalized with respect to L.

Ω is the factor of rotational stiffness.

ρ is the mass radius, normalized with respect to L. $\rho = \sqrt{\dfrac{(B/L)^2 + 1}{12 m_T}}$

H is the height of the structure.

m_T is the total mass of the structure.

E is the modulus of elasticity of the resisting element's material.

A.2 Highly torsionally stiff system

The X-system's vertical resisting elements are wall-type elements, with ratio $t / L_m = 0.1$. The in-plane dimension of the elements has been normalized with respect to the dimension of the element M1, which is the left element as shown in Fig. A.2. The in-plane dimension of the elements are obtained through equations A.4 to A.7. The out-of-plane dimension is obtained from the element dimensions ratio, $t_i = 0.1 L_{mi}$.

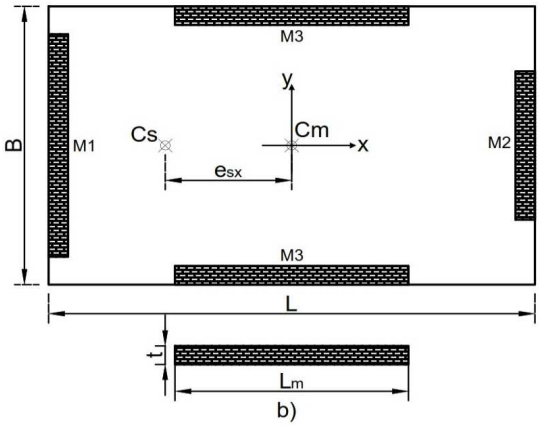

Fig. A.2. X-System*, element distribution and dimensions*

$$\left(L_1\right)^4 = \frac{40H^3 m_T}{E}\left(\frac{\pi}{T_y}\right)^2 \frac{1}{\left[1+\left(L_2^*\right)^4 + 0.01\left(L_3^*\right)^4 + 0.01\left(L_4^*\right)^4\right]} \quad \text{A.4}$$

$$\left(L_2^*\right)^4 = \frac{1+2e_{sx}}{1-2e_{sx}} \quad \text{A.5}$$

$$\left(L_3^*\right)^4 = \frac{R_T^2}{1-2e_{sx}} \quad \text{A.6}$$

$$\left(L_4^*\right)^4 = \frac{R_T^2}{\left(1-2e_{sx}\right)} \quad \text{A.7}$$

where:

L_i^* is the in-plane dimension of Mi, normalized with respect to L_1.

The distribution of the vertical resisting elements in this system represent a special case, in which de stiffness radii of the system is dependent of the value of e_x, and has a value of:

$$\Omega = \frac{1}{\rho}\sqrt{\frac{1}{4} - e_{sx}^2 + \frac{1}{4}\left(\frac{B}{L}\right)^2 {R_T}^2} \quad \text{A.8}$$